

Dear the reviewer for the manuscript entitled "Description and basic evaluation of simulated mean state, internal variability, and climate sensitivity in MIROC6" by Tatebe et al.

We would like to thank the reviewer for taking the time to carefully read our manuscript, for several very valuable suggestions and English grammatical corrections. We have much revised our manuscript and answered all the comments given by the reviewer. In the separate reply letter uploaded as a supplement, point-by-point responses to the reviewer's comments and how we revised the manuscript are described, referring to the revised manuscript and the manuscript with revision history which were also uploaded as supplements.

Hiroaki Tatebe

Research Center for Environmental Modeling and Application,

Japan Agency for Marine-Earth Science and Technology

3173-25 Showamachi, Kanazawaku, Yokohama, Kanagawa 236-0001, Japan

Response to reviewers' comments on " Description and basic evaluation of simulated mean state, internal variability, and climate sensitivity in MIROC6" by Tatebe et al.

Reply to the reviewer #1

General comments

This paper describes MIROC6, a new climate model aiming at participating in CMIP6, by developing the previous climate model MIROC5 that participated in CMIP5. Following the description of the model formulation focusing on the changes from MIROC5 together with the model's tuning procedure, the model's mean climate and variability in the preindustrial experiment are presented. Furthermore, climate sensitivity of the model and reproducibility of the past climate change are also evaluated. Although the manuscript is comprehensive, it is well-constructed and well-documented. Climate variabilities of the model has also been widely evaluated, which brings many useful scientific knowledges for future studies using this model. In addition, model tuning procedure is also described in detail, which contains very useful information to be helpful for climate model developers. It is recommended that it will be published after minor revisions.

We would like to thank the reviewer for taking the time to carefully read our manuscript, for several very valuable suggestions, and English grammatical corrections. We would like to answer the questions given by the reviewer and to describe how we have revised our manuscript point by point. Please note that our replies are written in red letters in this reply letter.

Reply to specific comments

L.355: The main parameters...in which the uncertainty of the climate sensitivity...

Does this mean that the model is tuned for a climate sensitivity as a result? If so, it is desirable to describe what is the target climate sensitivity (2.5 K?) for the tuning.

Here, the authors just wanted to mention that parameters listed in Shiogama et al. (2012) are mainly used for a tuning procedure. Climate sensitivity was not a tuning target. In the revised manuscript, we have rephrased the sentence as "The main parameters used in our tuning procedures are chosen referring to a perturbed parameter ensemble set made by Shiogama et al. (2012) in which parameter sensitivity to cloud-radiative processes is examined". Please see the lines 374 -377 in the revised manuscript.

L.374: interactions between anthropogenic aerosol emissions and...

“emissions” do not interact with cloud-radiation processes. Do you mean “aerosolcloud interaction”?
Rephrase it.

In the revised manuscript, the words are replaced by "aerosol-cloud interaction". Please see the lines 402-403. Thank you for your suggestion.

L.380: a present-day run

Is the run a fixed SST? Since the value of -0.9 Wm^{-2} by IPCC (2013) is for ERF, it should be evaluated by radiation change under the condition that SST does not change. Please explain.

The tuning was done under a coupled mode, namely, SST is not fixed. In the revised manuscript, we added the sentence "Note that MIROC6 in a coupled mode is used in this tuning procedure, and thus the sea surface temperature (SST) is not fixed. The estimated cooling effects here are not strictly the same as the effective radiative forcing estimated in IPCC (2013). However, by the present tuning procedure, the global-mean surface air temperature (SAT) change after the mid-19th century is well reproduced in the historical runs by MIROC6 (details are discussed in Section 4)". Please read the lines 411-416.

L.397: the global-mean ocean temperature shows a larger trend of...

On average there is 1.1 Wm^{-2} heating. Are these trends consistent with the radiation budget?

Discussions on the relationship between the warming trend of the ocean temperature and the TOA radiation budget/ocean heat uptake have been added in the revised manuscript. And we also added the explanation on the heat energy inconsistency between the TOA radiation budget and the ocean heat uptake in association with the model imperfection. We have rephrased the last paragraph of Section 2.5 as "The trend of the global-mean ocean temperature in the later period suggests slight but continuous warming of the deep ocean. The radiation budget at the TOA is 1.1 Wm^{-2} downward on average (linear trend of $9.5 \times 10^{-3} \text{ K/100 yr}$) and the net heat input at the sea surface is 0.32 Wm^{-2} . The deep ocean warming is explained by the net heat input. Note that there is about 0.78 Wm^{-2} inconsistency between the TOA radiation budget and the ocean heat uptake. This heat energy inconsistency is due to that internal energy associated with precipitation, water vapor and river runoff is not taken account in the atmospheric and land surface component in MIROC6 and that these waters with no temperature information implicitly set their temperature to the SST when they flow or fall into the ocean. Perpetual melting of the prescribed Antarctic ice-sheet with invariant ice thickness, which is occurred due to the warm SAT bias in the Antarctic region (details will be discussed in Section 3.1.3), is also a cause of the heat energy inconsistency".

L.477: consistent with the observed value of -0.81 Wm^{-2} .

The observed value is -0.8 Wm^{-2} because the system is warming in the present-day conditions. Ideally it should be 0 Wm^{-2} in the preindustrial conditions. The radiation imbalance of -1.1 Wm^{-2} is in the marginally acceptable range.

Thank you for your comment and the authors agree with the reviewer. In the revised manuscript, we added the sentence "However, the observed value is estimated in the present-day condition. Ideally, the model value in the preindustrial condition should be 0 Wm^{-2} and is in the marginally acceptable range". Please read the lines 521-523.

L.542: increase in precipitation (Figs. 8ce)

Increase in precipitation is found only in the North Pacific.

In the revised manuscript, the corresponding sentence is rewritten as "is accompanied by an associated increase in precipitation, especially in the North Pacific (Figs. 8ce)". Please read the lines 594-595.

Fig. 13 and 14: It is easy to understand if the biases are indicated by color shadings.

Following the comments, we have redrawn Figs. 13 and 14, and corresponding descriptions on ocean climatological hydrography have been rephrased partly in the revised manuscript. Please read the 1st and 2nd paragraphs of Section 3.1.2. Also, the revised manuscript with revision history is useful for checking the revision.

L.595: the Pacific sector (Figs. 13a-c) → "the Atlantic sector (Figs. 13a-c)" or "the Pacific sector (Figs. 14a-c)"

Carefully checking zonal-mean ocean temperature and salinity in the Pacific sector, the authors considered that representation of the northward intrusion of Antarctic Intermediate Water in the Southern Hemisphere in MIROC6 is not better than in MIROC5. In the revised manuscript, we deleted the sentence "Meanwhile, the northward intrusion of Antarctic Intermediate Water in the Southern Hemisphere around the 1000 m depth is better simulated in MIROC6 than in MIROC5, especially in the Pacific sector (Figs. 14a-c)".

L.622: better representation of cloud physics

How does cloud physics relate to trade wind? It seems to me that they are incoherent.

In the revised manuscript, we have described the details about the relationship between the stronger trade

wind and cumulus processes referring to the stand-alone AGCM experiments as "However, the thermocline depths in the western tropical Pacific are still larger in the models than in observations and are attributed to the stronger trade winds in the models. When both of MIROC6 and MIROC5 are executed as stand-alone AGCMs with the prescribed SST obtained from observations, the overestimate of the equatorial trade winds also appears due to overestimate of the upward winds over the maritime continent associated with deep cumulus convection and the resultant strengthening of the Walker circulation over the equatorial Pacific. Better parameterizing deep cumulus convection in the models could be required". Please read the lines 677-684.

L.648: present-day conditions. Specify the years of the observation. (1980-2009)?

In the revised manuscript, the years are specified as "while observations are taken in present-day conditions of 1980–2009...". Please read the lines 7070-711.

Figure 18: Adding a plot for the observed sea surface height will be helpful.

A figure of observed sea level height has been added as Fig. 18a and the reference for the observation data has been written in References (please see Rio et al. 2014).

L.687: strengthening of the Aleutian low lead to increase in southward transport...

I could not understand why the strengthening of the Aleutian low lead to increase in southward transport along the west coast.

We have rephrased the corresponding sentence as "Warm SAT and SST biases along the west coast of the North America are smaller in MIROC6 than in MIROC5. The reason is that an increase of southeastward Ekman transport in the eastern subarctic North Pacific due to the strengthening of the mid-latitude westerly jet (Fig. 10) and the Aleutian low tend to cancel out the relatively warm water supply from the subtropics to the subarctic region by the surface geostrophic current". Please read the lines 7555-759.

L.919: first 20 years

By the CMIP6 protocol, 150 year-long simulations are requested. ECS may change according to the length of analysis period. Describe why you made analysis for the first 20 years.

The authors agree that analysis for the first 20 years is not consistent with the CMIP6 protocol. Following the comment, we repeated the analysis using the first 150-yr-long data, and confirmed that the results were similar to the ones based on the first 20-yr-long data. The manuscript is updated based on the present

analysis. Please read Section 3.3 of the revised manuscript. Also, Figures 30, 31 and Tables 2 and 3 have been replaced by the revised ones.

L.939: are consistent with...→ “are correlated with”

In the revised manuscript, "are consistent with.." was replaced by "are correlated with". Please read the lines 1015-1019.

L.998: subarctic (tropical) region are underestimated (overestimated) in MIROC6 (MIROC5)

“subarctic (tropical) region are underestimated in MIROC6 (MIROC5)” or “subarctic region are underestimated (overestimated) in MIROC6 (MIROC5)”

Following the reviewer's comment, we have rewritten the sentence as "Signals associated with AMO in the subarctic (tropical) region are underestimated in MIROC6 (MIROC5)". Please read the lines 1073-1074.

Thank you very much.

L.1053: which is consistent with...in observations → which is in the acceptable range.

In the revised manuscript, the corresponding sentence is rewritten as "the global TOA radiation imbalance in MIROC6 is about -1.1 Wm^{-2} , which is in the acceptable range of observations". Please see the lines 1128-1130.

Technical corrections

L.185: is insufficient → delete : Deleted.

L.229: in order to to → in order to : Fixed.

L.433: , which has a shallow...: It is unnecessary as it already described in section 2.1.

The corresponding sentence was deleted in the revised manuscript.

L.481: $2.9 (3.1) \text{ Wm}^{-2}$ in MIROC5 → $2.9 (-3.1) \text{ Wm}^{-2}$ in MIROC5: We have added "-" in front of "3.1".

L.490: better simulated in MIROC5 → better simulated in MIROC6 : Fixed.

L.922: -1.5 Wm^{-2} → $-1.5 \text{ Wm}^{-2}\text{K}^{-1}$:Fixed. Thank you for your comment.

L.987: , qualitatively → delete. : Deleted.

Response to reviewers' comments on " Description and basic evaluation of simulated mean state, internal variability, and climate sensitivity in MIROC6" by Tatebe et al.

Reply to the reviewer #2

General comments

The authors describe in this manuscript version 6 of the climate model MIROC and its performance. Model description papers are useful to provide information that may be needed in future more science-oriented publications based on simulations with the respective model. Selecting the material for a model description paper is however a difficult task because it is clear that the information will always be insufficient to recreate the model from the description. I think that the authors present in general an appropriate selection of material. They only mention details of the model and its parameterizations where there are differences from the predecessor MIROC5, and they provide more or less typical evaluations of the simulated mean climatologies and variability based mostly on a pre-industrial control simulation. I appreciate that the authors describe the tuning procedure applied for arriving at the final model configuration. The presentation is in general clear and the use of language appropriate. I would recommend the editors to check in particular the use of articles, however. In general I would recommend publication of the article after introduction of minor revisions which I will list in the following.

We would like to thank the reviewer for taking the time to carefully read our manuscript, for several very valuable suggestions, and English grammatical corrections. We would like to answer the questions given by the reviewer and to describe how we have revised our manuscript point by point. Please note that our replies are written in red letters in this reply letter.

Reply to specific comments

L34 It's not clear to me what "directly resolved stratosphere" means. Could one resolve it indirectly?

In the revised manuscript, we rephrased it as "to the inclusion of the stratosphere". Please read the lines 34-35.

Introduction: I would recommend to shorten the introduction. This is a paper for specialists who know about global warming, IPCC, and the purposes of climate models. It would be good to report which specific goals the MIROC6 development had but I would cut the general introduction.

Thank you for your suggestions. Recently, the publication policy of GMD requires the short summary of a manuscript which is for non-specialists as well as specialist because simulation models are related scientific issues are of great concern of various fields of climate sciences and socio-economic sciences. Also, as stated in the WCRP conference in 2011, the decrease of the number of climate modelers is recognized as important problem to be solved for healthy progress of climate sciences and its application to mitigation and adaptation of human society to the changing climate (please see the slides 21-25; https://www.wcrp-climate.org/conference2011/orals/A4/Jakob_A4.pdf), suggesting that the importance of recruitment of students and younger scientists to climate model developments. As well as in climate centers in the world, we, Japanese climate modelling community, have faced the same problem for promoting climate modelers. In order to make some contributions to this issue, the authors wrote comprehensive description on motivations, purposes, and history of our model development to students and young researchers who may be interested in climate sciences as well as socio-economic scientist who will use our simulation data. We would be grateful if you could understand why we wrote rather long introduction in the present manuscript. On the other hand, the authors agree with your comment. So, we have revised, shortened, and reconstructed as possible as we could. Please read the introduction in the revised manuscript. Thank you very much for your suggestion again.

L42 "...has been already observed that..will drastically change": Rephrase if you want to keep this sentence. We have rephrased the sentence as "As the global warming due to increasing emissions of the anthropogenic greenhouse gases progresses, global and regional patterns of atmospheric circulations and precipitation as well as temperature are projected to be drastically changed at the end of the twentieth-first century". Please read the 1st sentence of Section 1.

L46 Not clear what "will increase" means e.g. for tropical cyclones. In size? Its number? Its strength?

We have rewritten the sentence as "occurrence frequency of extreme weather events such as heatwaves, droughts will be increased and extratropical cyclones will be stronger than in the present" in the revised manuscript. Please see the lines 46- 48.

L56 Why are only the two most recent ARs mentioned (if one wants to mention them at all)?

In revised manuscript, the citation of IPCC as (IPCC 2007; 2013) is deleted and IPCC (2007) is removed from the reference list. Please read the lines 57-59.

L64 Is there such a consensus that “sophisticating...parameterizations...are necessary” “to reduce uncertainties...in climate projections”?

In my opinion and as described in Chapter 9 of IPCC-AR5 WG1, climate model development towards resolving various processes or representing unresolved sub-grid scale phenomena based on process-oriented understanding of physical processes could contribute to more reliable climate projections. But, in the revised manuscript, we have avoided using affirmative expressions and have rewritten the corresponding sentence as "To reduce the uncertainties and errors in climate projections and predictions, utilizing observations, extracting essences of physical processes in the real climate, and investigating the response of the climate system to various external forcings based on a set of climate model simulations are necessary. In particular, a state-of-the-art climate model which can represent various processes in the Earth's climate system is a powerful tool for deeper understanding the Earth's climate system." Please read the lines 65-70.

L82 What means “K-1 model developers”

K-1 model developers (2004) is a technical report which was published by the Center for Climate System Research, the Univ. of Tokyo. The report was edited by H. Hasumi and S. Emori, but the first author is not specified. Although "K-1 model developers" doesn't look like a reference, a manuscript, which was published in GMD in 2011 (Watanabe et al. 2011, vol. 4, 845-874) cited this report in a same manner as in the present manuscript. So, "K-1 model developers" remains unchanged in the revised manuscript.

L116 As before: How may improvement of parameterizations “may result in reducing uncertainty”?

We have deleted "and may result in reducing uncertainty range of climate projections". Please see the line 116.

L126 The sentence on the “signal-to-noise ratio” is difficult to understand.

We have deleted " because the signal-to-noise ratio is smaller in the mid-latitude atmosphere than in the tropics". Please see the lines 126-128.

L139/140 I’d try to avoid terms like high-resolution” or “medium resolution” The notion of what is high, medium or low is very different among climate modelers and certainly changes over time.

I agree with the reviewer's comment. We have rephrased the sentence as "Considering that the computational costs of large ensemble predictions based on climate models with horizontal resolutions of,

for example, 50 km atmosphere and eddy-resolving ocean are still huge on recent computer systems, the use of relatively low resolution models such as MIROC6...". Please read the lines 136-140. Also, we have tried to avoid the use of terms like "medium" or "high" resolution through the text.

L151 I suggest to add a sentence on how MIROC relates to MIROC-ESM (which is referred to in Section 3.2.2). In my understanding MIROC6 is a climate model that concentrates on the physical part of the Earth system and it would be useful to mention that because many of the models used in CMIPs these days include some component cycles.

Following the comments, we have added a sentence on our earth system model and relationship between the earth system model and MIROC. Please read the lines 148-150.

Section 2: I'm missing some technical information in the model description. I guess that in particular time steps (atmosphere, ocean, coupling, exceptions for specific parameterizations) had to be changed in comparison to MIROC5.

Following the comment, we have written the timesteps used in the sub-models, coupling interval and specific parameterizations in MIROC6 and MIROC5. Please see the lines 178-181, 247-248, 287-288, and 364-366 in the revised manuscript.

Fig. 1: Do the marks indicate half levels or full levels or what else?

The marks indicate model half levels. We have revised the caption of Figure 1.

L164 Why is there a Table A1? I'd suggest to use a simple numbering for all tables.

The corresponding table is placed in Appendix. So, we numbered as Table A. But, we had typo in the previous manuscript. In the revised manuscript, "Table A1" is replaced by "Table A".

L174 I would speak of "model top", not "TOA".

"TOA" is replaced by "model top". If this replacement is adequate, other TOA in the manuscript is also replaced by "model top".

L184 Not clear what is meant with "dry air : : : is insufficient".

The sentence was not grammatically correct. We have corrected the sentence as " These biases appear to be the result of insufficient vertical mixing of the humid air in the planetary boundary layer and the dry air in

the free troposphere". Please read the lines 186-187.

L224 Remove "a": "a" is removed. Thank you for your comment.

L225 Not clear why there is reference to "future versions". Does the current model version use the described features or not?

The current model (MIROC6) use the described features. The authors just wanted to express "extended capability may be effective in future climate modeling study. To avoid confusion, the corresponding sentence has been removed in the revised manuscript.

L233 Tuning of gravity wave parameterizations. Often, the Hines parameterization is used with very simplified and globally homogeneous characteristics of the gravity waves at the launching levels? This may make it, however, difficult to tune as well the QBO and high-latitude circulations. In particular as this is a feature new to MIROC it would be useful to elaborate a bit more on the tuning of GW parameters.

We have revised the text to include some more explanations on the non-orographic gravity wave parameterization. In the revised manuscript, "Following Watanabe (2008), a present-day climatological source of non-orographic gravity waves, which is estimated using results of a gravity wave-resolving version of MIROC-AGCM (Watanabe et al., 2008), is launched at the 70 hPa level in the extratropics, while an isotropic source of non-orographic gravity waves is launched at the 650 hPa level in the tropics" has been added. Please read the lines 231-235. The corresponding references (Watanabe 2008; Watanabe et al. 2008) have been added to the reference list.

L244 Example of the SSNOWD parameterization: It is useful to mention that the new parameterization is "physically" based. But in general I would like to read what the motivation for introducing changes with respect to MIROC5, what the expectations were, and, later in the evaluation, if the expectations were met. This is done well for some of the changes (e.g. L271: "increased vertical layers have been adopted in order to .."), but less for others (e.g. the tripolar ocean grid mentioned at line 262). I would like to ask the authors to do this more consistently for the changes because it may help other modeling groups to judge if specific changes may be worthwhile to apply in other models or not.

Thank you for the comment. Regarding the SSNOWD, we have added the descriptions about the reason we implemented the scheme as "in order to improve seasonal cycle of snow cover". Please read the lines 250-252. For the ocean component, we have added the sentences "By introducing the horizontal tripolar

coordinate system, it is expected that theoretical westward propagation of the oceanic baroclinic Rossby can be represented with less numerical dispersions because of agreement of the coordinate system and the geographical coordinate system and that the horizontal resolutions in the Arctic Ocean where the Rossby radius of deformation is relatively small are higher than in the case where the bipolar warped coordinate system in MIROC5 is adopted". Please read the lines 274-279.

L309 Only extinction coefficients would not allow to compute the radiative effects of aerosols.

In the revised manuscript, the corresponding sentence has been rewritten as "Radiative forcing of stratospheric aerosols due to volcanic eruptions are computed by vertically integrating extinction coefficients for each radiation band, which are provided by Thomason et al. (2016), in the model layers above the tropopause". Please read the lines 321-323.

L322 "These" instead of "This": Done.

L328 I guess averages over these time periods are used?

Yes. In the revised manuscript, we added "averaged" in front of the periods.

L344 "land surface components are determined" sounds odd. I guess they are interpolated from some dataset. Please specify.

Following the comment, we have added the information on how to make coastline and topography of the atmospheric and land surface models as well as those in the ocean component. The corresponding sentences have been rewritten or added as "Ocean model coastline geometry and bottom bathymetry are specified based on horizontal interpolation of the land and sea-floor dataset of ETOPO5 (National Geophysical Data Center, 1993).", "the land-sea distribution and land-sea area ratios on the atmospheric and land surface model grids are determined according the coastline geometry of the ocean component", and "Surface topography in the atmospheric and land surface component are also made using the ETOPO5 dataset. Note that horizontal grid arrangement of the land surface model is exactly same as the atmospheric component". Please read the lines 349-351, 359-360, 361-365. The reference for ETOPO5 dataset has been added to the reference list.

L350 "Reproducibility" of what?

In the revised manuscript, we have rephrased as "reproducibility of climatic-mean state and internal climate

variations". Please see the lines 369-370.

L362 Here, the first tuning step for the coupled model is described. But there needs to be some procedure to specify tuning parameters in the component models, or not? Furthermore, I think it would be very useful for other modellers to be more specific about which parameters have been tuned to which effect. In some places this is described in acceptable detail, but in particular the first two sentences of this paragraph are very vague.

As pointed out by the reviewer, before coupling component models, parameter tuning was done in stand-alone component model. However, the tuning procedures were complex and depend on the component model group in our modeling community. So, it is better to describe only the parameter tuning procedure for coupled system, we think. Thank you for your suggestion.

Following the 2nd comment by the reviewer, we have described details on tuning parameters for tropical climate system as "Specifically, parameters of reference height for cumulus precipitation, efficiency of the cumulus entrainment of surrounding environment and maximum cumulus updraft velocity at the cumulus base are used to tune strength of the equatorial trade wind, climatological position and intensity of the Inter-Tropical Convergence Zone (ITCZ) and South Pacific Convergence Zone (SPCZ), and interannual variability of El-Niño/Southern Oscillation (ENSO). In particular, the parameter for the cumulus entrainment is known as a controlling factor of ENSO in MIROC5 (Watanabe et al., 2011). Summertime precipitation in the western tropical Pacific and characteristic of tropical intraseasonal oscillations are tuned by using the parameter for shallow convection describing the partitioning of turbulent kinetic energy between horizontal and vertical motions at the sub-cloud layer inversion". Please read the lines 385-393.

L376 Which "cooling effects" are meant, here? Aerosol-cloud effects as mentioned in the sentence before? Or total aerosol effects? I'd also prefer to speak of "radiative forcing" instead of cooling effects.

We tuned the total radiative forcing associated with aerosol-radiation interaction and aerosol-cloud interaction. In the revised manuscript, we have specified this and also have used "radiative forcing" instead of "cooling effects". Please read the lines 402-407.

L402 Apparently global mean SAT is not a tuning goal. It might be useful to mention this, and also why not. Additionally, I'd like to read a comment on the imbalance of about 1 Wm⁻² that seems to exist in equilibrium. It seems like there is some artificial energy source in the model. Is there any knowledge where

this originates from? Atmosphere, ocean, dynamical core, specific parameterizations? Is it known if this changes with the model state?

Following the comment, we have inserted the sentences "As above-mentioned, reproducibility of the global-mean SAT is not a tuning goal but is a typical metric which reflects results of the parameter tunings for individual processes of convections, dynamics, and radiative forcing" in the lines 416-418 in the revised manuscript. And following the 2nd comment of the reviewer, we have added the explanation on the heat energy inconsistency between the TOA radiation budget and the ocean heat uptake in association with the model imperfection. We have rephrased the last paragraph of Section 2.5 as "The trend of the global-mean ocean temperature in the later period suggests slight but continuous warming of the deep ocean. The radiation budget at the TOA is 1.1 Wm^{-2} downward on average (linear trend of $9.5 \times 10^{-3} \text{ K/100 yr}$) and the net heat input at the sea surface is 0.32 Wm^{-2} . The deep ocean warming is explained by the net heat input. Note that there is about 0.78 Wm^{-2} inconsistency between the TOA radiation budget and the ocean heat uptake. This heat energy inconsistency is due to that internal energy associated with precipitation, water vapor and river runoff is not taken account in the atmospheric and land surface component in MIROC6 and that these waters with no temperature information implicitly set their temperature to the SST when they flow or fall into the ocean. Perpetual melting of the prescribed Antarctic ice-sheet with invariant ice thickness, which is occurred due to the warm SAT bias in the Antarctic region (details will be discussed in Section 3.1.3), is also a cause of the heat energy inconsistency".

Fig. 4 and corresponding text: Names for the TOA fluxes are confusing. What is called NET is actually the total net flux, while what is called OSR is the net SW flux.

Thank you for the comment. To specify what NET, OSR, and OLR denote in the present manuscript, we have added the sentence "Hereafter, net shortwave, longwave, and the sum of them are denoted as OSR, OLR and NET, respectively, for simplicity" to the text and the caption of Figure 4. Please see the lines 473-474.

L426 The sentence on the consideration of "global-mean values" for RMSE calculations is difficult to understand. Maybe provide a formula or clearer description on how the RMSE are calculated? Is that true for all RMSE in this manuscript? It would be good to mention in every caption of Figures where RMSE are presented how these values are calculated, i.e. in particular if a global or some other mean have been subtracted before calculation of the error. The OLR in Fig. 4 looks particularly confusing without such information because while the RMSE is smaller in MIROC6 than in MIROC5 one would guess otherwise

from the color shading because of the dominance of red in the case of MIROC6.

In the present manuscript, all of RMSE were calculated without global-mean values. We have described this clearly in the revised manuscript as "In the present manuscript, RMSE is computed without model and observed global-mean quantities unless otherwise noted". Please read the lines 469-470 and the caption of Fig. 4. The above is not described in every figure where RMSE are presented in order to avoid lengthy caption, and a formula for RMSE calculation is not added because we use the most conventional formula. Thank you for your suggestion.

L476 I accept that for many climate variables it may not be essential if the evaluation is done for a pre-industrial or present-day simulation. But for some it is crucial. The energy balance is such a case, because the total net TOA flux should be zero in equilibrium. One can't say that the imbalance in the models is consistent with some observed imbalance, because the latter is related to the system not being in balance currently. It is also necessary to provide a reference for the observed value.

Following the comment, we have added the sentence "However, the observed value is estimated in the present-day condition. Ideally, the model value in the preindustrial condition should be 0 Wm^{-2} and is in the marginally acceptable range.". The reference of the observed values has been added as "(CERES; Loeb et al, 2009)". Please read the lines 521-522, and 520. Also, we have described possible cause of the non-zero TOA flux in our climate model. Please read our reply to the reviewer's comment to L. 402.

Fig. 4 and others. Parts of this and other figures are very blurred. This should be improved for the final publication.

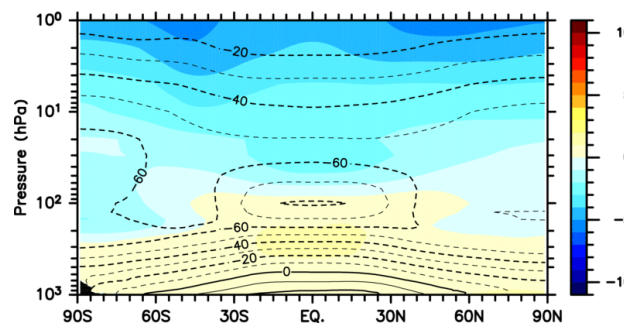
Although the figures in the automatically-generated PDF manuscript look blurred, all the figures in the present manuscript was originally prepared in the EPS format. In final publication, higher resolution figures based on the EPS figure files can be used.

L512 The region of the western tropical Pacific is singled out as a region of improvement in MIROC6. It should be mentioned that it seems that in other regions there is a clear worsening.

Following the comment, we have added the sentences "On the other hand, model representation of the precipitation in MIROC6 is not necessarily alleviated other than the western tropical Pacific. For example, the overestimate of wintertime precipitation over the Indian Ocean and the mid-latitude North Pacific is worse in MIROC6 than in MIROC5" in the lines 561-564.

L518 For the discussion of the upper stratospheric warm bias it also matters that present-day and pre-industrial are compared due to the known stratospheric cooling with increased GHGs and reduced ozone.

As shown in the figure just below and as suggested by the reviewer, the zonal-mean climatological temperature in 1980-2009 of a historical simulation is colder (warmer) than in the preindustrial simulation. Thus, the temperature bias shown in Fig. 7c can be smaller when the modeled temperature in the present-day simulation is compared with observations. In the revised manuscript, we have added the sentences "Note that the zonal-mean temperature bias in Fig. 7c is smaller when the climatological-mean temperature from 1980 to 2009 in a historical simulation are evaluated against observations because of the known stratospheric cooling with increased greenhouse gases and reduced O₃ concentrations." in the lines 579 -582.



Zonal-mean climatological temperature difference between a historical simulation (1980-2009) and the preindustrial simulation (shading). Contours denote values in a historical simulation.

L519: Again, I would prefer to speak of model top or lid and not of TOA.

In the revised manuscript, "model top" is used instead of TOA.

L522 It would be good to say that this is the stream function of zonal mean meridional winds and not of residual winds, I guess.

Following the comment, we have specified. Please read the line 571. Thank you for the comment.

L524 Please rephrase this sentence.

In the revised manuscript, we have rephrased the sentence as "It is considered that an increased upward advection of the temperature minimum around the tropopause in 30°S–30°N may lead to reduction of warm temperature bias in the stratosphere which is significant in MIROC5." Please read the lines 572-574.

L530 I guess the absorption of LW radiation plays a minor role compared to SW radiation.

We just had a wrong description. In the revised manuscript, "longwave" has been replaced by "shortwave". Please see the line 579. Thank you for your suggestion.

L561 "extend", not "extends"

Done.

L561 Not clear what "more active troposphere-stratosphere" interactions are supposed to mean (radiative, wave coupling, trace gas exchange?) and why the stream functions would indicate that.

As shown in Fig. 25 and its explanation described in Section 3.2.2, the stratosphere-troposphere interactions associated with the Northern Annular Mode is better simulated in MIROC6 than in MIROC5. Thus, we have specified and rephrased as " more active troposphere-stratosphere interactions associated with wave-coupling exist in MIROC6". Please read the lines 614-615.

L566 There is no "remarkable improvement" in May. Furthermore, I suggest to avoid subjective terms like "remarkable". Please check all the text.

In the revised manuscript, the corresponding sentence has been changed to "it can be seen that the former parameterization brings about significant improvement in the Northern Hemisphere snow cover fractions from the early to the late winter" and the sentences " Note that no clear improvement is found in May" has been added. Please see the lines 619-62 and 625. Following the comments, we have deleted or rephrased "remarkable" through the text. Thank you for your suggestion.

L586 "into which cold and dense water forms" Please rephrase.

The sentences have been rephrased and the associated sentences have been also rewritten for clear descriptions. Please read the lines 638-641.

L609 This is no sentence.

"and" at the last of the sentence has been removed in the revised manuscript.

L612 The caption of Fig. 15 says only "temperature" while here you speak of "potential temperature".

"potential" have been added in the caption of Fig. 15. Thank you for your comment.

L614 Please rephrase “is risen”: "risen" is replaced by "upwelled". Please see the line 671..

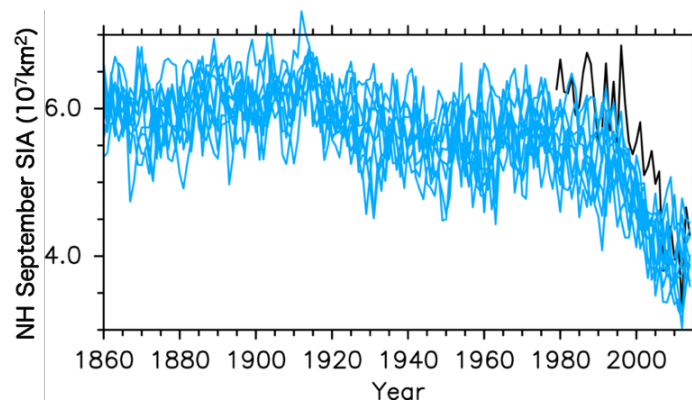
L623 “Better representation of cloud physics” would be “required” for what?

We have specified for "what" and have revised the corresponding sentences as " Better parameterizing deep cumulus convection in the models could be required for better representation of the equatorial trade winds and thus oceanic states." Please read the lines 682-684 and the lines just before.

L638 Remove “to”. : Done.

L648 It would be useful to check if the historical simulation shows more realistic numbers in the comparison to present-day sea ice.

As shown in the figure just below, the model does not capture the realistic number and amplitude of drastic decrease of the sea-ice area. However, the September sea-ice area in 1980–2009 of historical simulations in MIROC6 is smaller than the observations, indicating that decreasing trend of the sea-ice area in the twenties century in MIROC6 is slightly larger than in observations. In the revised manuscript, the corresponding descriptions have been added. Please read the lines 711- 715.



Time series of the Northern Hemisphere sea-ice area in historical simulations of MIROC6 (blue) and observations (black). Because data reliability before 1979 is not high in observations, the observed values are plotted only after 1979. Note that each blue line indicates the result from each ensemble historical simulation.

L649 Is there any idea why Antarctic sea ice is strongly underestimated?

The possible reason is described in the 2nd paragraph of Section 3.1.3 together with another prominent biases and their causes.

L655 Please specify what “sea level height” is presented in Fig. 18 and to which data it is compared in the text.

We have rewritten the corresponding sentence and the caption of Fig. 18 as "sea level height relative to the geoid" (L. 720). Also, a figure of observed sea level height has been added to the revised manuscript as Fig. 18a.

L676 “land surface variables” Actually I identify only one: snow cover.

"land surface variables" has been replaced by "the snow cover fractions in the Northern Hemisphere". Please see the line 744.

L678 Again, global mean SST and SAT are variables for which the comparison of preindustrial simulations and present-day observations is misleading.

Following the comment, we have added notes as " However, since the observed (model) value is estimated in the present-day (preindustrial) condition, the model global-mean SATs and SSTs are overestimated". Please read the lines 749-750.

L695 A prominent feature of SST and SAT biases is the strong warm bias close to Antarctica. This should be mentioned when discussing these variables.

I agree with the reviewer's comment. For example, you can find descriptions on the warm biases in the last sentence of the 3rd paragraph of Section 4 (Summary and Discussions) as "In the Southern Hemisphere, however, the underestimate of mid-level clouds and the corresponding warm SAT bias, the underestimate of sea-ice area, and the overestimate of incoming shortwave radiation in the Southern Ocean, all of which are attributed to errors in cloud radiative and planetary boundary layer processes (e.g., Bodas-Salcedo et al., 2012; Williams et al., 2013), remains the same as in MIROC5".

L718 It might be good to also mention the apparently missing features WIG and possibly EIG in the models. And what about anti-symmetric waves?

Thank you for your suggestion. In revised manuscript, we have mentioned the missing features of WIG and EIG waves. Also, we have added the figures for the zonal wavenumber–frequency power spectra of antisymmetric waves to Fig. 20 and descriptions on the antisymmetric waves. Please read the 1st paragraph of Section 3.2.1.

L727 Remove “and” : **Done.**

L743 Remove “MIROC6” : **Done.**

L760 “become” Rephrase.

In the revised manuscript, "become closer to observations" has been changed to "is consistent with observations". Please see the line 836.

L778 MIROC-ESM should be introduced in the beginning (or here)

Following the comments, we have added a sentence on our earth system model and relationship between the earth system model and MIROC. Please read the last sentence of Section 1.

L778 “whic”: "whic" is replaced by "which" in the revised manuscript. Thank you very much.

L787 Remove “that” : **Done.**

L787 What means “correlations...are not clear”? Insignificant? Small?

In the revised manuscript, "not clear" has been rephrased as "insignificant". Please see the line 864.

L793 SSWs are only a typical feature of the NH stratosphere.

In the revised manuscript, "a typical intraseasonal variability in the mid-latitude stratosphere" has been rephrased as "a typical intraseasonal variability of the mid-latitude stratosphere in the Northern Hemisphere". Please see the lines 869-870.

Fig. 24 and its discussion. I'd find it helpful to add Figures for January to make clear also the deficiencies of the model.

Following the comment, we have added January maps to Figure 14(d-f), and the figure caption and the text have been rewritten consistently with the new Fig. 14. Please read the paragraph starting from the line 869.

L807 One can't evaluate the polar night jet in Fig. 7e because it shows annual means. It might actually be an option to add some seasonal wind fields in Fig. 7. The paper has many figures anyhow, so I wouldn't mind adding a few more. Additionally there is a problem of chicken and egg with the wave-mean flow

interaction mentioned here.

Following the comment, we have added January maps to Figure 14 as written in the reply to the comment just above. And we have rephrased the corresponding sentence as " It is conjectured that the less frequent SSW in December–January could be attributed to less frequent stationary wave breakings due to overestimate of climatological zonal wind speed of the polar night jet in MIROC6 (Figs. 24d and e)". Please read the lines 884-887.

L846 Rephrase “existence depths”.

In the revised manuscript, we have replaced "However, the existence depths of the subsurface signals are larger in MIROC6 than in observations" with "However, the subsurface signals in MIROC6 reside deeper than in observations." Please read the line 924.

L885 “SLP anomalies are larger and better represented in MIROC6” The maximum is deeper, but otherwise I find it hard to judge which of the two models is better.

In the revised manuscript, the corresponding sentence is rephrased as "it can be seen that the amplitudes of the SLP anomalies in MIROC6 are larger than in MIROC5, which is closer to the observation". Please read the lines 962-963.

L889 I'd avoid words like “excessively” which are subjective statements.: "~~excessively~~" is deleted.

L918 In IPCC AR5 and also the paper by Andrews et al. (2012) which is cited, here, climate sensitivity and forcing are calculated from 150 years of the 4xCO2 simulation, not 20 years. I would suggest to follow this 150-year standard to ensure comparability. Some models show clear non-linearities during this period. It seems like the effect is relatively small in MIROC5, but this would need to be confirmed for MIROC6.

The authors agree that analysis for the first 20 years is not consistent with the CMIP6 protocol. Following the comment, we repeated the analysis using the first 150-yr-long data, and confirmed that the results were similar to the ones based on the first 20-yr-long data. The manuscript is updated based on the present analysis. Please read Section 3.3 of the revised manuscript. Also, Figures 30, 31 and Tables 2 and 3 have been replaced by the revised ones.

Tables 2 and 3: It would be convenient for the reader to combine the tables.

We consider the table may be more complex and the caption would be very long if the Tatebe 2 & 3 are

combined. So, Table 2 & 3 are not combined in the revised manuscript. Thank you for your comment.

L966, 979 Again, please avoid “remarkably”.: "remarkably" has been deleted.

L999 Why would ECS quantify uncertainty?

The sentence was not appropriate because ECS quantifies climate change itself, not uncertainty of climate change. We therefore rephrased the sentence "As a metric for climate change induced by atmospheric CO2 increase, ECS is also estimated". Please see the line 1075.

L1028 It's true that the hiatus is sometimes associated with the IPO, but there are plenty of other attempts to explain it and even arguments that the real reason maybe unidentifiable. So I'd suggest to not only mention the IPO.

We have added other candidate for the hiatus and we have rewritten the corresponding sentences as "The observed hiatus is considered to occur in association with a negative IPO phase as internal climate variations (e.g., Meehl et al., 2011; Watanabe et al., 2014). As external drivers of the hiatus, the weakening of solar activity and increase in stratospheric aerosols are given as possible candidates, for example (e.g., Solomon et al., 2010; Kaufmann et al., 2011)". Please read the lines 1103-1107 in the revised manuscript.

L1031 I don't understand this sentence. I agree that the simulated hiatus could be spurious, but the argument of the ensemble mean wouldn't support this.

After submitting the manuscript, we increased the number of ensemble historical simulations by MIROC6 up to 30 members. When we redrew the time series of the global-mean SAT anomalies using 30 members, the hiatus-like temperature change in the early 21th century is vanished and continuous temperature rise is appeared. We have replaced Fig. 32 by the new one with 30 ensemble members and we have rewritten the descriptions on the model hiatus as " The so-called recent hiatus of the global warming (Easterling and Wehner, 2009) in the first decade of the twenty-first century is not simulated in both of MIROC6 and MIROC5" and as " Failure of simulating the hiatus in the models could be attributed to uncertainties in the historical forcing datasets or cancellation of internal climate variations of the IPO by ensemble-mean manipulation of the individual historical simulations". Please read the lines 1101-1103 and 1107-1109 in the revised manuscript.

L1055 Should a new paragraph start here?

Because we would like to give an example of error compensation in oceanic processes, we did not start a new paragraph here. In the revised manuscript, we have rewritten the sentence describing the oceanic error compensation and have not started a new paragraph. Please read the line 1130-1135.

L1068 I have no idea why the final sentence suddenly makes a statement concerning component cycles which were not at all mentioned anywhere else in the text.

In the revised manuscript, the corresponding sentence has been deleted.

L1074 I don't know what the policy of GMD is concerning the availability of primary data (which I think should be the code of the model and all input data needed to redo the experiments), but I find it problematic that the code is only available under the condition of "collaborative research". As mentioned in my initial statement, a model description is necessarily incomplete. It can only be completed by the model code.

Following the reviewer's suggestions and that the simulation data used in the present manuscript have been distributed from December 2018 and the data are freely accessible, we have rewritten the code and data availability part as "Please contact the corresponding author if readers may want to validate the model configurations of MIROC6 and MIROC5 and to conduct replication experiments. The source codes and required input data will be provided by the modeling community where the author belongs. The model output from the CMIP6/CMIP5 pre-industrial control and historical simulations used in the present manuscript are distributed through the Earth System Grid Federation and are freely accessible. Details on ESGF are given on the CMIP Panel website (<https://www.wcrp-climate.org/wgcm-cmip>)."

1 Description and basic evaluation of simulated mean state, internal variability, and climate sensitivity
2 in MIROC6

3

4 Hiroaki Tatebe¹, Tomoo Ogura², Tomoko Nitta³, Yoshiki Komuro¹, Koji Ogochi¹, Toshihiko
5 Takemura⁴, Kengo Sudo⁵, Miho Sekiguchi⁶, Manabu Abe¹, Fuyuki Saito¹, Minoru Chikira³, Shingo
6 Watanabe¹, Masato Mori⁷, Nagio Hirota², Yoshio Kawatani¹, Takashi Mochizuki¹, Kei Yoshimura³,
7 Kumiko Takata², Ryouta O'ishi³, Dai Yamazaki⁸, Tatsuo Suzuki¹, Masao Kurogi¹, Takahito Kataoka¹,
8 Masahiro Watanabe³, and Masahide Kimoto³

9

10 1: Japan Agency for Marine-Earth Science and Technology, Yokohama, Japan

11 2: National Institute for Environmental Studies, Tsukuba, Japan

12 3: Atmosphere and Ocean Research Institute, University of Tokyo, Kashiwa, Japan

13 4: Research Institute for Applied Mechanics, Kyushu University, Kasuga, Japan

14 5: Graduate School of Environmental Studies, Nagoya University, Nagoya, Japan

15 6: Tokyo University of Marine Science and Technology, Tokyo, Japan

16 7: Research Center for Advanced Science and Technology, University of Tokyo, Tokyo, Japan

17 8: Institute of Industrial Sciences, University of Tokyo, Tokyo, Japan

18

19 Corresponding author: Hiroaki Tatebe ([E-mail: tatebe@jamstec.go.jp](mailto:tatebe@jamstec.go.jp))

20 [Research Center for Environmental Modeling and Application](#), ~~Project team for advanced climate~~

21 ~~modeling~~, Japan Agency for Marine-Earth Science and Technology

22 3173-25 Showa-machi, Kanazawa-ku, Yokohama, Kanagawa 236-0001, Japan

24 **Abstract**

25 The sixth version of the Model for Interdisciplinary Research on Climate (MIROC), called
26 MIROC6, was cooperatively developed by a Japanese modeling community. In the present manuscript,
27 simulated mean climate, internal climate variability, and climate sensitivity in MIROC6 are evaluated
28 and briefly summarized in comparison with the previous version of our climate model (MIROC5) and
29 observations. The results show that overall reproducibility of mean climate and internal climate
30 variability in MIROC6 is better than that in MIROC5. The tropical climate systems (e.g., summertime
31 precipitation in the western Pacific and the eastward propagating Madden-Julian Oscillation) and the
32 mid-latitude atmospheric circulations (e.g., the westerlies, the polar night jet, and troposphere-
33 stratosphere interactions) are significantly improved in MIROC6. These improvements can be
34 attributed to the newly implemented parameterization for shallow convective processes and to the
35 inclusion of the directly-resolved stratosphere. While there are significant differences in climates and
36 variabilities between the two models, the effective climate sensitivity of 2.5 K remains the same
37 because the differences in radiative forcing and climate feedback tend to offset each other. With an
38 aim towards contributing to the sixth phase of the Coupled Model Intercomparison Project, designated
39 simulations tackling a wide range of climate science issues, as well as seasonal-to-decadal climate
40 predictions and future climate projections, are currently ongoing using MIROC6.

41

42 1 Introduction

43 As the global warming due to increasing emissions of the anthropogenic greenhouse gases
44 progresses, ~~it is anticipated, or has been already observed that~~ global and regional patterns of ~~climate~~
45 ~~mean-atmospheric temperature, circulations,~~ and precipitation as well as temperature are projected to
46 be will drastically changed until the end of the twentieth-first century (e.g., Neelin et al., 2006; Zhang
47 et al., 2007; Bengtsson et al., 2009; Andrews et al., 2010; Scaife et al., 2012) and that occurrence
48 frequency of
49 extreme weather events such as heatwaves, droughts will be increased, and extratropical cyclones will
50 be stronger than in the present increase (e.g., Mizuta et al., 2012; Sillmann et al., 2013; Zappa et al.,
51 2013). Corresponding to the atmospheric changes under the global warming, the sea levels will rise
52 due to the thermal expansion of sea water and ice-sheet melting in the polar continental regions (e.g.,
53 Church and White, 2011; Bamber and Aspinall, 2013). Additionally, ocean acidification due to
54 absorption of atmospheric carbon dioxide (CO₂) and changes in carbon-nitrogen cycles are expected
55 to lead to the loss of Earth biodiversity (e.g., Riebesell et al., 2009; Rockström, et al. 2009; Taucher
56 and Oeschler, 2011; Watanabe et al., 2017). Societal demands for information on the global and
57 regional climate changes have increased significantly worldwide in order to meet information
58 requirements for political decision making related to mitigation and adaptation to the global warming.

59 The Intergovernmental Panel on Climate Change (IPCC) has continuously published the
60 assessment reports (ARs) in which a comprehensive view of past, present, and future climate changes
61 on various timescales, including the centennial global warming, are synthesized ~~(IPCC 2007; 2013).~~
62 Together with observations, climate models have been contributing to the IPCC-ARs through a broad
63 range of numerical simulations, especially, future climate projections after the twenty-first century.
64 However, there are many uncertainties in future climate projections and the range of uncertainties has
65 not been narrowed by an update of the IPCC reports. The uncertainties are arising from imperfections

66 of climate models in representing micro- to global-scale physical and dynamical processes in sub-
67 systems of the Earth's climate and their interactions. To reduce the uncertainties and errors in climate
68 projections and predictions, utilizing observations, extracting essences of physical processes in the
69 real climate, and investigating the response of the climate system to various external forcings based
70 on a set of climate model simulations ~~sophisticating physical parameterizations of climate models,~~
71 ~~which represent unresolved sub-grid scale phenomena,~~ are necessary. In particular, a state-of-the-art
72 climate model which can represent various processes in the Earth's climate system is a powerful tool
73 for deeper understanding the Earth's climate system.

74 One of Japanese climate models, which is called MIROC (Model for Interdisciplinary
75 Research on Climate), has been cooperatively developed at the Center for Climate System Research
76 (CCSR; the precursor of a part of the Atmosphere and Ocean Research Institute), the University of
77 Tokyo, the Japan Agency for Marine-Earth Science and Technology (JAMSTEC), and the National
78 Institute for Environmental Studies (NIES). Utilizing MIROC, our Japanese climate modelling group
79 has been tackling a wide range of climate science issues and seasonal-to-decadal climate predictions
80 and future climate projections. At the same time, by providing simulation data, we have been
81 participating to the third and fifth phases of the Coupled Model Intercomparison Projects (CMIP3 and
82 CMIP5; Meehl et al. 2007; Taylor et al. 2011) which have been contributing to the IPCC-ARs by
83 synthesizing multi-model ensemble datasets.

84 In the years up to the IPCC fifth assessment report (IPCC-AR5; IPCC 2013), we have
85 developed four versions of MIROC, three of which (MIROC3m, MIROC3h, and MIROC4h) have
86 almost the same dynamical and physical packages, but different resolutions. MIROC3m (K-1 model
87 developers, 2004) is composed of a medium-resolution model consisting of T42L20 atmosphere and
88 1.4°L43 ocean ~~components~~. Resolutions of MIROC3h (K-1 model developers, 2004) are higher than
89 MIROC3m and are T106L56 for the atmosphere and eddy-permitting for the ocean ($1/4^\circ \times 1/6^\circ$). Only

90 the horizontal resolution of the atmosphere of MIROC3h is changed to T213 in MIROC4h (Sakamoto
91 et al., 2012). MIROC5 is ~~a medium-resolution model~~ composed ~~nsisting~~ of T85L40 atmosphere and
92 1.4°L50 ocean ~~components~~, but with considerably updated physical and dynamical packages
93 (Watanabe et al., 2010). These models have been used to study various scientific issues such as the
94 detection of natural influences on climate changes (e.g., Nozawa et al., 2005; Mori et al., 2014;
95 Watanabe et al., 2014), uncertainty quantification of climate sensitivity (e.g., Shiogama et al., 2012;
96 Kamae et al., 2016), future projections of regional sea-level rises (e.g., Suzuki et al., 2005; Suzuki and
97 Ishii, 2011), and mechanism studies on tropical decadal variability (e.g., Tatebe et al., 2013; Mochizuki
98 et al., 2016).

99 During the last decade, our efforts have been preferentially devoted to providing science-
100 oriented risk information on climate changes that is beneficial to international, domestic, and
101 municipal communities. For example, so-called event attribution (EA) studies with large ensemble
102 simulations initiated from slightly different conditions have been conducted in order to statistically
103 evaluate influences of the global warming on the occurrence frequencies of observed individual
104 extremes (e.g., Imada et al., 2013; Watanabe et al., 2013; Shiogama et al., 2014). Seasonal-to-decadal
105 climate predictions are also of significant concerns. By initializing prognostic variables in our climate
106 models using observation-based data (Tatebe et al., 2012), significant prediction skills in several
107 specific phenomena, such as the El Niño/Southern Oscillation (ENSO) and the Arctic sea-ice extent
108 on seasonal timescales, the Pacific Decadal Oscillations (PDO; Mantua et al., 1997), the Atlantic
109 Multi-decadal Oscillations (AMO; Schlesinger and Ramankutty, 2004), and the tropical trans-basin
110 interactions between the Pacific and the Atlantic on decadal timescales, are detected (e.g., Mochizuki
111 et al., 2010; Chikamoto et al. 2015; Imada et al., 2015; Ono et al., 2018).

112 However, while the applicability of MIROC has been extended to a wide range of climate
113 science issues, almost all of the above-mentioned approaches were based on our medium-resolution

114 versions of MIROC (MIROC3m and MIROC5), and it is well known that higher-resolution models
115 are capable of better representing the model mean climate and internal climate variability, such as
116 regional extremes, orographic winds, and oceanic western boundary currents/eddies than lower-
117 resolution models (e.g., Shaffrey et al., 2009; Roberts et al., 2009; Sakamoto et al., 2012). Nevertheless,
118 ~~even in high-resolution models,~~ there remain persistent biases associated with, for example, cloud-
119 aerosol-radiative feedback and turbulent vertical mixing of the air in the planetary boundary layer (e.g.,
120 Bony and Dufresne, 2005; Bodas-Salcedo et al., 2012; Williams et al., 2013), which are tightly linked
121 with dominant uncertainties in climate projections. Therefore, improvement of physical
122 parameterizations for sub-grid scale processes is essential for better representing observed climatic-
123 mean states and internal climate variability ~~and may result in reducing uncertainty range of climate~~
124 ~~projections.~~ As well as physical parameterizations, enhanced vertical resolution in both of atmosphere
125 and ocean components, along with a highly accurate tracer advection scheme, have been suggested to
126 have impacts on reproducibility of model-climate and internal climate variations (e.g., Tatebe and
127 Hasumi, 2010; Ineson and Scaife, 2009; Scaife et al., 2012).

128 Recently, we have developed the sixth version of MIROC, called MIROC6. This newly
129 developed climate model has updated physical parameterizations in all sub-modules. In order to
130 suppress an increase of computational cost, the horizontal resolutions of MIROC6 are not significantly
131 higher than those of MIROC5. The reason is that a larger number of ensemble members are required
132 to realize significant seasonal predictions of, for example, the wintertime Eurasian climate (Murphy
133 et al., 1990; Scaife et al., 2014) ~~because the signal to noise ratio is smaller in the mid-latitude~~
134 ~~atmosphere than in the tropics.~~ Indeed, climate predictions by the older versions of MIROC having at
135 most 10 ensemble members are skillful only in the tropical climate ~~and~~ the mid-latitude ocean not
136 in the mid-latitude atmosphere. ~~In addition, when evaluating the contributions of internal variations,~~
137 ~~which will be done in preparation for use in the global stocktake, namely, a five-yearly review of each~~

138 ~~countries' provisions to climate changes, established by the Paris Agreement in 2015, I~~ large ensemble
139 predictions ~~are~~ may also be required in decadal-scale predictions in order to evaluate the human
140 influences on the near-term climate changes. ~~—~~ The model top ~~of the atmosphere (TOA)~~ in MIROC6
141 is placed at the 0.004 hPa pressure level which is higher than that of MIROC5 (3 hPa), and the
142 stratospheric vertical resolution has been enhanced in comparison to MIROC5 in order to represent
143 the stratospheric circulations. Overall, the reproducibility of the mean climate and internal variability
144 of MIROC6 is better than those of MIROC5, but the model's computational cost is about 3.6 times as
145 large as that of MIROC5. Considering that the computational costs of large ensemble predictions based
146 on climate high-resolution models with horizontal resolutions of, for example, 50 km atmosphere and
147 eddy-resolving ocean ~~ing~~ are still huge on recent computer systems, the use of relatively low ~~medium-~~
148 resolution models such as MIROC6 with further elaborated parameterizations can still be actively
149 useful in science-oriented climate studies and climate predictions produced for societal needs.

150 The rest of the present paper is organized as follows. We describe the model configuration,
151 tuning and spin-up procedures in Section 2, while simulated mean-state, internal variability, and
152 climate sensitivity are evaluated in Section 3. Simulation performance of MIROC6 and remaining
153 issues are briefly summarized and discussed in Section 4. Currently, MIROC6 is being used for various
154 simulations designed by the sixth phase of the CMIP (CMIP6; Eyring et al., 2016), which aims to
155 strengthen the scientific basis of the IPCC-AR6. ~~In addition, I~~ large ensemble simulations and climate
156 predictions using MIROC6 are also on-going ~~will be conducted~~ for science-oriented studies in our
157 modeling group, and for societal benefits. In addition, the latest earth system model version of MIROC
158 with the global carbon cycle, whose physical core will be MIROC6, has been developed for the CMIP6
159 towards further wide range issues of climate and societal applications (Hajima et al., in preparation).

160

161

162 **2 Model configurations and spinup procedures**

163 MIROC6 is composed of three sub-models: atmosphere, land, and sea ice-ocean. The
164 atmospheric model is based on the CCSR-NIES atmospheric general circulation model (AGCM;
165 Numaguti et al., 1997). The land surface model is based on Minimal Advanced Treatments of Surface
166 Interaction and Runoff (MATSIRO; Takata et al. 2003), which includes a river routing model of Oki
167 and Sud (2003) based on a kinematic wave flow equation (Ngo-Duc et al., 2007) and a lake module
168 where one-dimensional thermal diffusion and mass conservation are considered. The sea ice-ocean
169 model is based on the CCSR Ocean Component model (COCO; Hasumi, 2006). A coupler system
170 calculates heat and freshwater fluxes between the sub-models in order to ensure that all fluxes are
171 conserved within machine precision and then exchanges the fluxes among the sub-models (Suzuki et
172 al., 2009). No flux adjustments are used in MIROC6. In the remaining part of this section, we will
173 provide details of MIROC6 configurations, focusing on updates from MIROC5. Readers may also
174 refer to Table A+ [in Appendix](#) where the updates are briefly summarized.

175

176 **2.1 Atmospheric component**

177 MIROC6 employs a spectral dynamical core in its AGCM component as in MIROC5. The
178 horizontal resolution is a T85 spectral truncation that is an approximately 1.4° grid interval for both
179 latitude and longitude. The vertical grid coordinate is a hybrid σ - p coordinate (Arakawa and Konor,
180 1996). The [model top](#)^{TOA} is placed at 0.004 hPa, and there are 81 vertical levels (Fig. 1a). The vertical
181 grid arrangement in MIROC6 is considerably enhanced in comparison to that in MIROC5 (40 levels;
182 3 hPa) in order that the stratospheric circulations can be represented. ~~—~~ A sponge layer that damps
183 wave motions is set at the model top level by increasing Rayleigh friction to prevent extra wave
184 reflection near the [model top](#)^{TOA}. The atmospheric component of MIROC6 has standard physical
185 parameterizations for cumulus convections, radiation transfer, cloud microphysics, turbulence, and

186 gravity wave drag. It also has an aerosol module. These are basically the same as those used in
187 MIROC5, but several updates have been made, as will be detailed below. The parameterizations for
188 cloud micro-physics and planetary boundary layer processes in MIROC6 are the same as in MIROC5.
189 The standard timestep for MIROC6 is 6 minutes which is shorter than that of MIROC5 (12 minutes)
190 because stratospheric winds whose speed sometimes exceeds 150 ms^{-1} must be resolved in time
191 integration. The timestep for radiative transfer models is set separately and is 3 hours in both of
192 MIROC6 and MIROC5.

193 A cumulus parameterization proposed by Chikira and Sugiyama (2010), which uses an
194 entrainment formulation of Gregory (2001), is adopted in MIROC6 as in MIROC5. This
195 parameterization deals with multiple cloud types including shallow cumulus and deep convective
196 clouds. MIROC5, however, tends to overestimate the low-level cloud amounts over the low-latitude
197 oceans and has a dry bias in the free troposphere. These biases appear to be the result of insufficient
198 vertical mixing of the humid air in the planetary boundary layer and the dry air in the free troposphere
199 ~~is insufficient~~. To alleviate these biases, an additional parameterization for shallow cumulus
200 convection based on Park and Bretherton (2009) is implemented in MIROC6. Shallow convections
201 associated with the atmospheric instability are calculated by the Chikira and Sugiyama (2010) scheme,
202 and those associated with turbulence in the planetary boundary layer are represented by the Park and
203 Bretherton (2009) scheme. The shallow convective parameterization is a mass flux scheme based on
204 a buoyancy-sorting, entrainment-detrainment single plume model that calculates the vertical transport
205 of liquid water, potential temperature, total water mixing ratio, and horizontal winds in the lower
206 troposphere. The cloud-base mass flux is controlled by turbulent kinetic energy within the sub-cloud
207 layer and convective inhibition. The cloud-base height for shallow cumulus is set between the lifting
208 condensation level and the boundary layer top, which is diagnosed based on the vertical profile of
209 relative humidity. When implementing the parameterization in MIROC6, the following conditions for

210 triggering the shallow convection are specified: 1) The estimated inversion strength (Wood and
211 Bretherton, 2006) is smaller than a tuning parameter, and 2) the convection depth diagnosed by a
212 separate cumulus convection scheme (Chikira and Sugiyama, 2010) is smaller than a tuning parameter.

213 The Spectral Radiation-Transport Model for Aerosol Species (SPRINTARS; Takemura et
214 al., 2000, 2005, 2009) is used as an aerosol module for MIROC6 to predict the mass mixing ratios of
215 the main tropospheric aerosols which are black carbon, organic matter, sulfate, soil dust, and sea salt,
216 and the precursor gases of sulfate (sulfur dioxide, SO₂, and dimethylsulfide). By coupling the radiation
217 and cloud-precipitation schemes in MIROC, SPRINTARS calculates not only the aerosol transport
218 processes of emission, advection, diffusion, sulfur chemistry, wet deposition, dry deposition, and
219 gravitational settling, but also the aerosol-radiation and aerosol-cloud interactions. There are two
220 primary updates in SPRINTARS of MIROC6 that were not included in MIROC5. One is the treatment
221 of precursor gases of organic matters as prognostic variables. In the previous version, the conversion
222 rates from the precursor gases (e.g., terpene and isoprene) to organic matters are prescribed (Takemura
223 et al., 2000), while an explicit simplified scheme for secondary organic matters was introduced from
224 a global chemical climate model (Sudo et al., 2002). The other is a treatment of oceanic primary and
225 secondary organic matters. Emissions of primary organic matters are calculated with wind at a 10-m
226 height, the particle diameter of sea salt aerosols, and chlorophyll-*a* concentration at the ocean surface
227 (Gantt et al., 2011). The oceanic isoprene and monoterpene, which are precursor gases of organic
228 matters, are emitted depending on the photosynthetically active radiation, diffuse attenuation
229 coefficient at 490 nm, and the ocean surface chlorophyll-*a* concentration (Gantt et al., 2009).

230 The radiative transfer in MIROC6 is calculated by an updated version of the *k*-distribution
231 scheme used in MIROC5 (Sekiguchi and Nakajima 2008). The single scattering parameters have been
232 calculated and tabulated in advance, and liquid, ice, and five aerosol species can be treated in this
233 updated version. Given the significant effect of crystal habit on a particle's optical characteristics

234 (Baran, 2012), the assumption of ice particles habit has been updated from our previous simple
235 assumption of sphere used in MIROC5 to a hexagonal solid column (Yang et al., 2013) in MIROC6.
236 The upper limits of the mode radius of cloud particles have been extended from 32 μm to 0.2 mm for
237 liquids and from 80 μm to 0.5 mm for ice. Therefore, the scheme can now handle the large-sized water
238 particles (e.g., drizzle and rain) that have been shown to have a significant radiative impacts (Waliser
239 et al., 2011). ~~This extended capability is expected to be effective in our future model versions,~~
240 ~~especially in situations where mass mixing ratios of the large-sized particles are predicted or diagnosed~~
241 ~~in the cloud microphysics scheme.~~

242 Following Hines (1997) and Watanabe et al. (2011), a non-orographic gravity wave
243 parameterization is newly implemented into MIROC6 in order to ~~to~~ represent realistic large-scale
244 circulations and thermal structures in the stratosphere and mesosphere. Following Watanabe (2008), a
245 present-day climatological source of non-orographic gravity waves, which is estimated using results
246 of a gravity wave-resolving version of MIROC-AGCM (Watanabe et al., 2008), is launched at the 70
247 hPa level in the extratropics, while an isotropic source of non-orographic gravity waves is launched at
248 the 650 hPa level in the tropics. Together with this parameterization, an orographic gravity wave
249 parameterization of McFarlane (1987) is also adopted as in MIROC5. In both the orographic and non-
250 orographic gravity wave parametrizations, wave source parameters at launch levels are tuned so that
251 the realistic seasonal progress of the middle atmosphere circulations, frequency of sudden
252 stratospheric warmings, and period and amplitude of the equatorial quasi-biennial oscillations (QBOs)
253 can be represented.

254

255 **2.2 Land surface component**

256 The land surface model is also basically the same as in MIROC5. Energy and water
257 exchanges between land and atmosphere are calculated, considering the physical and physiological

258 effects of vegetation with a single layer canopy, and the thermal and hydrological effects of snow and
259 soil respectively with a three-layers snow and a six-layers soil down to a ~~14~~ 14-m depth. Sub-grid
260 fractions of land use and snow cover have also been considered. [The timestep for the land surface](#)
261 [model integration is 1 hour in MIROC6 which is the same as in MIROC5.](#) In addition to the standard
262 package in MIROC5, a few other physical parameterizations are implemented as described below.

263 A physically-based parameterization of sub-grid snow distribution (SSNOWD; Liston,
264 2004; Nitta et al., 2014) replaces the simple functional approach of snow water equivalent in
265 calculating sub-grid snow fractions in MIROC5 [in order to improve seasonal cycle of snow cover.](#) In
266 SSNOWD, the snow cover fraction is formulated for accumulation and ablation seasons separately.
267 For the ablation season, the snow cover fraction decreases based on the sub-grid distribution of the
268 snow water equivalent. A lognormal distribution function is assumed and the coefficient of variation
269 category is diagnosed from the standard deviation of the sub-grid topography, coldness index, and
270 vegetation type that is a proxy of surface winds. While the cold degree month was adopted for coldness
271 in the original SSNOWD, we decided instead to introduce the annually averaged temperature over the
272 latest 30 years using the time-relaxation method of Krinner et al. (2005), in which the timescale
273 parameter is set to 16 years. The temperature threshold for a category diagnosis is set to 0°C and 10°C.
274 In addition, a scheme representing a snow-fed wetland that takes into consideration sub-grid terrain
275 complexity (Nitta et al., 2017) is incorporated. The river routing model and lake module are the same
276 as those used in MIROC5, but the river network map is updated to keep the consistency to the new
277 land-sea mask (Yamazaki et al., 2009).

278

279 **2.3 Ocean and sea-ice component**

280 The ocean component of MIROC6 is basically the same as that used in MIROC5, but
281 several updates are implemented as described below. The warped bipolar horizontal coordinate system

282 in MIROC5 has been replaced by the tripolar coordinate system proposed by Murray (1996). Two
283 singular points in the bipolar region to the north of about 63°N are placed at (63°N, 60°E) in Canada
284 and (63°N, 120°W) in Siberia (Fig. 2). In the spherical coordinate portion to the south of 63°N, the
285 longitudinal grid spacing is 1° and the meridional grid spacing varies from about 0.5° near the equator
286 to 1° in the mid-latitudes. In the central Arctic Ocean where the bipole coordinate system is applied,
287 the grid spacings are about 60 km in zonal and 33 km in meridional, respectively. By introducing the
288 horizontal tripolar coordinate system, it is expected that theoretical westward propagation of the
289 oceanic baroclinic Rossby can be represented with less numerical dispersions because of agreement
290 of the coordinate system and the geographical coordinate system and that the horizontal resolutions in
291 the Arctic Ocean where the Rossby radius of deformation is relatively small are higher than in the case
292 where the bipolar warped coordinate system in MIROC5 is adopted. There are 62 vertical levels in a
293 hybrid σ -z coordinate system. The horizontal grid spacing in MIROC5 is nominally 1.4°, except for
294 the equatorial region and there are 49 vertical levels. The resolutions in MIROC6 are higher than in
295 MIROC5. In particular, 31 (23) of the 62 (49) vertical layers in MIROC6 (MIROC5) are within the
296 upper 500 m depth (Fig. 1b). The increased vertical layers in MIROC6 have been adopted in order to
297 better represent the equatorial thermocline and observed complex hydrography in the Arctic Ocean.
298 An increase in computational costs of the ocean component due to higher resolutions in MIROC6 is
299 suppressed by implementing a time-staggered scheme for the tracer and baroclinic momentum
300 equations (Griffies et al., 2005). Owing to the time-staggered scheme, the timestep for the ocean and
301 sea-ice components of MIROC6 is 20 minutes which is longer than that in MIROC5 (15 minutes).

302 The tracer advection scheme (Prather, 1986), the surface mixed layer parameterization
303 (Noh and Kim, 1999), and the parameterization for eddy isopycnal diffusion (Gent et al., 1995) used
304 in MIROC6 are the same as those used in MIROC5. Also as in MIROC5, the bottom boundary layer
305 parameterization of Nakano and Suginozawa (2002) is introduced south (north) of 54°S (49°N) for

306 representing the down-sloping flow of dense waters. The constant parameters used in the above-
307 mentioned parameterizations are determined in the same manner as that of MIROC5, except for the
308 Arctic region. An empirical profile of background vertical diffusivity, which is proposed in Tsujino et
309 al. (2000), is modified above the 50 m depth to the north of 65°N. It is $1.0 \times 10^{-6} \text{ m}^2 \text{ s}^{-1}$ in the uppermost
310 29 m and gradually increases to $1.0 \times 10^{-5} \text{ m}^2 \text{ s}^{-1}$ at the 50 m depth. Additionally, the turbulent mixing
311 process in the surface mixed layer is changed so that there is no surface wave breaking and no resultant
312 near-surface mixing in regions covered by sea ice. The combination of the weak background vertical
313 diffusivity and suppression of turbulent mixing under the sea-ice contributes to better representations
314 of the surface stratification in the Arctic Ocean with little impact on the rest of the global oceans
315 (Komuro, 2014).

316 The sea-ice component in MIROC6 is almost the same as in MIROC5. A brief description,
317 along with some major parameters, is given here. Readers may refer to Komuro et al. (2012) and
318 Komuro and Suzuki (2013) for further details. A subgrid-scale sea-ice thickness distribution is
319 incorporated by following Bitz et al. (2001). There are five ice categories (plus one additional category
320 for open water), and the lower bounds of the ice thickness for these categories are set to 0.3, 0.6, 1,
321 2.5, and 5 m. The momentum equation for sea-ice dynamics is solved using elastic-viscous-plastic
322 rheology (Hunke and Dukowicz, 1997). The strength of the ice per unit thickness and concentration is
323 set at $2.0 \times 10^4 \text{ N m}^{-2}$, and the ice–ocean drag coefficient is set to 0.02. The surface albedo for bare ice
324 surface is 0.85 (0.65) for the visible (infrared) radiation. The surface albedo in snow-covered areas is
325 0.95 (0.80) when the surface temperature is lower than -5°C for the visible (infrared) radiation, and it
326 is 0.85 (0.65) when the temperature is 0°C. Note that the albedo changes linearly between -5°C and
327 0°C. These parameter values listed here are the same as those listed in MIROC5.

328

329 **2.4 Boundary conditions**

330 A set of external forcing data recommended by the CMIP6 protocol are used. The historical
331 solar irradiance spectra, greenhouse gas concentrations, anthropogenic aerosol emissions, and biomass
332 burning emissions are given by Matthes et al. (2017), Meinshausen et al. (2017), Hoesly et al. (2018),
333 and van Marle et al. (2017), respectively. The concentrations of greenhouse gases averaged globally
334 and annually are given to MIROC6. Radiative forcing of stratospheric aerosols due to volcanic
335 eruptions are computed by vertically integrating extinction coefficients for each radiation band, which
336 are provided by Thomason et al. (2016), in the model layers above the tropopause~~are taken into~~
337 ~~account as extinction coefficients for each radiation band~~. Three-dimensional atmospheric
338 concentrations of historical ozone (O₃) are produced by the Chemistry-Climate Model Initiative
339 (Hegglin et al., in preparation; the data are available at [http://blogs.reading.ac.uk/ccmi/forcing-](http://blogs.reading.ac.uk/ccmi/forcing-databases-in-support-of-cmip6/)
340 [databases-in-support-of-cmip6/](http://blogs.reading.ac.uk/ccmi/forcing-databases-in-support-of-cmip6/)). Three dimensional concentrations of the OH radical, hydrogen
341 peroxide (H₂O₂) and Nitrate (NO₃) are precalculated by a chemical atmospheric model of Sudo et al.
342 (2002). As precursors of secondary organic aerosol, emission data of terpenes and isoprene provided
343 by the Global Emissions Inventory Activity (Guenther et al., 1995) are normally used, although
344 simulated emissions from the land ecosystem model of Ito and Inatmoni (2012) are also used
345 alternatively.

346 For specifying the soil types and area fractions of natural vegetation and crop-land on grids
347 of the land-surface component, the harmonized land-use dataset (Hurtt et al., in prep.), Center for
348 Sustainability and the Global Environment global potential vegetation dataset (Ramankutty and Foley,
349 1999), and the dataset provided by the International Satellite Land Surface Climatology Project
350 Initiative I (Sellers et al., 1996) are used. ~~These is~~ datasets are also used in prescribing background
351 reflectance at the land surface. Leaf-area index data are prepared based on the Moderate Resolution
352 Imaging Spectroradiometer Leaf-area index products of Myneni et al. (2002).

353 The forcing dataset used for the preindustrial control simulation is basically composed of

354 the data for the year 1850, which are included in the above-mentioned historical dataset. The
355 stratospheric aerosols and solar irradiance in the preindustrial simulation are given as monthly
356 climatology averaged in 1850 – 2014 and in 1850 – 1873, respectively. The total solar irradiance is
357 about 1361 Wm^{-2} , and the global-mean concentrations of CO_2 , methane (CH_4), and nitrous oxide (N_2O)
358 are 284.32 ppm, 808.25 ppb, and 273.02 ppb, respectively.

359

360 **2.5 Spin-up and tuning procedures**

361 Firstly, the stand-alone ocean component of MIROC6, which includes the sea-ice
362 processes, is integrated from the initial motionless state with the observed temperature and salinity
363 distribution of the Polar Science Center hydrographic climatology (Steele et al., 2001). Ocean model
364 coastline geometry and bottom bathymetry are specified based on horizontal interpolation of the land
365 and sea-floor dataset of ETOPO5 (National Geophysical Data Center, 1993). The ocean component is
366 spun-up for 1000 years by the monthly climatological surface fluxes of Röske (2006). An acceleration
367 method of Bryan (1984) is used in the spin-up stage in order to obtain a thermally and dynamically
368 quasi-steady state. After the spin-up, additional integration for 200 years is performed without the
369 acceleration method. By analyzing the last 50-yr-long data from the stand-alone ocean component, the
370 monthly climatology of typical variables (e.g., zonal-mean temperature and salinity in several basins,
371 volume transports across major straits and archipelagos, meridional overturning circulations, and sea-
372 ice distributions) are compared with observations. Once the configuration of the ocean component is
373 frozen, the land-sea distribution and land-sea area ratios on the ~~model grids of the~~ atmospheric and
374 land surface model grids are and land surface components are determined according the coastline
375 geometry of the ocean component, after which the atmospheric and the land surface components are
376 coupled with the ocean component. Surface topography in the atmospheric and land surface
377 component are also made using the ETOPO5 dataset. Note that horizontal grid arrangement of the

378 land surface model is exactly same as the atmospheric component. The coupling interval among the
379 sub-models is 1 hour. An initial condition of the ocean component in MIROC6 is given by the stand-
380 alone ocean experiment, and those of the atmosphere and land are taken from an arbitrary year of the
381 pre-industrial control run of MIROC5.

382 After coupling the sub-models, climate model tuning is done under the pre-industrial
383 boundary conditions. Conventionally, the climate models of our modeling community are retuned in
384 coupled modes after stand-alone sub-model tuning. This is because reproducibility of climatic-mean
385 state and internal climate variations is not necessarily guaranteed in climate models with the same
386 parameters determined in stand-alone sub-model tuning, which is particularly the case in the tropical
387 climate. In our tuning procedures described below, many of the 10-yr-long climate model runs are
388 conducted with different parameter values. There are numerous parameters associated with physical
389 parameterizations, whose upper/lower bounds are constrained by empirical or physical reasoning. The
390 main parameters used in our tuning procedures are chosen referring to a perturbed parameter ensemble
391 set made by Shiogama et al. (2012) in which parameter sensitivity to cloud-radiative processes is
392 examined.~~stated in the next paragraph and are chosen primarily referring to Shiogama et al. (2012), in~~
393 ~~which the uncertainty of the climate sensitivity in MIROC5 is extensively measured using a perturbed~~
394 ~~parameter ensemble set.~~ The impact of parameter tuning on the present climate is also discussed by
395 Ogura et al (2017), focusing on the top-of-the-atmosphere (TOA) radiation and clouds. Any objective
396 and optimal methods for parameter tuning are not used in our modeling group and the tuning
397 procedures are like those in other climate modeling groups as summarized in Hourdin et al. (2017).

398 In the first model tuning step, climatology, seasonal progression, and internal climate
399 variability in the tropical coupled system are tuned in order that departures from observations or
400 reanalysis datasets are reduced. Here, it should be noted that representation of the tropical system in
401 MIROC6 is sensitive to the parameters for ~~cumulus~~convections and planetary boundary layer

402 processes. Specifically, parameters of reference height for cumulus precipitation, efficiency of the
403 cumulus entrainment of surrounding environment and maximum cumulus updraft velocity at the
404 cumulus base are used to tune strength of the equatorial trade wind, climatological position and
405 intensity of the Inter-Tropical Convergence Zone (ITCZ) and South Pacific Convergence Zone (SPCZ),
406 and interannual variability of El-Niño/Southern Oscillation (ENSO). In particular, the parameter for
407 the cumulus entrainment is known as a controlling factor of ENSO in MIROC5 (Watanabe et al., 2011).
408 Summertime precipitation in the western tropical Pacific and characteristic of tropical intraseasonal
409 oscillations are tuned by using the parameter for shallow convection describing the partitioning of
410 turbulent kinetic energy between horizontal and vertical motions at the sub-cloud layer inversion. Next,
411 the wintertime mid-latitude westerly jets and the stationary waves in the troposphere are tuned using
412 the parameters of the orographic gravity wave drag and the hyper diffusion of momentum. The
413 parameters of the hyper diffusion and the non-orographic gravity wave drag are also used when tuning
414 stratospheric circulations of the polar vortex and QBO. Finally, the radiation budget at the TOA is
415 tuned, primarily using the parameters for the auto-conversion process so that excess downward
416 radiation can be minimized and maintained closer to 0.0 Wm^{-2} . The surface albedos for bare sea-ice
417 and snow-covered sea-ice are set to higher values than in observations (see Section 2.3) in order to
418 avoid underestimating of the summertime sea-ice extent in the Arctic Ocean due to excess downward
419 shortwave radiation in this region. In addition, parameter tuning for the total radiative forcing
420 associated with aerosol-radiation and aerosol-cloud interactions~~cooling effects due to interactions~~
421 ~~between anthropogenic aerosol emissions and cloud radiative processes is~~ are done. In order that the
422 total radiative forcing ~~cooling effects~~ can be closer to the estimate of -0.9 Wm^{-2} (IPCC, 2013; negative
423 value indicates cooling) with an uncertainty range of -1.9 to -0.1 Wm^{-2} , parameters of cloud
424 microphysics and the aerosol transport module, such as timescale for cloud droplet nucleation, in-
425 cloud properties of aerosol removal by precipitation, and minimum threshold of number concentration

426 of cloud droplets, are perturbed. To determine a suitable parameter set, several pairs of a present-day
427 run under the anthropogenic aerosol emissions at the year 2000 and a pre-industrial run are conducted.
428 A pair of the present and preindustrial runs has exactly the same parameters, and differences of
429 tropospheric radiations between two runs are considered as anthropogenic radiative forcing~~cooling~~
430 effects. Note that MIROC6 in a coupled mode is used in this tuning procedure, and thus the sea surface
431 temperature (SST) is not fixed. The estimated radiative forcing here is not strictly the same as the
432 effective radiative forcing estimated in IPCC (2013). However, by the present tuning procedure, the
433 global-mean surface air temperature (SAT) change after the mid-19th century is well reproduced in
434 the historical runs by MIROC6 (details are discussed in Section 4). As above-mentioned,
435 reproducibility of the global-mean SAT is not a tuning goal but is a typical metric which reflects results
436 of the parameter tunings for individual processes of convections, dynamics, and radiative forcing.

437 After fixing the model parameters, the climate model is spun-up for 2000 years. During
438 the first several hundred years, waters contained in the land surface are drained to the ocean via river
439 runoff, which leads to a temporal weakening of the meridional overturning circulations in the ocean
440 and a rising of the global-mean sea level. After the global hydrological cycle reaches to an equilibrium
441 state, the strengths of the meridional overturning circulations recover and keep quasi steady state. The
442 above-mentioned processes spend about 1000 years, after which an additional 1000-yr-long
443 integration is performed in order to obtain a thermally and dynamically quasi-steady ocean state.

444 Figure 3 shows the time series of the global-mean quantities after the spin-up. The labeled
445 year in Fig. 3 indicates the elapsed year after the spin-up duration of 2000 years. Linear trend of the
446 global-mean SAT is 9.5×10^{-3} K/100 yr and ~~The global-mean surface air temperature (SAT) and the~~
447 ~~radiation budget at the TOA show no significant drifts, thereby indicating that they are in a quasi-~~
448 ~~steady state. Linear trends of the global-mean SAT and the radiation budget are 9.5×10^{-3} K/100yr and~~
449 ~~2.1×10^{-3} Wm⁻²/100yr, respectively. The trend of the SAT is much smaller than the observed value of~~

450 about $0.62 \text{ K}/100 \text{ yr}$ in the twentieth century, indicating that there is no significant drift and the
451 global-mean SAT is in a quasi-steady state. While the global-mean ~~sea surface temperature~~ (SST) is
452 in a quasi-steady state (linear trend of $7.0 \times 10^{-3} \text{ K}/100 \text{ yr}$), the global-mean ocean temperature shows
453 a larger trend of $6.8 \times 10^{-3} \text{ K}/100 \text{ yr}$ in the first 500 years than that of $1.3 \times 10^{-3} \text{ K}/100 \text{ yr}$ in the
454 later period. In the later sections, the 200-yr-long data between the 500-th and 699-th years are
455 analyzed.

456 _____ The ~~larger~~ trend of the global-mean ocean temperature in the later period suggests slight
457 but continuous warming of the deep ocean. The radiation budget at the TOA is 1.1 Wm^{-2} downward
458 on average (linear trend of $9.5 \times 10^{-3} \text{ K}/100 \text{ yr}$) and the net heat input at the sea surface is 0.32 Wm^{-2} .
459 The deep ocean warming is explained by the net heat input.~~global-mean ocean temperature suggests~~
460 ~~that the deep ocean continues to warm slightly.~~ Note that there is about 0.78 Wm^{-2} inconsistency
461 between the TOA radiation budget and the ocean heat uptake. This heat energy inconsistency is due to
462 that internal energy associated with precipitation, water vapor and river runoff is not taken account in
463 the atmospheric and land surface component in MIROC6 and that these waters with no temperature
464 information implicitly set their temperature to the SST when they flow or fall into the ocean. Perpetual
465 melting of the prescribed Antarctic ice-sheet with invariant ice thickness, which is occurred due to the
466 warm SAT bias in the Antarctic region (details will be discussed in Section 3.1.3), is also a cause of
467 the heat energy inconsistency.

468 ~~In the later sections, the 200-yr-long data between the 500-th and 699-th years are analyzed.~~

469

470 **3 Results of pre-industrial simulation**

471 Representations of climatic-mean field and internal climate variability in MIROC6 are
472 evaluated in comparison with MIROC5 and observations. The 200-yr-long data of the preindustrial
473 control simulation by MIROC5 are used. The observations and reanalysis datasets used in the

474 comparison are listed in Table 1.

475 Here, the model climatology in the pre-industrial simulations is compared with
476 observations in the recent decades. Because observations are obtained concurrently with the progress
477 of the global-warming due to increasing anthropogenic radiative forcing, the model climate under the
478 pre-industrial conditions may not be adequate for use when making comparisons with recent
479 observations. However, the root-mean-squared (RMS) errors of typical variables (e.g., the global-
480 mean SAT) in the climate models with respect to observations are much larger than the RMS
481 differences between the model climatology in the pre-industrial simulation and those in the last 30-yr-
482 long period in the historical simulations. Therefore, the era differences where climatology is defined
483 are not significant concern in comparisons among the climate models and observations.

484

485 **3.1 Climatology**

486 **3.1.1 Atmosphere and Land-surface**

487 First, model systematic biases in radiations at the TOA are evaluated because they reflect
488 model deficiencies in cloud-radiative processes that contribute to a large degree of uncertainty in
489 climate modelling. Figure 4 shows annual-mean biases in radiative fluxes at the TOA in MIROC6 and
490 MIROC5 with respect to the recent Clouds and the Earth's Radiant Energy System (CERES) estimate
491 (Loeb et al., 2009; the data are available at <https://ceres.larc.nasa.gov/>). At the top-right of each panel,
492 a global-mean (GM) value and a root-mean-squared error (RMSE) with respect to observations are
493 written. In the present manuscript, RMSE is computed without model and observed global-mean
494 quantities unless otherwise noted.

495 ~~Because the modeled and observed global-mean values are not considered when~~
496 ~~calculating the RMSE, the RMSE reflects model errors in spatial distribution.~~

497 ~~Persistent overestimates~~ of net shortwave radiative flux and the in the sum of net shortwave

498 ~~and net longwave fluxes net and outgoing shortwave radiative fluxes (hereafter, NET and OSR,~~
499 ~~respectively)~~ over low-latitude oceans in MIROC5 are significantly reduced in MIROC6. Hereafter,
500 net shortwave, longwave, and the sum of them are denoted as OSR, OLR and NET, respectively, for
501 simplicity. As described in Ogura et al. (2017), since parameter tuning cannot eliminate the above-
502 mentioned excess upward radiations, it is suggested that implementing a shallow convective
503 parameterization is required in order to reduce the biases. Figure 5 shows annual-mean moistening
504 rates associated with deep and shallow convections at the 850 hPa pressure level in MIROC6, ~~which~~
505 ~~has a shallow convective parameterization based on Park and Bretherton (2009).~~ Moistening due to
506 shallow convections occurs mainly over the low-latitude oceans, especially the eastern subtropical
507 Pacific and the western Atlantic and Indian oceans. These active regions of shallow convections occur
508 separately from regions with active deep convections in the western tropical Pacific and the ~~ITCZ~~
509 ~~Tropical Convergence Zone (ITCZ).~~ The clear separation of the two convection types is consistent
510 with satellite-based observations (Williams and Tselioudis, 2007). Owing to the shallow convective
511 process that mixes the humid air in the planetary boundary layer with the dry air in the free troposphere,
512 low-level cloud cover over the low-latitude oceans is better represented in MIROC6 than in MIROC5.
513 Figure 6 shows annual-mean biases in cloud covers with respect to the International Satellite Cloud
514 Climatology Project (ISCCP; Rosso et al., 1996; Zhang et al., 2004; the data are available at
515 <https://isccp.giss.nasa.gov/>). Overestimate of low-level cloud cover over the low-latitude oceans in
516 MIROC5 (Fig. 6b) is apparently reduced in MIROC6 (Fig. 6a), which results in the smaller biases in
517 NET and OSR biases (Fig. 4). RMS error in low-level cloud cover in MIROC6 is 9% lower than that
518 in MIROC5.

519 OSR in the mid-latitudes are also better represented in MIROC6 than in MIROC5. Zonally
520 distributed downward OSR bias in MIROC5 is reduced or becomes a relatively small upward bias in
521 MIROC6 (Figs. 4cd). This difference in the OSR bias is commonly found in both hemispheres. Cloud

522 covers at middle and high levels are larger in MIROC6 over the subarctic North Pacific, North Atlantic,
523 and the Southern Ocean (Figs. 6c-f), while low-level cloud cover over the same regions is smaller in
524 MIROC6 than in MIROC5 over the same regions (Figs. 6ab). The smaller low-level cloud cover in
525 MIROC6 is inconsistent with the larger upward OSR bias in MIROC6. The wintertime mid-latitude
526 westerlies are stronger and are located more poleward in MIROC6 than in MIROC5. Correspondingly,
527 activity of sub-weekly disturbances in the mid-latitudes is strengthened in MIROC6 (details are
528 described later). These differences in the mid-latitude atmospheric circulations between MIROC6 and
529 MIROC5 lead to an enhanced poleward moist air transport from the subtropics to the subarctic region,
530 which could result in an increase in the mid- and high-level cloud covers in MIROC6, as reported in
531 previous modeling studies (e.g., Bodas-Salcedo et al., 2012; Williams et al., 2013). Consequently, the
532 downward OSR bias in the mid-latitudes is smaller in MIROC6 than in MIROC5. In polar regions,
533 both biases in OSR and NET remain the same as in MIROC5.

534 Systematic bias in the outgoing longwave radiative flux (hereafter, OLR) is worse in
535 MIROC6 than in MIROC5 because MIROC6 tends to underestimate OLR over almost the entire
536 global domain, except for Antarctica (Figs. 4ef). The global-mean of the high-level cloud cover in
537 MIROC6 is larger than in MIROC5 by 0.04 (Figs. 6ef), which is consistent with the smaller OLR in
538 MIROC6. The increased moisture transport due to the strengthening of the westerlies and sub-weekly
539 disturbances can partly explain the increase in the mid-latitude high-level clouds in MIROC6, but
540 high-level cloud cover is also larger in the low-latitudes. Hirota et al. (2018) reported that moistening
541 of the free troposphere due to shallow convections creates favorable conditions for atmospheric
542 instabilities that leads to the resultant activation of deep convections in the low-latitudes. Such
543 processes may contribute to the inferior representation of OLR in MIROC6.

544 Next, we will discuss on the global budget of the radiative fluxes and the RMS errors
545 between models and observations. Note that only deviations from the global means are considered

546 when calculating RMS errors. As written on the upper right of panels in Fig. 4ab, the global-mean
547 (RMS errors) NETs are -1.11 (12.7) Wm^{-2} in MIROC6 and -0.98 (15.9) Wm^{-2} in MIROC5, respectively,
548 and these values are consistent with the observed value of -0.81 Wm^{-2} (CERES; Loeb et al, 2009).
549 However, the observed value is estimated in the present-day condition. Ideally, the model value in the
550 preindustrial condition should be 0 Wm^{-2} and is in the marginally acceptable range. If However, if
551 NET is divided into OSR and OLR, so-called error compensation becomes apparent. The global means
552 of OSR (OLR) are -231.3 (230.2) Wm^{-2} in MIROC6 and -237.6 (236.6) Wm^{-2} in MIROC5,
553 respectively (Figs. 4c-f). The observed global-means of OSR and OLR are -240.5 Wm^{-2} and 239.7
554 Wm^{-2} . Biases in the global-mean OSR (OLR) with respect to observations are 9.2 (-9.5) Wm^{-2} in
555 MIROC6 and 2.9 (-3.1) Wm^{-2} in MIROC5, respectively. Thus, the global-mean OSR and OLR in
556 MIROC6 are worse than those in MIROC5. Further division of OSR and OLR into cloud-radiative
557 forcing and clear-sky shortwave (longwave) radiative components shows that shortwave cloud-
558 radiative forcing is dominant on the biases in radiative fluxes. The biases in the global-mean shortwave
559 (longwave) cloud-radiative forcing with respect to observations are 12.0 (6.7) Wm^{-2} in MIROC6 and
560 -4.0 (-0.2) Wm^{-2} in MIROC5, respectively.

561 The global radiation budget in MIROC6 is inferior to that in MIROC5, while
562 reproducibility of climatic means of typical model variables, other than radiative fluxes, and internal
563 variations are better simulated in MIROC6 (details are shown later). As described in Section 2.5, the
564 intensive tuning by perturbing model parameters is done focusing on reproducibility of climatic means,
565 internal variations, and radiative forcing due to anthropogenic aerosols. During this procedure, the
566 global radiation budget is traded-off. On the other hand, RMS errors in NET, OSR, and OLR are 12.7 ,
567 16.2 , and 6.3 Wm^{-2} in MIROC6 and 15.9 , 18.9 , and 6.8 Wm^{-2} in MIROC5, respectively, thereby
568 indicating that the errors in MIROC6 have been reduced by 7% to 20%. This is also the case for
569 shortwave and longwave cloud radiative forcings, where the corresponding errors have been reduced

570 by 17% and 13 %, respectively. Taken together, these results show that the spatial patterns of the
571 radiative fluxes are better simulated in MIROC6 than in MIROC5.

572 The improvement in spatial radiation patterns, especially in low-latitude OSR, is
573 explained primarily by the implementation of shallow convective processes, which results in a moister
574 free troposphere in MIROC6 than in MIROC5. Figures 7ab show zonal-mean biases in annual-mean
575 specific humidity with respect to the European Centre for Medium-Range Weather Forecast interim
576 reanalysis (ERA-I; Dee et al., 2011; the data are available at
577 <https://www.ecmwf.int/en/forecasts/datasets/archive-datasets/reanalysis-datasets/era-interim>). Dry
578 bias in 30°S–30°N, which occurs persistently in MIROC5, are largely reduced in MIROC6 owing to
579 vertical mixing at the interface of the planetary boundary layer and the free troposphere. On the other
580 hand, moist bias below the 600 hPa pressure level in the mid-latitudes is somewhat worse in MIROC6
581 than in MIROC5. Shallow convections also contribute to the improvement of precipitations in the low
582 latitudes. Figure 8 shows global maps for climatological precipitation in boreal winter (December–
583 February) and summer (June–August). The second version of the Global Precipitation Climatology
584 Project (GPCP; the data are available at <https://precip.gsfc.nasa.gov/>) Monthly Precipitation Analysis
585 (Adler et al., 2003) is used for the observations. While MIROC5 suffers from underestimate of
586 summertime precipitation over the western tropical Pacific, the underestimate is largely reduced in
587 MIROC6 (Figs. 8df). The increase of precipitations is associated with deep convections because the
588 moister free troposphere in MIROC6 is more favorable for the occurrence of deep convections (Hirota
589 et al., 2018). On the other hand, model representation of the precipitation in MIROC6 is not necessarily
590 alleviated other than the western tropical Pacific. For example, the overestimate of wintertime
591 precipitation over the Indian Ocean and the mid-latitude North Pacific is worse in MIROC6 than in
592 MIROC5.

593 Zonal-mean biases in annual-mean air temperature and zonal wind velocity are also better

594 represented in MIROC6 than in MIROC5 (Figs. 7c-f). The ~~remarkable~~ upper stratospheric warm bias
595 in 50°S–50°N in MIROC5 is significantly reduced in MIROC6. The ~~model top of T_{OA} in~~ MIROC6 is
596 located at the 0.004 hPa pressure level and there are 42 vertical layers above the 50 hPa pressure level,
597 while the ~~model top T_{OA}~~ of MIROC5 is placed at the 3 hPa pressure level. As a result, there are
598 significant differences in stratospheric circulations between the models. As shown in the annual-mean
599 mass stream function calculated using zonal-mean meridional winds with log₁₀ vertical scale (Fig. 9),
600 an upward wind continuing from the low-latitude troposphere to the stratosphere is stronger in
601 MIROC6 than in MIROC5. It is considered that an increased upward advection of the temperature
602 minimum around the tropopause in 30°S–30°N may lead to reduction of warm temperature bias in the
603 stratosphere which is significant in MIROC5. ~~from the tropopause to the stratopause is apparent in~~
604 ~~low latitudes of MIROC6. This upward wind transports the cold air in the temperature minimum~~
605 ~~around the tropopause in 30°S–30°N, which reduces the warm bias in the stratosphere.~~
606 Correspondingly, the stratospheric westerly bias in low latitudes of MIROC5 is also considerably
607 alleviated in MIROC6. Note that the atmospheric O₃ concentration data used in MIROC5 is different
608 from those in MIROC6, and the concentration in the stratosphere is higher than the data used in
609 MIROC6. About 25% of the above-mentioned reduction in the stratospheric warm biases is explained
610 by the smaller absorption of ~~short~~longwave radiation by O₃. Note that the zonal-mean temperature
611 bias in Fig. 7c is smaller when the climatological-mean temperature from 1980 to 2009 in a historical
612 simulation are evaluated against observations because of the known stratospheric cooling with
613 increased greenhouse gases and reduced O₃ concentrations.

614 The zonal-means of the air temperature and zonal wind in MIROC6 are also better
615 simulated in the mid- and high latitudes. A pair of easterly and westerly biases in MIROC5, which is
616 in the troposphere of the Northern Hemisphere, is associated with a weaker mid-latitude westerly jet
617 and its southward shift with respect to observations. The pair of the biases is reduced in MIROC6,

618 thereby suggesting that a strengthening and northward shift of the westerly jet occurs in MIROC6.
619 Indeed, as shown in the upper panels of Fig. 10, the meridional contrast of high and low biases in the
620 500 hPa pressure level (Z500) along the wintertime westerly jet is weaker in MIROC6 than in
621 MIROC5. The latitudes with the maximal meridional gradient of Z500 are located further northward
622 in MIROC6 than in MIROC5, especially over the North Atlantic. Correspondingly, wintertime storm
623 track activity (STA), which is defined as an 8-day-high-pass-filtered eddy meridional temperature flux
624 at the 850 hPa pressure level, is stronger over the North Pacific and Atlantic in MIROC6 than in
625 MIROC5 (see upper panels of Fig. 11) and is accompanied by an associated increase in precipitation,
626 especially in the North Pacific (Figs. 8ce). In the stratosphere above the 10 hPa pressure level, the
627 polar night jet is reasonably captured in MIROC6, although the westerly is somewhat overestimated
628 in 30°N–60°N. Also, in the Southern Hemisphere, representation of the tropospheric westerly and the
629 polar night jets are better in MIROC6 than in MIROC5, and the easterly bias centered at 60°S in the
630 troposphere is clearly reduced in MIROC6. Although causality is unclear, the warm air temperature
631 bias above the tropopause to the south of 60°S is smaller in MIROC6 than in MIROC5.

632 The enhanced wintertime STA in MIROC6 leads to a strengthening of the Ferrel circulation
633 in the Northern Hemisphere and a broadening of its meridional width. As shown in Fig. 9, the northern
634 edge of the Ferrel cell is located further northward in MIROC6 than in MIROC5. Because the Ferrel
635 cell is a thermally indirect circulation driven primarily by eddy temperature and momentum fluxes,
636 the stronger STA in MIROC6 possibly causes the Ferrel cell differences between the two models.
637 Associated with the northward extension of the Ferrel cell, the upward wind between the Ferrel cell
638 and the polar cell centered at 65°N is stronger in MIROC6 than in MIROC5 and the meridional width
639 of the polar cell is smaller. Also, in the Southern Hemisphere, the upward wind around 60°S at the
640 southern edge of the Ferrel cell is stronger in MIROC6 than in MIROC5. Correspondingly, high sea
641 level pressure (SLP) biases in polar region in MIROC5 are significantly reduced in MIROC6 (figures

642 are omitted) and RMS errors with respect to observations (ERA-I) are decreased by 30 %. Meanwhile,
643 in the stratosphere, anti-clockwise (clockwise) circulations to the north (south) of 50°N (S) are stronger
644 and extends further upward in MIROC6 than in MIROC5. These circulations seem to continue from
645 the troposphere into the stratosphere, thereby implying that more active troposphere-stratosphere
646 interactions associated with wave-coupling exist in MIROC6. Further details will be described later,
647 focusing on the occurrence of the sudden stratospheric warmings.

648 Parameterizations of SSNOWD (Liston, 2004; Nitta et al., 2014) and a wetland due to
649 snow-melting water have been newly implemented into MIROC6 (Nitta et al., 2017). In comparison
650 of MIROC6 with MIROC5, it can be seen that the former parameterization brings about significant
651 ~~remarkable~~ improvement in the Northern Hemisphere snow cover fractions from the early to the late
652 winter (Fig. 12). Compared with observations of the Northern Hemisphere EASE-Grid 2.0 (Brodzik
653 and Armstrong, 2013; the data are available at <https://nsidc.org/data/ease/>), the distribution of the snow
654 cover fractions is more realistic in MIROC6 than MIROC5, especially where and when the snow water
655 equivalent is relatively small (e.g., mid- and high latitudes in November, over Siberia in February).
656 Note that no clear improvement is found in May. This is because the newly implemented SSNOWD
657 represents hysteresis in the snow water equivalent-snow cover fraction relationship in both the
658 accumulation and ablation seasons. MIROC6 underestimates the snow cover fraction in the partially
659 snow-covered regions and overestimates it on the Tibetan plateau and in some parts of China. We note
660 that meteorological (e.g., precipitation or temperature) phenomena might affect these biases, but
661 further investigation will be necessary to identify their causes. Nevertheless, in spite of those
662 discrepancies, it can be said that the seasonal changes of the snow cover fraction are better simulated
663 in MIROC6 than in MIROC5 (Fig. 12j).

664

665 **3.1.2 Ocean**

666 Next, we evaluate the climatological fields of the ocean hydrographic structure, meridional
667 overturning circulations (MOCs), and sea-ice distribution. The zonal-mean potential temperature and
668 salinity are displayed in Figs. 13 and 14, respectively. Both MIROC6 and MIROC5 capture the general
669 features of the observed climatological hydrography (ProjD; Ishii et al., 2003). ~~However, in the deep~~
670 ~~and bottom layers to the south of 60°S, into which cold and dense water forms due to intense surface~~
671 ~~cooling around Antarctica sinks,~~ the potential temperatures in the deep and bottom layers to the south
672 of 60°S in the two models are warmer than observations because of ~~in the two models are warmer than~~
673 ~~observations~~ insufficient formation and sinking of cold and dense water due to intense surface cooling
674 around Antarctica (Figs. 13a-c and 14a-c). Such warm temperature bias associated with deep water
675 formation is also found in northern high latitudes of the Atlantic sector (Figs. 13a-c). ~~(Figs. 13a-e~~
676 ~~and 14a-e), as are the potential temperatures in northern high latitudes of the Atlantic sector (Figs.~~
677 ~~13a-e).~~ By horizontal advection of the warm temperature biases associated with the Pacific and
678 Atlantic MOCs, the model temperatures in deep layers apart other from than polar regions are also
679 warmer than in observations. The warm potential temperature bias in ~~In general,~~ the deep layer is
680 worse in MIROC6 than in MIROC5 in both of the Atlantic and Pacific sectors and the warm bias
681 influences the subsurface and the intermediate layers above the 3000 m depth, which might be
682 attributed to the excess ocean heat uptake and longer integration time in MIROC6 than in MIROC5
683 (the spinup duration of MIROC6 is 2000 years and that of MIROC5 is about 1000 years, respectively).
684 Also the low salinity bias below the 2000 m depth is worse in MIROC6 than in MIROC5, especially
685 in the Pacific sector (Figs. 14ef). This worsening can be explained the excess supply of the freshwater
686 in the Southern Ocean and weaker northward intrusion of the less saline water in MIROC6.
687 ~~water distribution in MIROC6 remains the same as in MIROC5.~~

688 ~~Meanwhile, the northward intrusion of Antarctic Intermediate Water in the Southern~~
689 ~~Hemisphere around the 1000-m depth is better simulated in MIROC6 than in MIROC5, especially in~~

690 ~~the Pacific sector (Figs. 13a-c).~~ In the Arctic Ocean, the halocline above the upper 500 m depth is
691 sharper and more realistic in MIROC6 than in MIROC5 and the high salinity bias below the 500 m
692 depth in MIROC5 is alleviated in MIROC6 (Figs. 13ef) because, as described in Section 2.3, there are
693 many more vertical levels in the surface and subsurface layers of MIROC6. In addition, vertical
694 diffusivity in the Arctic Ocean is set to smaller values in MIROC6 than in MIROC5, and the turbulent
695 kinetic energy input induced by surface wave breaking, as a function of the sea-ice concentration in
696 each grid cell, is reduced in MIROC6, as shown in Komuro (2014). ~~These differences in the ocean~~
697 ~~model configuration are considered likely to contribute to the improved oceanic structures in the~~
698 ~~surface and intermediate layers.~~ In the North Pacific, the southward intrusion of North Pacific
699 Intermediate Water (NPIW) around the 1000 m depth retreats northward in MIROC6. Strong tide-
700 induced vertical mixing of sea water is observed along the Kuril Islands (e.g., Katsumata et al., 2004).
701 The locally enhanced tide-induced mixing is known to reinforce the southward intrusion of the
702 Oyashio and associated water mass transport from the subarctic to subtropical North Pacific, and to
703 feed the salinity minimum of NPIW (Nakamura et al., 2004; Tatebe and Yasuda, 2004). Hence, ~~in~~
704 ~~situations where enhanced tidal mixing is considered,~~ NPIW reproducibility is better in MIROC5
705 where enhanced tidal mixing is considered than in MIROC6. Because we encountered significant
706 uncertainty in implementing the tidal mixing, ~~and~~ we decided to quit implementing it in developing
707 phase of MIROC6, at the expense of NPIW reproducibility.

708 The annual-mean potential temperature and zonal currents along the equator in MIROC6
709 are better simulated in MIROC6 than in MIROC5 (Fig. 15). Relatively cold water below the equatorial
710 thermocline is upwelled ~~is~~ in MIROC6, especially in the eastern tropical Pacific, which leads to a
711 strengthening of the vertical temperature gradient across the thermocline. The eastward speed of the
712 Equatorial Undercurrent in MIROC6 is over 80 cm s^{-1} , and is closer to the products of Simple Ocean
713 Data Assimilation (SODA; Carton and Giese, 2008; the data are available at

714 http://www.atmos.umd.edu/~lchen/SODA3.3_Description.html) than in MIROC5. These
715 improvements are mainly attributed to the higher vertical resolution of MIROC6 in the surface and
716 subsurface layers. However, the thermocline depths in the western tropical Pacific are still larger in
717 the models than in observations and are attributed. ~~This is due~~ to the stronger trade winds in the
718 models. When both of MIROC6 and MIROC5 are executed as stand-alone AGCMs with the
719 prescribed SST obtained from observations, the overestimate of the equatorial trade winds also appears
720 due to overestimate of the upward winds over the maritime continent associated with deep cumulus
721 convection and the resultant strengthening of the Walker circulation over the equatorial Pacific. ~~;~~
722 ~~which is a deficiency that also appears in stand-alone AGCM experiments. Hence, b~~ Better
723 parameterizing deep cumulus convection ~~representation of cloud physics~~ in the models could ~~may~~ be
724 required for better representation of the equatorial trade winds and thus oceanic states. ~~in the future.~~

725 Figure 16 displays annual-mean [YK1]Atlantic and Pacific MOCs. In the Atlantic, two
726 deep circulation cells associated with North Atlantic Deep Water (NADW; upper cell) and Antarctic
727 Bottom Water (AABW, lower cell) are found in both of the models. NADW transport across 26.5°N
728 is 17.2 (17.6) Sv ($1 \text{ Sv} = 10^6 \text{ m}^3 \text{ s}^{-1}$) in MIROC6 (MIROC5). These values are consistent with the
729 observational estimate of 17.2 Sv (McCarthy et al., 2015). RMS amplitudes of NADW transport are
730 about 0.9 Sv in MIROC6 and 1.1 Sv in MIROC5 on longer-than-interannual timescales, respectively.
731 These are smaller than the observed amplitude of 1.6 Sv in 2005–2014. Because observations include
732 the weakening trend of the Atlantic MOC due to the global warming, they can be larger than the model
733 variability under the preindustrial conditions. In the Pacific Ocean, both the models have the deep
734 circulation associated with Circumpolar Deep Water (CDW), but the northward transport of CDW
735 across 10°S is 8.6 Sv in MIROC6, which is slightly larger than 7.5 Sv of MIROC5. Although these
736 models values are somewhat smaller than observations, they are within the uncertainty range of
737 observations (Talley et al., 2003; Kawabe and Fujio, 2010).

738 Northern Hemisphere sea-ice concentrations are shown in Fig. 17. Here, it can be seen that
739 both the March and September sea-ice distributions in MIROC6 resemble ~~to~~ the satellite-based
740 observation (SSM/I; Cavarieli et al., 1991; the data are available at <https://nsidc.org/>). In general, the
741 spatial patterns of the models resemble the observations. Sea-ice areas in March (September) are 12.4
742 (6.1), 13.0 (6.9), and 14.9 (5.7) Million km² in MIROC6, MIROC5, and observations, respectively.
743 The model estimates are smaller (larger) in March (September) than in observations. The
744 underestimate in March is still found in MIROC6 and is attributed to the underestimate of sea-ice area
745 in the Sea of Okhotsk and the Gulf of St. Lawrence, even though the sea-ice area in the former region
746 is better simulated in MIROC6 than in MIROC5. Meanwhile, the eastward retreat of the sea-ice in the
747 Barents Sea is better represented in MIROC6 than in MIROC5. The overestimates in September in the
748 models are due to that the model climatology is defined under the pre-industrial conditions while
749 observations are taken in present-day conditions of 1980–2009, where a rapid decreasing trend of
750 summertime sea-ice area (including a few events of drastic decreases) is on-going (e.g., Comiso et al.,
751 2008). Note that the model September sea-ice area in 1980–2009 of historical simulations is smaller
752 than the observations and the sea-ice area does not show year-to-year drastic sea-ice decrease with
753 comparable amplitude with observations. The underestimate of the mean September sea-ice area in
754 MIROC6 might be attributed to slightly rapid warming of the Arctic climate in MIROC6 than in
755 observations. On the other hand, the modeled sea-ice areas in the Southern Ocean are unrealistically
756 smaller than in observations. Southern Hemisphere sea-ice areas in March (September) are 0.1 (3.4),
757 0.2 (5.2), and 5.0 (18.4) Million km² in MIROC6, MIROC5, and observations, respectively. Since
758 there are no ~~significant~~remarkable differences between the two models, the spatial maps for the sea-
759 ice area in the southern hemisphere are omitted.

760 Figure 18 shows the global maps of annual-mean sea level height relative to the geoid. The
761 absolute dynamic height data provided by Archiving, Validation, and Interpretation of Satellite

762 Oceanographic (AVISO; Rio et al. 2014) data are used as observed sea level height (the data are
763 available at <https://www.aviso.altimetry.fr/en/home.html>). ~~Although~~ Overall oceanic gyre
764 structures in the two models are consistent with observations. Although representation of the gyres in
765 MIROC6 remain generally the same as in MIROC5, there are a few improvements in the North Pacific
766 and the North Atlantic. The mid-latitude westerly in MIROC6 is stronger and is shifted further
767 northward than in MIROC5 (Fig. 10), which results in the strengthening of the subtropical gyres,
768 northward shifts of the western boundary currents, and their extensions. In particular, the current speed
769 of the Gulf Stream and the North Atlantic Current are faster in MIROC6 than in MIROC5, and the
770 contours emanating from the North Atlantic reach the Barents Sea in MIROC6. A corresponding
771 increase in warm water transport from the North Atlantic to the Barents Sea leads to sea-ice melting
772 and an eastward retreat of the wintertime sea-ice there in MIROC6 (Figs. 17a-c). An ~~remarkable~~
773 improvement in MIROC6 is also found in the Subtropical Countercurrent (STCC) in the North Pacific
774 along 20°N. As reported in Kubokawa and Inui (1999), the low potential vorticity water associated
775 with a wintertime mixed layer deepening in the western boundary current region is transported
776 southward in the subsurface layer and it pushes up isopycnal surfaces around 25°N. Thus, the
777 eastward-flowing STCC is induced around 25°N. Although both of the models show the wintertime
778 mixed layer deepening, the ocean stratification along 160°E is weaker in MIROC6 than in MIROC5
779 (not shown). This suggests that the isopycnal advection of low potential vorticity water in MIROC6
780 is more realistic than in MIROC5.

782 3.1.3 Discussions on model climatological biases

783 We have evaluated the simulated climatology in MIROC6 in comparison with MIROC5
784 and observations. The model climatology in MIROC6 shows certain improvements in simulating
785 radiations, atmospheric and oceanic circulations, and the snow cover fractions in the Northern

786 ~~Hemisphere. land surface variables.~~ In Fig. 19, we display the model biases in annual-mean SAT and
787 SST (Fig. 19) because these are typical variables that reflect errors in individual processes in the
788 climate system. The global-mean of SAT (SST) is 15.2 (18.1) °C in MIROC6, 14.6 (18.0) °C in
789 MIROC5, and 14.4 (18.1) °C in observations. The modeled global-mean SATs and SSTs are generally
790 consistent with observations. However, since the observed (model) value is estimated in the present-
791 day (preindustrial) condition, the model global-mean SATs and SSTs are overestimated. Here, it
792 should be noted that while the spatial patterns of the SAT and SST biases in MIROC6 resemble those
793 in MIROC5, there are several improvements. For example, cold SAT bias in MIROC5 extending from
794 the Barents Sea to Eurasia is significantly smaller in MIROC6, possibly owing to the increase in warm
795 water transport by the North Atlantic Current and the resultant eastward retreat of the sea ice in the
796 Barents Sea (Figs. 17 and 18). Warm SAT and SST biases along the west coast of the North America
797 are smaller in MIROC6 than in MIROC5. ~~The reason is that an thereby suggesting that the~~
798 ~~strengthening of the mid-latitude westerly jet (Fig. 10) and the associated strengthening of the Aleutian~~
799 ~~low~~ increase of southeastward Ekman transport in the eastern subarctic North Pacific due to the
800 strengthening of the mid-latitude westerly jet (Fig. 10) and the Aleutian low tend to cancel out the
801 relatively warm water supply from the subtropics to the subarctic region by the surface geostrophic
802 current. ~~lead to increase in southward transport of relatively cold water in the subarctic region.~~
803 Although it is not clear from Fig. 19, the SAT and SST in the subtropical North Pacific around 20°N
804 are warmer by 2 K in MIROC6 than in MIROC5. Also in the Atlantic, the SAT in the western tropics
805 is warmer in MIROC6. These warmer surface temperatures in MIROC6 indicates a reduction of the
806 cold SAT and SST biases that can be alleviated by an increase in the downward OSR in MIROC6 due
807 to the implementation of a shallow convective parameterization (Fig. 4), and by an increase in
808 eastward transport of the warm pool temperature associated with the stronger STCC in MIROC6 (Fig.
809 18).

810 On the other hand, the warm SAT and SST biases in the Southern Ocean and the warm
811 SAT bias in Middle East and the Mediterranean are worse in MIROC6 than in MIROC5. Consequently,
812 the RMS error in SAT is larger in MIROC6 (2.4 K) than in MIROC5 (2.2 K). The former is due
813 essentially to the underestimate of mid-level cloud covers, excess downward OSR, and the resultant
814 underestimate of the sea ice in the Southern Ocean. Such bias commonly occurs in many of climate
815 models and is normally attributed to errors in cloud radiative processes (e.g., Bodas-Salcedo et al.,
816 2012; Williams et al., 2013). In addition, poor representations of mixed layer depths and open ocean
817 deep convections due to the lack of mesoscale processes in the Antarctic Circumpolar Current are
818 causes of the warm bias (Olbers et al., 2004; Downes and Hogg, 2013). The latter warm bias, seen in
819 Middle East around the Mediterranean, can be explained by a tendency to underestimate the radiative
820 forcing cooling effects of aerosol-radiation interactions due to underestimate of dust emissions from
821 the Sahara Desert in MIROC6 (not shown).

822

823 **3.2 Internal climate variations**

824 **3.2.1 Madden-Julian oscillation and East Asian Monsoon**

825 In this section, we will evaluate the reproducibility of internal climate variations in
826 MIROC6 in comparison with MIROC5 and observations, beginning with an examination of the
827 equatorial waves in the atmosphere. Zonal wavenumber–frequency power spectra normalized by
828 background spectra for the symmetric and antisymmetric components of OLR are calculated following
829 Wheeler and Kiladis (1999) and are shown in Fig. 20. The daily-mean OLR data derived from the
830 Advanced Very High-Resolution Radiometer (AVHRR) of the National Oceanic and Atmospheric
831 Administration (NOAA) satellites (Liebmann and Smith, 1996; the data are available at
832 https://www.esrl.noaa.gov/psd/data/gridded/data.interp_OLR.html) are used for observational
833 references. The signals corresponding to the Madden-Julian oscillation (MJO), equatorial Kelvin (EK),

834 ~~and equatorial~~ Rossby-waves (ER), eastward inertia-gravity (n=1 EIG), and westward inertia-gravity
835 (WIG) waves in the symmetric component and mixed Rossby-gravity (MRG) and eastward inertia-
836 gravity (n=0 EIG) waves in the antisymmetric component stand out from the background spectra in
837 observations. MIROC5 qualitatively reproduces these spectral maxima of the symmetric MJO, EK,
838 and ER qualitatively, while the amplitudes of the MJO and the EK are underestimated. These
839 underestimates are partially mitigated in MIROC6. The power summed over the eastward
840 wavenumber 1–3 and periods of 30–60 days corresponding to the MJO are 20% larger in MIROC6
841 than in MIROC5. Furthermore, some additional analyses indicate that many aspects of the MJO,
842 including its eastward propagation over the western tropical Pacific, are improved in MIROC6. Those
843 improvements are primarily associated with the implementation of the shallow convective scheme that
844 moistens the lower troposphere. The results of these additional analyses, along with ~~and~~ some
845 sensitivity experiments, are described in a separate paper (Hirota et al., 2018). The EIG and WIG in
846 the symmetric component and the MRG and the EIG in the antisymmetric component are missing in
847 both MIROC6 and MIROC5.

848 Figure 21 shows the June–August (JJA) climatology of precipitation and circulations in
849 the East Asia. As shown in observations (ERA-I; Fig. 21a), the East Asian summer monsoon (EASM)
850 is characterized by the monsoon low over the warmer Eurasian continent and the subtropical high over
851 the colder Pacific Ocean (e.g., Ninomiya and Akiyama, 1992). The southwesterly between these
852 pressure systems transports moist air to the mid-latitudes forming a rainband called *Baiu* in Japanese.
853 The general circulation pattern of the EASM and the rainband are well simulated in both MIROC6
854 and MIROC5. It should be noted that one of major deficiencies in MIROC5, the underestimate of the
855 precipitation around the Philippines, has been largely alleviated in MIROC6. This improvement is,
856 again, associated with the moistening of the lower troposphere by shallow convective processes.
857 Interannual EASM variabilities are examined using an empirical orthogonal function (EOF) analysis

858 of vorticity at the 850 hPa pressure level over [100°E–150°E, 0°N–60°N] following Kosaka and
859 Nakamura (2010). The regressions of precipitation and 850hPa vorticity with respect to the time series
860 of the first mode (EOF1) are shown in the lower panels of Fig. 21. In observations, precipitation and
861 vorticity anomalies show a tripolar pattern with centers located around the Philippines, Japan, and the
862 Sea of Okhotsk (Hirota and Takahashi, 2012). The anomalies around the Philippines and Japan
863 correspond to the so-called Pacific-Japan pattern (Nitta et al., 1987). ~~In MIROC6,~~ The southwest-
864 northeast orientation of the wave-like anomalies is better simulated in MIROC6 than in MIROC5.

865 Figure 22 shows the wintertime (December–February) climatology of circulations and the
866 STA in the East Asia. The East Asian winter monsoon (EAWM) is characterized by northwesterly
867 between the Siberian high and the Aleutian low in observations (ERA-I; e.g. Zhang et al., 1997). The
868 monsoon northwesterly advects cold air to East Asia, enhancing the meridional temperature gradients
869 and strengthening the subtropical jet around Japan. The jet’s strength influences synoptic wave
870 activities in the storm track. MIROC5 captures the circulation pattern, but significantly underestimates
871 the STA. The STA in MIROC6 is better simulated than in MIROC5, but it is still smaller than in
872 observations. Interannual variability of the EAWM is also better represented in MIROC6 than in
873 MIROC5. The dominant variability of the monsoon northwesterly is extracted as the EOF1 of the
874 meridional wind at the 850 hPa pressure level over the region [30°N–60°N, 120°E–150°E]. In
875 observations, the regressions with respect to the time series of the EOF1 show stronger northwesterly
876 accompanied with suppressed STA, which is consistent with previous studies (Fig. 22d; e.g.,
877 Nakamura, 1992). This relationship between the circulations and the STA can be found in MIROC6
878 but not in MIROC5 (Figs. 22e, f). The explained variance of the EOF1 is 46.0% in observations, 37.1%
879 in MIROC5, and 47.1% in MIROC6, suggesting that the amplitude of this variability in MIROC6 is
880 consistent with ~~has become closer to~~ observations.

881

882 3.2.2 Stratospheric circulations

883 A few of the major changes in the model setting from MIROC5 to MIROC6 are higher
884 vertical resolution and higher model top altitude in MIROC6, namely, representation of the
885 stratospheric circulations. Here, we examine representation of the Quasi-Biennial Oscillations (QBOs)
886 in MIROC6. Figure 23 shows the time-height cross-sections of the monthly mean, zonal-mean zonal
887 wind over the equator for observations (ERA-I) and MIROC6. In this figure, an obvious QBO with
888 mean period of approximately 22 months can be seen in MIROC6. The mean period is slightly shorter
889 than that of ~28 months in observations, and the simulated QBO period varies slightly from cycle to
890 cycle. The maximum speed of the easterly at the 20 hPa pressure level is approximately -25 m s^{-1} in
891 MIROC6 and that of the westerly is 15 m s^{-1} . On the other hand, the observed maximum wind speeds
892 are -35 m s^{-1} for the easterly and 20 m s^{-1} westerly, respectively. The simulated QBO has somewhat
893 weaker amplitude in MIROC6 than observations, but the same east-west phase asymmetry. The QBO
894 in the MIROC6 shifts upward compared with that in observations, and the simulated amplitude is
895 larger above the 5 hPa pressure level and smaller in the lower stratosphere. The simulated downward
896 propagation of the westerly shear zones of zonal wind ($\partial\bar{u}/\partial z > 0$, where z is the altitude) is faster
897 than the downward propagation of easterly shear zones ($\partial\bar{u}/\partial z < 0$), which agrees with observations.
898 The QBOs in MIROC6 are qualitatively similar to that represented in the MIROC-ESM, which is an
899 Earth system model with a similar vertical resolution that participated in the CMIP5 (Watanabe et al.,
900 2011). Note that nothing resembling a realistic QBO was simulated in the previous low-top version
901 MIROC5, which only has a few vertical layers in the stratosphere.

902 Recently, Yoo and Son (2016) found that the observed MJO amplitude in the boreal winter
903 is stronger than normal during the QBO easterly phase at the 50 hPa pressure level. They also showed
904 that the QBO exerted greater influence on the MJO than did ENSO. Marshall et al. (2016) pointed out
905 the improvement in forecast skill during the easterly phase of the QBO and indicated that the QBO

906 could be a potential source of the MJO predictability. MIROC6 successfully simulates both the MJO
907 and QBO in a way ~~that~~ consistent with observations, as mentioned above, but correlations between
908 the QBO and MJO are ~~insignificant~~~~not clear~~. One possible reason is smaller amplitude of the simulated
909 QBO in the lowermost stratosphere. The QBO contribution to tropical temperature variation at the 100
910 hPa pressure level is ~0.1 K in the MIROC6, which is much smaller than the observed value of ~0.5
911 K (Randel et al., 2000). The simulated QBO has little effects on static stability and vertical wind shear
912 in the tropical upper troposphere.

913 MIROC6 can also simulate Sudden Stratospheric Warming (SSW), which is a typical intra-
914 seasonal variability ~~of in~~ the mid-latitude stratosphere ~~in the Northern Hemisphere~~. ~~Figure 24 shows~~
915 ~~the~~ standard deviation of monthly and zonal-mean zonal wind (colors) ~~superimposed on monthly~~
916 ~~climatology of zonal-mean zonal wind (black contours) in~~ February ~~are shown in Fig. 24 (a)-(c)~~.
917 ~~There are two maxima of the standard deviations over the equatorial stratosphere and the mid-to-high~~
918 ~~latitude upper stratosphere in the Northern Hemisphere in observations (Fig. 24a), which correspond~~
919 ~~to QBO and polar vortex variability. This feature is well captured in MIROC6 (Fig. 24b), while there~~
920 ~~are too small variations in MIROC5 where the stratosphere cannot be well resolved (Fig. 24c). Here,~~
921 ~~a prominent variation is observed over the equatorial stratosphere and the extratropical upper~~
922 ~~stratosphere. These two maxima, which correspond to QBO and polar vortex variability, respectively,~~
923 ~~are well captured in MIROC6. Although MIROC6 still has biases for magnitude and structure, no~~
924 ~~variation with a realistic magnitude appears when the stratosphere is not well resolved (Fig. 24e). The~~
925 ~~better representation~~ ~~improvement in the simulation~~ of the polar vortex variability ~~in MIROC6~~ is
926 closely ~~related~~ ~~associated with~~ ~~to~~ that of the SSW. As shown in the ~~bottom~~ ~~lower~~ panels of Fig. 24,
927 abrupt and short-lived warming events associated with SSW are detected in MIROC6, which are
928 reproduced comparably to observations in terms of magnitude, but are not detected in MIROC5. This
929 is consistent with previous modeling studies that reported the importance of ~~the~~ well-resolved

930 stratosphere for better simulation of stratospheric variability (e.g., Cagnazzo and Manzini, 2009;
931 Charlton-Perez et al., 2013; Osprey et al., 2013). ~~In December–January, however, On the other hand,~~
932 MIROC6 ~~still tends to underestimate~~s the frequency of SSW events ~~in December and January,~~ which
933 is a common bias ~~found in common with~~ other high-top climate models (e.g., Inatsu et al., 2007;
934 Charlton-Perez et al., 2013; Osprey et al., 2013). It is conjectured that the less frequent SSW in
935 December–January could be attributed to less frequent stationary wave breakings due to overestimate
936 of climatological zonal wind speed of the polar night jet in MIROC6 (Figs. 24d and e).
937 ~~It is conjectured that less frequent stationary wave breaking due to overestimate of climatological wind~~
938 ~~speeds associated with the polar night jet (Fig. 7e) have the effect to reducing the SSW frequency in~~
939 ~~December and January.~~

940 The inclusion of a well-resolved stratosphere in MIROC6 is also considered to be
941 important for improvement in representation of stratosphere-troposphere coupling. In order to evaluate
942 this, we examine the time-development of the Northern Annular Modes (NAM) associated with
943 strongly weakened polar vortex events in the stratosphere. The NAM indices are defined by the first
944 EOF mode of the zonal-mean year-round daily geopotential height anomalies over the Northern
945 Hemisphere and are computed separately at each pressure level (Baldwin and Thompson, 2009). The
946 height anomalies are first filtered by a 10-day low-pass filter to remove transient eddies. Figure 25
947 shows the composite of time development of the NAM index for weak polar vortex events. The events
948 are determined by the dates on which the 10 hPa NAM index exceeded -3.0 standard deviations
949 (Baldwin and Dunkerton, 2001). Note that the NAM index is multiplied by the square root of the
950 eigenvalue in each level before the composite, that is, the composite having the geopotential height
951 dimension. The weak polar vortex signal in the stratosphere propagates downward to the surface and
952 persists approximately 60 days in the lower stratosphere and upper troposphere. These observational
953 features are well represented in MIROC6 (Figs. 25ab). Although MIROC5 has also captured

954 downward propagating signals, its magnitude is approximately half in the stratosphere, and its
955 persistency is weak in the lower stratosphere and upper troposphere. Therefore, these results strongly
956 indicate that the inclusion of a well-resolved stratosphere in a model is important for representing not
957 only stratospheric variability, but also stratosphere-troposphere coupling.

958

959 **3.2.3 El Niño/Southern Oscillation and Indian Ocean Dipole mode**

960 Among the various internal climate variabilities on interannual timescales, ENSO is of
961 great importance because it can influence climate not only in tropics but also mid- and high latitudes
962 of both hemispheres through atmospheric teleconnections associated with wave propagations (e.g.,
963 Hoskins and Karoly, 1981; Alexander et al., 2002). Here, we describe representation of ENSO and
964 related teleconnection pattern. Figure 26 shows anomalies of SST, precipitation, the 500 hPa pressure
965 height, and the equatorial ocean temperature regressed onto the NINO3 index which is defined as the
966 area average of the SST in [5°S–5°N, 150°W–90°W]. ProjD and ERA-I in 1980–2009 are used as
967 observations. Although the maximum of the SST anomalies in the tropical Pacific is shifted more
968 westward than in observations, the ENSO-related SST anomalies simulated in both of MIROC6 and
969 MIROC5 are globally consistent with observations (Figs. 26a-c). Simulated positive precipitation
970 anomalies in MIROC6 still overextend to the western Pacific (Figs. 26d-f). Meanwhile, dry anomalies
971 over the maritime continent, the eastern equatorial Indian Ocean, and ~~the SPCZ~~
972 ~~South Pacific Convergence Zone (SPCZ)~~ are better simulated in MIROC6 than in MIROC5. ENSO teleconnection
973 patterns in Z500 (Figs. 26g-i) are also realistically simulated as seen in, for example, the Pacific-North
974 American pattern (Wallace and Gutzler, 1981). Equatorial subsurface ocean temperature anomalies in
975 MIROC6 are more confined within the thermocline than in MIROC5 (Figs. 26j-l), and the signals in
976 MIROC6 are closer to observations. However, the subsurface signals in MIROC6 reside deeper than
977 in observations. ~~However, the existence depths of the subsurface signals are larger in MIROC6 than in~~

978 ~~observations~~. This is due to the difference in the climatological structure of the equatorial thermocline,
979 which is attributed to the overestimate of the trade winds over the equatorial Pacific, as mentioned in
980 Section 3.1.2.

981 As well as ENSO, the Indian Ocean Dipole (IOD) mode is recognized as a prominent
982 interannual variability (Saji et al., 1999; Webster et al., 1999). Figure 27 shows anomalies of SST, 10
983 m wind, and precipitation regressed onto the autumn (September–November) dipole mode index
984 (DMI) which is defined as the zonal difference of the anomalous SST averaged over $[10^{\circ}\text{S}–10^{\circ}\text{N},$
985 $50^{\circ}\text{E}–70^{\circ}\text{E}]$ and that averaged in $[10^{\circ}\text{S}–10^{\circ}\text{N}, 90^{\circ}\text{E}–110^{\circ}\text{E}]$. ProjD and ERA-I in 1980–2009 are used
986 as observations. The observed positive IOD phase is characterized by a basin-wide zonal mode with
987 positive (negative) SST anomalies in the western (eastern) Indian Ocean, and precipitation is increased
988 (decreased) over the positive (negative) SST anomalies (Figs. 27ad). The dipole SST pattern is better
989 simulated in MIROC6 than in MIROC5 where the eastern SST anomalies are located more southward
990 than in observations (Figs. 27a-c). Correspondingly, a meridional dipole pattern in the precipitation of
991 MIROC5 is alleviated, and MIROC6 shows a zonal dipole precipitation pattern, as in observations
992 (Figs. 27d-f). Seasonal IOD phase locking to boreal autumn, which is assessed based on RMS
993 amplitude of the DMI, is also better simulated in MIROC6 than in MIROC5 (not shown). Seasonal
994 shoaling of the eastern equatorial thermocline in the Indian Ocean is realistically simulated in
995 MIROC6 during boreal summer to autumn. The shallower thermocline leads the stronger thermocline
996 feedback which is evaluated based on the SST anomalies regressed onto the 20°C isotherm depth
997 anomalies averaged over the eastern part of the IOD region. As displayed in the top of the upper panels
998 of Fig. 27, the thermocline feedback in MIROC6 is comparable to observations. This larger
999 thermocline feedback in MIROC6 possibly leads to the above-mentioned improvements in the IOD
1000 pattern. Note that the simulated surface wind anomalies are more realistic in MIROC6 than in
1001 MIROC5, although the magnitude of SST anomalies is overestimated in MIROC6. The overestimate

1002 of the SST anomalies may have arisen from an excessive response of the equatorial and coastal Ekman
1003 up- and down-welling to the wind changes, which are favorable in coarse-resolution ocean models.

1004

1005 **3.2.4 Decadal-scale variations in the Pacific and Atlantic Oceans**

1006 On longer-than-interannual timescales, the PDO (Mantua et al., 1997) or the Interdecadal
1007 Pacific Oscillations (IPO; Power et al., 1999) is known to be a dominant climate mode that is detected
1008 in the SST and the SLP over the North Pacific. To examine simulated PDO patterns, monthly SST and
1009 wintertime (December–February) SLP anomalies are regressed onto the PDO index defined as the 1st
1010 EOF mode of the North Pacific SST to the north of 20°N and are shown in Fig. 28. In order to detect
1011 the decadal-scale variation, the COBE-SST2/SLP2 data (Hirahara et al., 2014) from 1900 to 2013 are
1012 used as observations. Negative SST anomalies in the western and central North Pacific and positive
1013 SST anomalies in the eastern North Pacific are found in observations. These signals are also
1014 represented in both of MIROC6 and MIROC5. The regression of SLP anomalies corresponding to the
1015 deepening of the Aleutian low are well simulated in the models over the subarctic North Pacific, and
1016 it can be seen that the amplitudes of the SLP anomalies are larger in MIROC6 than in MIROC5, which
1017 is closer to the observation and ~~better represented in MIROC6 than in MIROC5~~. In the tropical Pacific,
1018 positive SST anomalies, which are among the more important driving processes of the PDO (e.g.
1019 Alexander et al., 2002), are seen in both the models and the observations. In MIROC5, the 5-yr running
1020 means of the wintertime (November–March) North Pacific Index (NPI), defined as the SLP averaged
1021 over [30°N–65°N, 160°E–140°W], are ~~excessively~~ less sensitive to the NINO3 index (correlation
1022 coefficient $r = -0.37$) than to the NINO4 index ($r = -0.64$). Note that the NINO4 index is defined as
1023 the area average of the SST in [5°S–5°N, 160°E–150°W]. The distorted response of the extratropical
1024 atmosphere to the tropical SST variations works to unsuitably modify the extratropical ocean and plays
1025 a major role in limiting the decadal predictability of the PDO index in MIROC5 (Mochizuki et al.,

1026 2014). In contrast, those in MIROC6 are well correlated with the NINO3 index ($r = -0.61$) in addition
1027 to the NINO4 index ($r = -0.62$). Overestimate of the tropical signals of MIROC5 in the western tropical
1028 Pacific are also alleviated in MIROC6. The above-mentioned PDO improvement and the linkage
1029 between the tropics and the mid-latitude North Pacific imply a potential for improved skills in
1030 initialized decadal climate predictions.

1031 In the Atlantic Ocean, there is another decadal-scale variability, which is called the AMO
1032 (Schlesinger and Ramankutty, 2004). Figure 29 shows anomalies of SST and SLP regressed onto the
1033 AMO index, which is defined as the area average of the SST anomalies in the North Atlantic [0° –
1034 60° N, 0° – 80° W] with the global-mean SST anomalies subtracted (Trenberth and Shea, 2006). As in
1035 the PDO, the centennial-long data of the COBE-SST2/SLP2 data in 1900–2013 are used as
1036 observations. The observed AMO spatial pattern in its positive phase is characterized by positive SST
1037 anomalies in the off-equator and the subarctic North Atlantic, and by negative or weakly-positive SST
1038 anomalies in the western subtropical North Atlantic (Fig. 29a). Corresponding to negative (positive)
1039 SLP anomalies over the subtropical (subarctic) North Atlantic, the mid-latitude westerly jet is weaker
1040 in a positive AMO phase than in normal years. These spatial patterns in the SST and SLP are simulated
1041 in both of MIROC6 and MIROC5. It is especially noteworthy that the positive SST anomalies in low
1042 latitudes have larger amplitudes in MIROC6 than in MIROC5, and they extend to the South Atlantic
1043 as in observations (Figs. 29bc). On the other hand, the positive SST anomalies in the subarctic region
1044 are underestimated in MIROC6, which may be due to the smaller RMS amplitudes of NADW transport
1045 in MIROC6 (see Section 3.1).

1046

1047 **3.3 Climate sensitivity**

1048 Following the regression method by Gregory et al. (2004) and Gregory and Webb (2008),
1049 we conducted abrupt CO₂ quadrupling experiments with MIROC6 and MIROC5 in order to evaluate

1050 effective climate sensitivity (ECS), radiative forcing, and climate feedback. The CO₂ quadrupling
1051 experiments were initiated from the pre-industrial control runs. Data from the first 1250 years after
1052 the CO₂ increase were used for the analysis.

1053 ECS, 2 × CO₂ radiative forcing, and climate feedback for MIROC6 are estimated to be
1054 2.56 K, 3.87 Wm⁻², and -1.54 Wm⁻²K⁻¹, respectively (Fig. 30a and Table 2). The ECS, radiative forcing,
1055 and climate feedback in MIROC6 are lower, higher, and negatively larger than those of the CMIP5
1056 multi-model ensemble means, although these estimates for MIROC6 are within the ensemble spread
1057 of the multi-models (Andrews et al., 2012). The ECS of MIROC6 is almost the same as MIROC5
1058 because the decrease in radiative forcing is counterbalanced by the positive increase in climate
1059 feedback, although the change in climate feedback is small and not statistically significant. The
1060 decrease in radiative forcing of MIROC6 relative to MIROC5 is evident in the longwave and
1061 shortwave cloud components (LCRE and SCRE in Fig. 30b and Table 3). On the other hand, the clear-
1062 sky shortwave component (SWclr) increases in MIROC6 relative to MIROC5, which partially cancels
1063 the differences between the two models. The positive increase in climate feedback is pronounced in
1064 the SCRE, which is partially offset by the decrease in the clear sky longwave (LWclr) and SWclr (Fig.
1065 30c and Table 3).

1066 We now focus on the SCRE of the radiative forcing and climate feedback, which show the
1067 largest differences between the two models, and compare the geographical distribution (Fig. 31). The
1068 distribution is calculated by regressing the changes in SCRE caused by the CO₂ increase at each
1069 latitude-longitude grid box against the change in the global-mean SAT. There is a large difference in
1070 the geographical distribution between MIROC6 and MIROC5, with the former showing more
1071 pronounced zonal contrast in the tropical Pacific than the latter. The changes in the global mean from
1072 MIROC5 to MIROC6 (Figs. 30bc) are correlated consistent with the changes in the western tropical
1073 Pacific, showing more negative radiative forcing and more positive climate feedback, which are

1074 partially offset by the changes in the central tropical Pacific with opposite signs. Interestingly, ~~the~~
1075 radiative forcing and climate feedback tend to show similar geographical patterns with opposite signs
1076 in each model.

1077

1078 **4. Summary and discussions**

1079 The sixth version of a climate model, MIROC6, was developed by a Japanese climate
1080 modeling community, aiming at contributing to the CMIP6 through deeper understanding of a wide
1081 range of climate science issues and seasonal-to-decadal climate predictions and future climate
1082 projections. The model configurations and basic performances in the pre-industrial control simulation
1083 have been described and evaluated in the present manuscript. Major changes from MIROC5, which
1084 was our official model for the CMIP5, to MIROC6 are mainly done in the atmospheric component.
1085 These include implementation of a parameterization of shallow convective processes, the higher model
1086 ~~top and TOA,~~ vertical resolution in the stratosphere. The ocean and land-surface components have
1087 been also updated in terms of the horizontal grid coordinate system and higher vertical resolution in
1088 the former, and parameterizations for sub-grid scale snow distribution and wet lands due to snow-
1089 melting water in the latter. Overall, the model climatology and internal climate variability of MIROC6,
1090 which are assessed in comparison with observations, are better simulated than in MIROC5.

1091 Overestimate of low-level cloud amounts in low latitudes, which can be partly attributed
1092 to insufficient representation of shallow convective processes, are significantly alleviated in MIROC6.
1093 The free atmosphere becomes wetter and the precipitation over the western tropical Pacific becomes
1094 larger in MIROC6 than in MIROC5, primarily due to vertical mixing of the humid air in the planetary
1095 boundary layer with the dry air in the free troposphere. Shallow convections also contribute to better
1096 propagation characteristics of intra-seasonal variability associated with MJO in MIROC6, as well as
1097 East Asian summer monsoon variability on interannual timescales. In addition, QBO, which is absent

1098 in MIROC5, appears in MIROC6 because of its better stratospheric resolution and non-orographic
1099 gravity wave drag parameterization.

1100 Climatic mean and internal climate variability in the mid-latitudes are also ~~remarkably~~
1101 improved in MIROC6. Together with enhanced activity of sub-weekly disturbances, the tropospheric
1102 westerly jets in MIROC6 are shifted more poleward and are stronger than in MIROC5, especially in
1103 the Northern Hemisphere. Overestimates in zonal wind speed of the polar night jet are reduced in
1104 MIROC6. These advanced representations lead to tighter interactions between the troposphere and the
1105 stratosphere in MIROC6. SSW events in the form of polar vortex destructions induced by upward
1106 momentum transfer from the troposphere to the stratosphere (e.g., Matsuno, 1971), are well captured
1107 in MIROC6. On interannual timescales, the improvement of the westerly jet results in better
1108 representations of the spatial wind pattern of the wintertime East Asian monsoon. Associated with
1109 changes in the large-scale atmospheric circulations, the western boundary currents in the oceans, the
1110 Kuroshio-Oyashio current system, the Gulf Stream, and their extensions are better simulated in
1111 MIROC6. The increase in warm water transport from the subtropical North Atlantic to the Barents Sea
1112 seems to melt the sea ice in the Barents Sea, and to alleviate the overestimate of the wintertime sea-
1113 ice area that is seen in that region in MIROC5. Another ~~remarkable~~ improvement in MIROC6 is found
1114 in the climatological snow cover fractions in the early winter over the Northern Hemisphere continents.
1115 In the Southern Hemisphere, however, the underestimate of mid-level clouds and the corresponding
1116 warm SAT bias, the underestimate of sea-ice area, and the overestimate of incoming shortwave
1117 radiation in the Southern Ocean, all of which are attributed to errors in cloud radiative and planetary
1118 boundary layer processes (e.g., Bodas-Salcedo et al., 2012; Williams et al., 2013), remains the same
1119 as in MIROC5.

1120 Qualitatively, the linkage representations between the tropics and the mid-latitudes
1121 associated with ENSO in MIROC6 are mostly the same as in MIROC5, ~~qualitatively~~. Meanwhile,

1122 oceanic subsurface signals, which partly control ENSO characteristics, are more confined along the
1123 equatorial thermocline in MIROC6, which is consistent with observations. Regarding the PDO,
1124 tropical influence on the mid-latitudes is more dominant in MIROC6 than in MIROC5, suggesting
1125 improvements in decadal-scale atmospheric teleconnections in MIROC6.

1126 The above descriptions are mainly on the Pacific internal climate variabilities. Regarding
1127 the Indian Ocean, the zonal dipole structures in the SST and precipitation associated with the
1128 interannual variability, known as the IOD, are better simulated in MIROC6 than in MIROC5, which
1129 has a bias of a false meridional precipitation pattern. In the Atlantic, the multi-decadal variability,
1130 known as the AMO, is represented in both ~~of~~ the models roughly consistent with observations, but
1131 their reproducibility shows both drawbacks and advantage. Signals associated with AMO in the
1132 subarctic (tropical) region are underestimated (~~overestimated~~) in MIROC6 (MIROC5).

1133 As a metric for climate change induced by atmospheric CO₂ increase, ~~one of important~~
1134 ~~metrics for quantifying uncertainty in future climate projections~~, ECS is also estimated. Although the
1135 model configurations and performances are different between the models, the ECS is almost the same
1136 (2.5 K). However, looking at geographical distributions of radiative forcing and climate feedback, the
1137 amplitudes of shortwave cloud components are much larger in MIROC6 than in MIROC5. Since the
1138 larger negative (positive) radiative forcing and positive (negative) climate feedback in the western
1139 (central) tropical Pacific cancel each other, global-mean quantities in MIROC6 almost remain the same
1140 as in MIROC5. As a topic of future study, estimating radiative forcing and climate feedback with
1141 Atmospheric Model Intercomparison Project-type experiments in order to check robustness of the
1142 present study would be desirable. Elucidating the impact of different geographical patterns of radiative
1143 forcing and climate feedback on the projected future climates would also be useful.

1144 After conducting the pre-industrial control simulation and evaluating the model
1145 reproducibility of the mean climate and the internal climate variability, ensemble historical simulations

1146 that were initiated from the pre-industrial simulations were executed using the historical forcing data
1147 recommended by the CMIP6 protocol. Figure 32 shows a time series of the global-mean SAT
1148 anomalies with respect to the 1961–1990 mean. There are 30 (5) ensemble members in the MIROC6
1149 (MIROC5) historical simulations. Note that the MIROC5 historical simulations are executed using the
1150 forcing datasets of the CMIP5 protocol. As shown in Fig. 32, the simulated SAT variations in both of
1151 MIROC6 and MIROC5 follow observations (HadCRUTv4.4.0; Morice et al., 2012; the data are
1152 available at <https://crudata.uea.ac.uk/cru/data/temperature/>) on a centennial timescale. The
1153 temperature rises from the nineteenth century to the early twenty-first century are about 0.72 K in
1154 MIROC6, 0.85 K in MIROC5, and 0.82 K in observations, respectively. Focusing on the period from
1155 the 1940s to the 1960s, the SAT variations seem to be better simulated in MIROC6 than in MIROC5,
1156 which can be due to both of an update of the forcing datasets and the larger ensemble number in
1157 MIROC6. On the other hand, the warming trend during the first half of the twentieth century in the
1158 models is about half as large as in observations. Whether it can be attributed to internal climate
1159 variability (e.g., Thompson et al., 2014; Kosaka and Xie, 2016) or to an externally forced mode (e.g.,
1160 Meehl et al., 2003; Nozawa et al., 2005) is still being debated. ~~Interestingly,~~ the so-called recent
1161 hiatus of the global warming (Easterling and Wehner, 2009) in the first decade of the twenty-first
1162 century is ~~not reasonably simulated in both of MIROC6 and MIROC5. captured in MIROC6.~~ The
1163 observed hiatus is considered to occur in association with a negative IPO phase as internal climate
1164 variations (e.g., Meehl et al., 2011; Watanabe et al., 2014). As external drivers of the hiatus, the
1165 increase in stratospheric water vapor and the weakening of solar activity are given as possible
1166 candidates, for example (e.g., Solomon et al., 2010; Kaufmann et al., 2011). Failure of simulating the
1167 hiatus in the models could be attributed to uncertainties in the historical forcing datasets or cancellation
1168 of internal climate variations of the IPO by ensemble-mean manipulation of the individual historical
1169 simulations. ~~while the simulated spatial pattern of the SAT trends in the first decade of the twenty-~~

1170 ~~first century does not have a negative IPO pattern (not shown). Considering that the ensemble mean~~
1171 ~~of the individual simulations reflects only externally forced variations and that signals of internal~~
1172 ~~climate variations have been roughly removed, the simulated hiatus in MIROC6 could be spurious and~~
1173 ~~the SAT trend difference between MIROC6 and MIROC5 could be attributed to the difference in the~~
1174 ~~forcing datasets.~~

1175 As summarized above, the overall reproducibility of the mean climate and the internal
1176 variability in the latest version of our climate model, MIROC6, has progressed, as well as the historical
1177 warming trend of the climate system. During the first trial of the preindustrial simulation conducted
1178 just after the model configuration was frozen, however, the model reproducibility was not as good as
1179 seen in MIROC5. As described in Section 2.5, we intensively tuned the model by perturbing
1180 parameters associated with, especially, cumulus and shallow convections, and planetary boundary
1181 processes. In addition, before starting the historical simulations, we estimated and tuned the radiative
1182 forcing ~~cooling effects~~ due to aerosol-radiation and aerosol-cloud interactions by changing the
1183 parameters of cloud microphysics in order to ensure that the estimated radiative forcing ~~cooling~~ would
1184 be closer to the best-estimate of the IPCC-AR5 (IPCC, 2013). Without this parameter tuning, the
1185 simulated warming trend after the 1960s was 70% as large as seen in observations. This dependence
1186 of radiative forcing and reproducibility of the warming trend on cloud microphysics has also been
1187 reported in other climate models (Golaz et al., 2013). A recent comparison of cloud microphysical
1188 statistics between climate models and satellite-based observations has pointed out that "tuned" model
1189 parameters that were adjusted for adequate radiative forcing ~~cooling~~ and realistic SAT changes do not
1190 necessarily ensure cloud properties and rain/snow formations will be consistent with observations and
1191 implies the presence of error compensations in climate models (e.g., Suzuki et al., 2013; Michibata et
1192 al., 2016). Error compensations are found also in both of global and regional aspects. As described in
1193 Section 3.1, the global TOA radiation imbalance in MIROC6 is about -1.1 Wm^{-2} , which is in the

1194 acceptable range of ~~consistent with -0.8 Wm^{-2} in~~ observations. However, when the TOA imbalance is
1195 examined in parts, cloud radiative components in the model contain non-negligible biases with respect
1196 to satellite-based observations. Regarding error compensations in the oceanic processes, for example,
1197 ~~Pacific Ocean,~~ the modeled northward transport of CDW, which ~~is about 8.6 Sv and~~ is within the
1198 uncertainty range of observations, is. ~~Although this transport is realistic, it is~~ maintained by spurious
1199 open ocean convections in the Southern Ocean, ~~which occur apart from the coastal region of Antarctica~~
1200 ~~and reach the sea floor,~~ which often that are artifacts appear in coarse-resolution ocean models where
1201 oceanic mesoscale eddies and coastal bottom water formation cannot be represented (e.g., Olbers et
1202 al., 2004; Downes and Hogg, 2013).

1203 There remain several key foci of ongoing model development efforts. These include
1204 process-oriented refinements of cloud microphysics and convective systems based on constraints from
1205 satellite data and feedbacks from cloud-resolving atmospheric models (e.g., Satoh et al., 2014), higher
1206 resolutions for representations of regional extremes, oceanic eddies and river floods, and
1207 parameterization of tide-induced micro-scale mixing of sea water. Improvement of computational
1208 efficiency, especially on massive parallel computing systems, is among the urgent issues for long-term
1209 and large ensemble simulations. ~~In terms of model architecture, giving each sub-module in a climate~~
1210 ~~model greater independence for effective model development may be required.~~ These improvements
1211 can contribute to deeper understanding of the Earth's climate, reducing uncertainties in climate
1212 projections and predictions, and more precise evaluations of human influences on carbon-nitrogen
1213 cycles when applied to Earth system models.

1214

1215 *Code and data availability.* ~~Please contact the corresponding author if readers may want to validate~~
1216 ~~the model configurations of MIROC6 and MIROC5 and to conduct replication experiments. The~~
1217 ~~source codes and required input data will be provided by the modeling community where the author~~

1218 belongs. The model output from the CMIP6/CMIP5 pre-industrial control and historical simulations
1219 used in the present manuscript are distributed through the Earth System Grid Federation and are
1220 freely accessible. Details on ESGF are given on the CMIP Panel website (<https://www.wcrp->
1221 [climate.org/wgcm-cmip](https://www.wcrp-climate.org/wgcm-cmip)).

1222

~~1223 Source code of MIROC6 and MIROC5 associated with this study is available to those who conduct~~
~~1224 collaborative research with the model users under license from copyright holders. For further~~
~~1225 information on how to obtain the code, please contact the corresponding author. The data from the~~
~~1226 model simulations and observations used in the analyses are available from the corresponding author~~
~~1227 upon request.~~

1228

1229 *Competing interests. The authors declare that they have no conflict of interest.*

1230

1231 **Acknowledgements**

1232 This research is supported by the “Integrated Research Program for Advancing Climate Models
1233 (TOUGOU Program)” from the Ministry of Education, Culture, Sports, Science, and Technology
1234 (MEXT), Japan. Model simulations were performed on the Earth Simulator at JAMSTEC and NEC
1235 SX-ACE at NIES. The authors are much indebted to Dr. Teruyuki Nishimura and Mr. Hiroaki Kanai
1236 for their long-term support in areas related to model developments and server administration. The
1237 authors also wish to express thanks to our anonymous reviewers for their suggestions and careful
1238 reading of the manuscript.

1239

1240 **References**

1241 Adcroft, A., Hill, C., and Marshall, J.: Representation of topography by shaved cells in a height

1242 coordinate ocean model, *Mon. Wea. Rev.*, 125, 2293–2315, 1997.

1243 Adler, R. F., Huffman, G. J., Chang, A., Ferraro, R., Xie, P., Janowiak, J., Rudolf, B., Schneider, U.,
1244 Curtis, S., Bolvin, D., Gruber, A., Susskind, J., and Arkin, P.: The Version 2 Global Precipitation
1245 Climatology Project (GPCP) Monthly Precipitation Analysis (1979–Present), *J. Hydrometeor.*, 4,
1246 1147–1167, 2003.

1247 Alexander, M. A., Bladé, I., Newman, M., Lanzante, J. R., Lau, N.-C., and Scott, J. D.: The
1248 atmospheric bridge: The influence of ENSO teleconnections on air–sea interaction over the global
1249 oceans, *J. Clim.*, 15, 2205–2231, 2002.

1250 Andrews, T., Foster, P., Boucher, O., Bellouin, N., and Jones, A.: Precipitation, radiative forcing and
1251 global temperature change. *Geophys. Res. Lett.*, 37, doi:10.1029/2010GL043991, 2010.

1252 Andrews, T., Gregory, J. M., Webb, M. J., and Taylor, K. E.: Forcing, feedbacks and climate sensitivity
1253 in CMIP5 coupled atmosphere-ocean climate models, *Geophys. Res. Lett.*, 39, L09712,
1254 doi:10.1029/2012GL051607, 2012.

1255 Arakawa, A. and Konor, C. S.: Vertical differencing of the primitive equations based on the Charney-
1256 Phillips grid in hybrid σ -p vertical coordinates, *Mon. Wea. Rev.*, 124, 511-528, 1996.

1257 Baldwin, M. P. and Dunkerton, T. J.: Stratospheric harbingers of anomalous weather regimes, *Science*,
1258 294, 581-584, 2001.

1259 Baldwin, M. P. and Thompson, D. W. J.: A critical comparison of stratosphere-troposphere coupling
1260 indices, *Quart. J. Roy. Meteorol. Soc.*, 135, 1661–1672, 2009.

1261 Bamber, J. L. and Aspinall, W. P.: An expert judgement assessment of future sea level rise from the
1262 ice sheets, *Nature Clim. Change*, 3, 424–427, 2013.

1263 Baran, A. J.: From the single-scattering properties of ice crystals to climate prediction: A way forward,
1264 *Atmospheric Res.*, 112, 45-69, 2012.

1265 Bengtsson, L., Hodges, K. I., and Keenlyside, N.: Will extratropical storms intensify in a warmer

1266 climate? *J. Clim.*, 22, 2276-2301, 2009.

1267 Bitz, C., Holland, M., Weaver, A., and Eby, M.: Simulating the ice-thickness distribution in a coupled
1268 climate model, *J. Geophys. Res.*, 106, 2441–2463, 2001.

1269 Bryan, K.: Accelerating the convergence to equilibrium of ocean-climate models, *J. Phys. Oceanogr.*,
1270 14, 666-673.

1271 Brodzik, M. and Armstrong, R.: Northern Hemisphere EASE-Grid 2.0 Weekly Snow Cover and Sea
1272 Ice Extent. Version 4, Boulder, Colorado USA: NASA DAAC at the National Snow and Ice Data
1273 Center, 2013.

1274 Cagnazzo, C. and Manzini, E.: Impact of the stratosphere on the winter tropospheric teleconnections
1275 between ENSO and the North Atlantic and European region, *J. Clim.*, 22, 1223-1238, 2009.

1276 Carton, J. A. and Giese, B. S.: A reanalysis of ocean climate using simple ocean data assimilation,
1277 *Mon. Wea. Rev.*, 136, 2999–3017, 2008.

1278 Cavarieli, D. J., Corawford, J. P., Drinkwater M. R., Eppler, D. T., Farmer, L. D., Jentz, R. R., and
1279 Wackerman, C. C.: Aircraft active and passive microwave validation of sea ice concentrations from
1280 the DMSP SSM/I, *J. Geophys. Res.*, 96, 21989-22088, 1991.

1281 Charlton-Perez, A. J., and co-authors: On the lack of stratospheric dynamical variability in low-top
1282 versions of the CMIP5 models, *J. Geophys. Res.*, 118, 2494-2505, 2013.

1283 Chikamoto, Y., Timmermann, A., Luo, J.-J., Mochizuki, T., Kimoto, M., Watanabe, M., Ishii, M., Xie,
1284 S.-P., and Jin, F.-F.: Skillful multi-year predictions of tropical trans-basin climate variability, *Nature*.
1285 *commun.*, 6, doi:10.1038/ncomms7869, 2015.

1286 Chikira, M. and Sugiyama, M.: A cumulus parameterization with state-dependent entrainment rate.
1287 Part I: Description and sensitivity to temperature and humidity profiles, *J. Atmos. Sci.*, 67, 2171-2193,
1288 2010.

1289 Church, J. A. and White, N. J.: Sea-level rise from the late 19th to the early 21st century, *Surv.*

1290 Geophys., 32, 585–602, 2011.

1291 Comiso, J. C., Parkinson, C. L., Gersten, R., and Stock, L.: Accelerated decline in the Arctic sea ice
1292 cover, Geophys. Res. Lett., 35, doi:10.1029/2007GL031972, 2008.

1293 Dee, D. and co-authors: The ERA-Interim reanalysis: configuration and performance of the data
1294 assimilation system. Quart J Roy Met. Soc., 137, 535–597, 2011.

1295 Downes, S. M. and Hogg, A. M.: Southern Ocean circulation and eddy compensation in CMIP5
1296 models, J. Clim., 26, 7198-7220, 2013.

1297 Easterling, D. R. and Wehner, M. F.: Is the climate warming or cooling? Geophys. Res. Lett., 36,
1298 doi:10.1029/2009GL037810, 2009.

1299 Eyring, V., Bony, S., Meehl, G. A., Senior, C. A., Stevens, B., Stouffer, R. J., and Taylor, K. E.:
1300 Overview of the Coupled Model Intercomparison Project Phase 6 (CMIP6) experimental design and
1301 organization, Geosci. Model. Dev., 9, 1937-1958, 2016.

1302 Gantt, B., Meskhidze, N., and Kamykowski, D.: A new physically-based quantification of marine
1303 isoprene and primary organic aerosol emissions, Atmos. Chem. Phys., 9, 4915-4927, doi:10.5194/acp-
1304 9-4915-2009, 2009.

1305 Gantt, B., Meskhidze, N., Facchini, M. C., Rinaldi, M., Ceburnis, D., and O’Dowd, C. D.: Wind speed
1306 dependent size-resolved parameterization for the organic mass fraction of sea spray aerosol, Atmos.
1307 Chem. Phys., 11, 8777-8790, doi:10.5194/acp-11-8777-2011, 2011.

1308 Gent, P.R., Willebrand, J., McDougall, T.J., and McWilliams, J.C: Parameterizing eddy-induced tracer
1309 transports in ocean circulation models, J. Phys. Oceanogr., 25, 463-474, 1995.

1310 Golaz, J. C., Horowitz, L. W., and Levy II, H.: Cloud tuning in a coupled climate model: Impact on
1311 20th century warming, Geophys. Res. Lett., 40, 2246-2251, 2013.

1312 Gregory, D.: Estimation of entrainment rate in simple models of convective clouds, Quart. J. Roy.
1313 Meteor. Soc., 127, 53–72, 2001.

1314 Gregory, J. M., Ingram, W. J., Palmer, M. A., Jones, G. S., Stott, P. A., Thorpe, R. B., Lowe, J. A.,
1315 Johns, T. C., and Williams, K. D.: A new method for diagnosing radiative forcing and climate
1316 sensitivity, *Geophys. Res. Lett.*, 31, L03205, doi:10.1029/2003GL018747, 2004.

1317 Gregory, J. and Webb, M.: Tropospheric adjustment induces a cloud component in CO₂ forcing, *J.*
1318 *Clim.*, 21, 58-71, 2008.

1319 Griffies, S. M., Gnanadesikan, A., Dixon, K. W., Dunne, J. P., Gerdes, R., Harrison, M. J., Rosati, A.,
1320 Russell, J. L., Samuels, B. L., Spelman, M. J., Winton, M., and Zhang, R.: Formulation of an ocean
1321 model for global climate simulations, *Ocean Sci.*, 1, 45-79, 2005.

1322 Guenther, A., Hewitt, N., Erickson, D., Fall, R., Geron, C., Graedel, T., Harley, P., Klinger, L., Lerdau,
1323 M., McKay, W., Pierce, T., Scholes, B., Steinbrecher, R., Tallamraju, R., Taylor, J., and Zim-merman,
1324 P.: A global model of natural volatile organic compound emissions, *J. Geophys. Res.*, 100, 8873–8892,
1325 1995.

1326 [Hajima, T., and co-authors: Model description of a new Earth system model “MIROC-ES2L” and the](#)
1327 [sensitivity analysis of the biogeochemical feedbacks, in preparation.](#)

1328 Hasumi, H.: CCSR Ocean Component Model (COCO) version 4.0, Center for Climate System
1329 Research Rep., 25, 103 pp., 2006. [Available online at [http://www.ccsr.u-](http://www.ccsr.u-
1330 tokyo.ac.jp/hasumi/COCO/coco4.pdf)

1331 Hegglin, M. I., and co-authors: Historical and future ozone database (1850-2100) in support of CMIP6,
1332 in prep.

1333 Hines, C. O.: Doppler-spread parameterization of gravity wave momentum deposition in the middle
1334 atmosphere, Part 2: Broad and quasi monochromatic spectra, and implementation, *J. Atmos. Solar Terr.*
1335 *Phys.*, 59, 387–400, 1997.

1336 Hirahara, S., Ishii, M., and Fukuda, Y.: Centennial-scale sea surface temperature analysis and its
1337 uncertainty, *J. Clim.*, 27, 57-75, 2014.

1338 Hirota, N., Ogura, T., Tatebe, H., Shiogama, H., Kimoto, M., and Watanabe, M.: Roles of shallow
1339 convective moistening in the eastward propagation of the MJO in MIROC6, *J. Clim.*, 31, 3033-3034,
1340 2018.

1341 Hirota, N. and Takahashi, M.: A tripolar pattern as an internal mode of the East Asian summer
1342 monsoon, *Clim. Dyn.*, 39, 2219–2238, doi:10.1007/s00382-012-1416-y, 2012.

1343 Hoesly, R.M., and co-authors: Historical (1750-2014) anthropogenic emissions of reactive gases and
1344 aerosols from the Community Emission Data System (CEDS), *Geosci. Model Dev.*, 11, 369-408,
1345 doi:10.5194/gmd-11-369-2018, 2018.

1346 Hourdin, F., Maurisen, T., Getteleman, A., Golaz, J.-C., Balaji, V., Duan, Q., Folini, D., Klocke, D.,
1347 Qian, Y., Rauser, F., Rio, C., Tomassini, L., Watanabe, M., and Williamson, D.: The art and science of
1348 climate model tuning, *Bull. Amer. Meteor. Soc.*, 98, 589-602, 2017.

1349 Hoskins, B. J. and Karoly, D. J.: The steady linear response of a spherical atmosphere to thermal and
1350 orographic forcing, *J. Atmos. Sci.*, 38, 1179-1196, 1981.

1351 Hunke, E. and Dukowicz, J.: An elastic–viscous–plastic model for sea ice dynamics, *J. Phys.*
1352 *Oceanogr.*, 27, 1849–1867, 1997.

1353 Hurtt, G., and co-authors: Harmonization of global land-use change and management for the period
1354 850-2100, *Geosci. Model Dev.*, in preparation.

1355 Inatsu, M., Kimoto, M. and Sumi, A.: Stratospheric sudden warming with projected global warming
1356 and related tropospheric wave activity, *SOLA*, 3, 105-108, 2007.

1357 Ineson, S. and Scaife, A. A.: The role of the stratosphere in the European climate response to El Niño,
1358 *Nature Geosci.*, 2, 32-36, 2009.

1359 ~~[IPCC: Climate Change 2007: The Physical Science Basis. Contribution of Working Group I to the](#)~~
1360 ~~[Fourth Assessment Report of the Intergovernmental Panel on Climate Change, edited by Solomon, S.,](#)~~
1361 ~~[Qin, D., Manning, M., Chen, Z., Marquis, M., Averyt, K. B., Tignor, M. and Miller, H. L., Cambridge](#)~~

1362 ~~University Press, Cambridge, United Kingdom and New York, NY, USA, 996 pp.~~

1363 IPCC: Climate Change 2013: The Physical Science Basis. Contribution of Working Group I to the
1364 Fifth Assessment Report of the Intergovernmental Panel on Climate Change, edited by Stocker, T.F.
1365 et al., Cambridge University Press, Cambridge, United Kingdom and New York, NY, USA, 1535 pp,
1366 2013.

1367 Ishii, M., Kimoto, M., and Kachi, M.: Historical ocean subsurface temperature analysis with error
1368 estimate, *Mon. Wea. Rev.*, 131, 51-73, 2003.

1369 Imada, Y., Watanabe, M., Mori, M., Kimoto, M., Shiogama, H., and Ishii, M.: Contribution of
1370 atmospheric circulation change to the 2012 heavy rainfall in southwestern Japan, *Bull. Amer. Meteor.*
1371 *Soc.*, 95, S52-S54, 2013.

1372 Imada, Y., Tatebe, H., Ishii, M., Chikamoto, Y., Mori, M., Arai, M., Watanabe, M., and Kimoto, M.:
1373 Predictability of two types of El-Niño assessed using an extended seasonal prediction system by
1374 MIROC, *Mon. Wea. Rev.*, 143, 4597-4617, 2015.

1375 Ito, A. and Inatomi, M.: Use of a process-based model for assessing the methane budgets of global
1376 terrestrial ecosystems and evaluation of uncertainty, *Biogeosciences*, 9, 759-773, 2012.

1377 K-1 model developers: K-1 coupled GCM (MIROC) description, K-1 Tech. Rep., 1, edited by H.
1378 Hasumi, H., and Emori, S., 34 pp., Center for Climate System Research, the Univ. of Tokyo, Tokyo,
1379 2004.

1380 Kamae, Y., Shiogama, H., Watanabe, M., Ogura, T., Yokohata, T., and Kimoto, M.: Lower tropospheric
1381 mixing as a constraint on cloud feedback in a multiparameter multiphysics ensemble, *J. Clim.*, 29,
1382 6259-6275, 2016.

1383 Katsumate, K., Ohshima, K. I., Kono, T., Itoh, M., Yasuda, I., Volkov, Y., and Wakatsuchi, M.: Water
1384 exchange and tidal current through the Bussol's Strait revealed by direct current measurements, *J.*
1385 *Geophys. Res.*, 109, doi:10.1019/2003JC001864, 2004.

1386 [Kaufmann, R. K., Kauppi, H., Mann, M. L., and Stock, J. H.: Reconciling anthropogenic climate](#)
1387 [change with observed temperature 1998–2008, Proc. Natl. Acad. Sci. USA, 108, 11790-11793, 2011.](#)

1388 Kawabe, M. and Fujio, S.: Pacific Ocean circulation based on observation, *J. Oceanogr.*, 66, 389-403,
1389 doi:10.1007/s10872-010-0034-8, 2010.

1390 Krinner, G., Viovy, N., de Noblet-Ducoudre, N., Ogee, J., Polcher, J., Friedlingstein, P., Ciais, P., Sitch,
1391 S., and Prentice, I. C.: A dynamic global vegetation model for studies of the coupled atmosphere-
1392 biosphere system, *Global Biogeochem. Cycles*, 19, GB1015, doi:10.1029/2003GB002199, 2005.

1393 Komuro, Y., Suzuki, T., Sakamoto, T. T., Hasumi, H., Ishii, M., Watanabe, M., Nozawa, T., Yokohata,
1394 T., Nishimura, T., Ogochi, K., Emori, S., and Kimoto, M.: Sea-ice in twentieth-century simulations by
1395 new MIROC coupled models: a comparison between models with high resolution and with ice
1396 thickness distribution, *J. Meteor. Soc. Japan*, 90A, 213–232, 2012.

1397 Komuro, Y. and Suzuki, T.: Impact of subgrid-scale ice thickness distribution on heat flux on and
1398 through sea ice, *Ocean Modell.*, 71, 13–25, 2013.

1399 Komuro, Y.: The Impact of Surface Mixing on the Arctic River Water Distribution and Stratification
1400 in a Global Ice–Ocean Model, *J. Clim.*, 27, 4359-4370, 2014.

1401 Kosaka, Y. and Nakamura, H.: Mechanisms of meridional teleconnection observed between a summer
1402 monsoon system and a subtropical anticyclone. Part I: The Pacific-Japan pattern, *J. Clim.*, 23, 5085–
1403 5108, 2010.

1404 Kosaka, Y. and Xie, S.-P.: The tropical Pacific as a key pacemaker of the variable rates of global
1405 warming, *Nature Geosci.*, 9, 669-673, 2016.

1406 Kubokawa, A., and Inui, T.: Subtropical Countercurrent in an idealized Ocean OGCM, *J. Phys.*
1407 *Oceanogr.*, 29, 1303-1313, 1999.

1408 Liebmann, B.: Description of a complete (interpolated) outgoing longwave radiation dataset, *Bull.*
1409 *Amer. Meteor. Soc.*, 77, 1275–1277, 1996.

1410 Liston, G.E.: Representing subgrid snow cover heterogeneities in regional and global models, *J. Clim.*,
1411 17, 1381-1397, 2014.

1412 Loeb, N. G., Wielicki, B. A., Doelling, D. R., Smith, G.L., Keyes, D.F., Kato, S., Manalo-Smith, N.,
1413 and Wong, T.: Toward optimal closure of the earth's top-of-atmosphere radiation budget, *J. Clim.*, 22,
1414 748–766, 2009.

1415 Mantua, N. J., Hare, S. R., Zhang, Y., Wallace, J. M., and Francis, R. C: A Pacific interdecadal climate
1416 oscillation with impacts on salmon production, *Bull. Amer. Meteor. Soc.*, 78, 1069-1079, 1997.

1417 Meehl, G. A., Covey, C., Delworth, T., Latif, M., McAvaney, B., Mitchell, J. F. B., Stouffer, R. J., and
1418 Taylor, K. E.: The WCRP CMIP3 multi-model dataset: a new era in climate change research. *Bull.*
1419 *Amer. Meteor. Soc.*, 88, 1383-1394, 2007.

1420 Myneni, R. B., and co-authors: Global products of vegetation leaf area and fraction absorbed PAR
1421 from year one of MODIS data, *Remote Sens. Environ.*, 83, 214–231, 2002.

1422 Mori, M., Watanabe, M., Shiogama, H., Inoue, J., and Kimoto, M.: Robust Arctic sea-ice influence on
1423 the frequent Eurasian cold winters in past decades, *Nature Geosci.*, 7, 869-873, 2014.

1424 Marshall, A. G., Hendon, H. H., Son, S. W., and Lim, Y.: Impact of the quasi-biennial oscillation on
1425 predictability of the Madden–Julian oscillation, *Clim. Dyn.*, doi:10.1007/s00382-016-3392-0, 2016.

1426 McCarthy, G. D., Smeed, D. A., Johns, W. E., Frajka-Williams, E., Moat, B. I., Rayner, D., Baringer,
1427 M. O., Meinen, C. S., Collins, J., and Bryden, H. L.: Measuring the Atlantic Meridional Overturning
1428 Circulation at 26°N, *Prog. Oceanogr.*, 130, 91-111, doi: 10.1016/j.pocean.2014.10.006, 2015.

1429 Matsuno, T.: A dynamical mode of the stratospheric sudden warming, *J. Atmos. Sci.*, 28, 1479-1494,
1430 1971.

1431 Matthes, K., and co-authors: Solar forcing for CMIP6 (v3.2), *Geosc. Model Dev.*, 10, 2247-2302,
1432 doi:10.5194/gmd-10-2247-2017, 2017.

1433 Meehl, G. A., Washington, W. M., Wigley, T. M. L., Arblaster, J. M., and Dai, A.: Solar and greenhouse

1434 gas forcing and climate response in the twentieth century, *J. Clim.*, 16, 426-444, 2003.

1435 Meehl, G. A., Arblaster, J. M., Fasullo, J. T., Hu, A., and Trenberth, K. E.: Model-based evidence of
1436 deep-ocean heat uptake during surface temperature hiatus periods, *Nature Clim. Change*, 1, 360-364,
1437 2011.

1438 Meinshausen, M., and co-authors: Historical greenhouse gas concentrations for climate modelling
1439 (CMIP6), *Geosci. Model Dev.*, 10, 2057-2116, doi:10.5194/gmd-10-2057-2017, 2017.

1440 Michibata, T., Suzuki, K., Sato, Y., and Takemura, T.: The sources of discrepancies in aerosol-cloud-
1441 precipitation interactions between GCM and A-Train retrievals, *Atmos. Chem. Phys.*, 16, 15413-
1442 15424, 2016.

1443 Mizuta, R.: Intensification of extratropical cyclones associated with the polar jet change in the CMIP5
1444 global warming projections, *Geophys. Res. Lett.*, 39, doi:10.1029/2012GL053032, 2012.

1445 Mochizuki, M., and co-authors: Pacific decadal oscillation hindcasts relevant to near-term climate
1446 prediction, *Proc. Natl. Acad. Sci. U.S.A.*, 107, 1833-1837, 2010.

1447 Mochizuki, T., Kimoto, M., Chikamoto, Y., Mori, M., Watanabe, M., and Ishii, M.: Error sensitivity
1448 to initial climate states in Pacific decadal hindcasts, *SOLA*, 10, 39-44, 2014.

1449 Mochizuki, T., Kimoto, M., Watanabe, M., Chikamoto, Y., and Ishii, M.: Interbasin effects of the
1450 Indian Ocean on Pacific decadal climate change, *Geophys. Res. Lett.*, 43, 7168-7175, 2016.

1451 Morice, C. P., Kennedy, J. J., Rayner, N. A., and Jones, P. D.: Quantifying uncertainties in global and
1452 regional temperature change using an ensemble of observational estimates: The HadCRUT4 dataset,
1453 *J. Geophys. Res.*, doi:10.1029/2011JD017187, 2012.

1454 Murphy, J. M.: Assessment of the practical utility of extended range ensemble forecasts, *Q. J. R.*
1455 *Meteorol. Soc.*, 116, 89-125, 1990.

1456 Murray, R. J.: Explicit generation of orthogonal grids for ocean models, *J. Comput. Phys.*, 126, 251-
1457 273, 1996.

1458 Nakamura, H.: Midwinter suppression of baroclinic wave activity in the Pacific, *J. Atmos. Sci.*, 49,
1459 1629–1642, 1992.

1460 Nakamura, T., Toyoda, T., Ishikawa, Y., and Awaji, T.: Tidal mixing in the Kuril Straits and its impact
1461 on ventilation in the North Pacific Ocean, *J. Oceanogr.*, 60, 411-423, 2004.

1462 Nakano, H., and Suginozawa, N.: Effects of bottom boundary layer parameterization on reproducing
1463 deep and bottom waters in a world ocean model, *J. Phys. Oceanogr.*, 32, 1209–1227, 2002.

1464 [National Geophysical Data Center, 1993: 5-minute Gridded Global Relief Data \(ETOPO5\), National](#)
1465 [Geophysical Data Center, NOAA, doi:10.7289/V5D798BF.](#)

1466 Neeling, J. D., Munnich, M., Su, H., Meyerson, J. E., and Holloway, C. E.: Tropical drying trends in
1467 global warming models and observations, *Proc. Natl. Acad. Sci. U.S.A.*, 103, 6110-6115, 2006.

1468 Ngo-Duc, T., Oki, T., and Kanae, S.: A variable streamflow velocity method for global river routing
1469 model: model description and preliminary results, *Hydrol. Earth Syst. Sci. Discuss.*, 4, 4389-4414,
1470 doi:10.5194/hessd-4-4389-2007, 2007.

1471 Ninomiya, K., and Akiyama, T.: Multi-scale features of Baiu, the summer monsoon over Japan and
1472 East Asia, *J. Meteor. Res. Japan*, 70, 467–495, 1992.

1473 Nitta, T., Yoshimura, K., and Abe-Ouchi, A.: Impact of arctic wetlands on the climate system: Model
1474 sensitivity simulations with the MIROC5 AGCM and a snow-fed wetland scheme, *J. Hydrometeor.*,
1475 18, 2923-2936, 2017.

1476 Nitta, T., Yoshimura, K., Takata, K., O'ishi, R., Sueyoshi, T., Kanae, S., Oki, T., Abe-Ouchi, A., and
1477 Liston, G. E.: Representing variability in subgrid snow cover and snow depth in a global land model,
1478 *J. Clim.*, 27, 3318-3330, doi:10.1175/JCLI-D-13-003, 2014.

1479 Nozawa, T., Nagashima, T., Shiogama, H., and Crooks, S.A.: Detecting natural influence on surface
1480 air temperature change in the early twentieth century, *Geophys. Res. Lett.*, 32,
1481 doi:10.1029/2005GL023540, 2005.

1482 Numaguti, A., Takahashi, M., Nakajima, T., and Sumi, A.: Description of CCSR/NIES atmospheric
1483 general circulation model. National Institute for Environmental Studies, Center for Global
1484 Environmental Research Supercomputer Monograph Rep., 3, 1-48, 1997.

1485 Olbers, D., Borowski, D., Volker, C., and Wolff, J.-O.: The dynamical balance, transport and
1486 circulation of the Antarctic Circumpolar Current. *Antarctic Sci.*, 14, 439-470, 2004.

1487 Oki, T. and Sud, Y.C.: Design of Total Runoff Integrating Pathways (TRIP) - A global river channel
1488 network, *Earth Interact.*, 2, 1-37, 1998.

1489 Ono, J., Tatebe, H., Komuro, Y., Nodzu, M. I., and Ishii, M.: Mechanisms influencing seasonal to
1490 inter-annual prediction skill of sea ice extent in the Arctic Ocean in MIROC, *The Cryosphere*, 12, 675-
1491 683, 2018.

1492 Osprey, S. M., Gray, L. J., Hardiman, S. C., Butchart, N., and Hinton, T. J.: Stratospheric variability
1493 in twentieth-century CMIP5 simulations of the Met Office climate model: High top versus low top, *J.*
1494 *Clim.*, 26, 1595-1606, 2013.

1495 Park, S. and Bretherton, C. S.: The University of Washington shallow convection and moist turbulence
1496 schemes and their impact on climate simulations with the Community Atmosphere Model, *J. Clim.*,
1497 22, 3449-3469, 2009.

1498 Power, S., Casey, T., Folland, C., Colman, A., and Mehta, V.: Interdecadal modulation of the impact
1499 of ENSO on Australia, *Clim. Dyn.*, 15, 319-324, 1999.

1500 Prather, M. J.: Numerical advection by conservation of second-order moments, *J. Geophys. Res.* 91,
1501 6671–6681, 1986.

1502 Ramankutty, N. and Foley, J.A.: Estimating historical changes in global land cover: croplands from
1503 1700 to 1992, *Global Biogeochem. Cycles*, 13, 997-1027, 1999.

1504 [Rio, M.-H., Mullet, S., and Picot, N.: Beyond GOCE for the ocean circulation estimate: Synergetic](#)
1505 [use of altimetry, gravimetry, and in-situ data provides new insight into geostrophic and Ekman currents,](#)

1506 [Geophys. Res. Lett., 41, 8192-8925, doi:10.1002/2014GL061773.](#)

1507 Rockström, J., and co-authors: A safe operating space for humanity, *Nature*, 461, 472-475, 2009.

1508 Riebesell, U., Körtzinger, A., and Oschlies, A.: Sensitivities of marine carbon fluxes to ocean change,
 1509 *Proc. Natl. Acad. Sci. U.S.A.*, 106, 20602–20609, 2009.

1510 Roberts, M. J., Clayton, A., Demory, M.-E., Donners, J., Vidale, P. L., Norton, W., Shaffrey, L.,
 1511 Stevens, D. P., Stevens, I., Wood, R. A., and Slingo, J.: Impact of resolution on the tropical Pacific
 1512 circulation in a matrix of coupled models. *J. Clim.*, 22, 2541–2556, 2009.

1513 Röske, F.: A global heat and freshwater forcing dataset for ocean models, *Ocean Modell.*, 11, 235-297,
 1514 2006.

1515 Rossow, W. B., Walker, A. W., Beuschel, D., and Roiter, M.: International Satellite Cloud Climatology
 1516 Project (ISCCP) documentation of new cloud datasets, World Climate Research Programme (ICSU
 1517 and WMO), WMO/TD 737, 115pp, 1996.

1518 Scaife, A. A., and co-authors: Climate change projections and stratosphere-troposphere interaction,
 1519 *Clim. Dyn.*, 38, 2089-2097, 2012.

1520 Scaife, A. A., and co-authors: Skillful long-range predictions of European and North American winters,
 1521 *Geophys. Res. Lett.*, 41, 2514-2519, 2014.

1522 Saji, N. H., Goswami, B. N., Vinayachandran, P. N., and Yamagata, T.: A dipole mode in the tropical
 1523 Indian Ocean, *Nature*, 401, 360–363, 1999.

1524 Sakamoto, T., and co-authors: MIROC4h - A new high-resolution atmosphere-ocean coupled general
 1525 circulation model, *J. Meteor. Soc. Jpn.*, 90A, 325-359, 2012.

1526 Satoh, M., and co-authors: The non-hydrostatic icosahedral atmospheric model: description and
 1527 development, *Prog. Earth Planet Sci.*, 1:18, doi:10.1186/s40645-017-014-0018-1, 2014.

1528 Schlesinger, M. E. and Ramankutty, N.: An oscillation in the global climate system of period 65-70
 1529 years, *Nature*, 376, 723 – 726, 1994.

1530 Sekiguchi, M. and Nakajima, T.: A k-distribution-based radiation code and its computational
1531 optimization for an atmospheric general circulation model, *J. Quant. Spectrosc. Radiat. Transfer*,
1532 doi:10.1016/j.jqsrt.2008.07.13, 2008.

1533 Sellers, P.J., and co-authors: The ISLSCP Initiative I global datasets: surface boundary conditions and
1534 atmospheric forcings for land-atmosphere studies, *Bull. Amer. Meteor. Soc.*, 1987-2005, 1997.

1535 Shaffrey, L., and co-authors: U.K. HiGEM: The new U.K. high resolution global environment model
1536 - Model description and basic evaluation, *J. Clim.*, 22, 1861–1896, 2009.

1537 [Shiogama, H., Watanabe, M., Yoshimori, M., Yokohata, T., Ogura, T., Annan, J.D., Hargreaves, J.C.,](#)
1538 [Abe, M., Kamae, Y., O'ishi, R., Nobui, R., Emori, S., Nozawa, T., Abe-Ouchi, A., and Kimoto, M.:](#)
1539 [Perturbed physics ensemble using the MIROC5 coupled atmosphere-ocean GCM without flux](#)
1540 [corrections: experimental design and results, *Clim. Dyn.*, 39, 3041-3056, 2012.](#)

1541 ~~[Shiogama, H., Watanabe, M., Yoshimori, M., Yokohata, T., Ogura, T., Annan, J.D., Hargreaves, J.C.,](#)~~
1542 ~~[Abe, M., Kamae, Y., O'ishi, R., Nobui, R., Emori, S., Nozawa, T., Abe-Ouchi, A., and Kimoto, M.:](#)~~
1543 ~~[Perturbed physics ensemble using the MIROC5 coupled atmosphere-ocean GCM without flux](#)~~
1544 ~~[corrections: experimental design and results, *Clim. Dyn.*, 39, 3041-3056, 2012.](#)~~

1545 Shiogama, H., Watanabe, M., Imada, Y., Mori, M., Kamae, Y., Ishii, M., and Kimoto, M.: Attribution
1546 of the June-July 2013 heat wave in the southwestern United States, *SOLA*, 10, 122-126, 2014.

1547 Sillmann, J., Kharin, V. V., Zwiers, F. W., Zhang, X., and Bronaugh, D.: Climate extremes indices in
1548 the CMIP5 multimodel ensemble: Part 2. Future climate projections, *J. Geophys. Res.*, 118, 2473-
1549 2493, 2013.

1550 [Solomon, S., Rosenlot, K. H., Portmann, R. W., Daniel, J. S., Davis, S. M., Sanford, T. J., and Plattner,](#)
1551 [G.-K.: Contributions of stratospheric water vapor to decadal changes in the rate of global warming,](#)
1552 [Science, 327, 1219-1223.](#)

1553 Steele, M., Morley, R., and Ermold, W.: PHC: A global ocean hydrography with a high-quality Arctic

1554 Ocean, *J. Clim.*, 14, 2079-2087, 2001.

1555 Stott, P. A., Stone, D. A. and Allen, M. R.: Human contribution to the European heatwave of 2003,
1556 *Nature*, 432, 610-614, 2004.

1557 Sudo, K., Takahashi, M., Kurokawa, J., and Akimoto, H.: CHASER: A global chemical model of the
1558 troposphere 1. Model description, *J. Geophys. Res.*, 107, 4339, doi:10.1029/2001JD001113, 2002.

1559 Suzuki, K., Golaz, J.-C, and Stephens, G. L., 2013: Evaluating cloud tuning in a climate model with
1560 satellite observations, *Geophys. Res. Lett.*, 40, 4464-4468, 2013.

1561 Suzuki, T., Saito, F., Nishimura, T., and Ogochi, K.: Heat and freshwater exchanges between sub-
1562 models of MIROC version 4, *JAMSTEC Rep. Res. Dev.*, 9, 2009 (in Japanese).

1563 Suzuki, T., Hasumi, H., Sakamoto, T. T., Nishimura, T., Abe-Ouchi, A., Segawa, T., Okada, N., Oka,
1564 A., and Emori, S.: Projection of future sea level and its variability in a high-resolution climate model:
1565 ocean processes and Greenland and Antarctic ice-melt contributions, *Geophys. Res. Lett.*, 32,
1566 doi:10.1029/2005GL023677, 2005.

1567 Suzuki, T. and Ishii, M.: Regional distribution of sea level changes resulting from enhanced
1568 greenhouse warming in the Model for Interdisciplinary Research on Climate version 3.2, *Geophys.*
1569 *Res. Lett.*, 38, doi:10.1029/2010GL045693, 2011.

1570 Takata, K., Emori, S., and Watanabe, T.: Development of the Minimal Advanced Treatments of
1571 Surface Interaction and RunOff (MATSIRO), *Global and Planetary Change*, 38, 209-222, 2003.

1572 Takemura, T., Okamoto, H., Maruyama, Y., Numaguti, A., Higurashi, A., and Nakajima, T.: Global
1573 three-dimensional simulation of aerosol optical thickness distribution of various origins, *J. Geophys.*
1574 *Res.*, 105, 17853-17873, 2000.

1575 Takemura, T., Nakajima, T., Dubovik, O., Holben, B. N., and Kinne, S.: Single-scattering albedo and
1576 radiative forcing of various aerosol species with a global three-dimensional model, *J. Clim.*, 15, 333-
1577 352, 2002.

1578 Takemura, T., Nozawa, T., Emori, S., Nakajima, T. Y., and Nakajima, T.: Simulation of climate
1579 response to aerosol direct and indirect effects with aerosol transport-radiation model, *J. Geophys. Res.*,
1580 110, D02202, doi:10.1029/2004JD005029, 2005.

1581 Takemura, T., Egashira, M., Matsuzawa, K., Ichijo, H., O'ishi, R., and Abe-Ouchi, A.: A simulation of
1582 the global distribution and radiative forcing of soil dust aerosols at the Last Glacial Maximum, *Atmos.*
1583 *Chem. Phys.*, 9, 3061-3073, doi:10.5194/acp-9-3061-2009, 2009.

1584 Talley, L. D., Reid, J. L., and Robbins, P. E.: Date-based meridional overturning streamfunctions for
1585 the global ocean, *J. Clim.*, 16, 3213-3226, 2003.

1586 Tatebe, H. and Yasuda, I.: Oyashio southward intrusion and cross-gyre transport related to diapycnal
1587 upwelling in the Okhotsk Sea, *J. Phys. Oceanogr.*, 34, 2327-2341, 2004.

1588 Tatebe, H. and Hasumi, H.: Formation mechanism of the Pacific equatorial thermocline revealed by a
1589 general circulation model with a high accuracy tracer advection scheme, *Ocean Modell.*, 35, 245-252,
1590 2010.

1591 Tatebe, H., and co-authors: The initialization of the MIROC climate models with hydrographic data
1592 assimilation for decadal prediction, *J. Meteor. Soc. Jpn.*, 90A, 275-294, 2012.

1593 Tatebe, H., Imada, Y., Mori, M., Kimoto, M., and Hasumi, H.: Control of decadal and bidecadal
1594 climate variability in the tropical Pacific by the off-equatorial South Pacific Ocean, *J. Clim.*, 26, 6524-
1595 6534, 2013.

1596 Taucher, J. and Oschlies, A.: Can we predict the direction of marine primary production change under
1597 global warming? *Geophys. Res. Lett.*, 38, doi:10.1029/2010GL045934, 2011.

1598 Taylor, K. E., Stouffer, R. J., and Meehl, G. A.: A summary of the CMIP5 experiment design.
1599 https://pcmdi.llnl.gov/?cmip5/docs/Taylor_CMIP5_22Jan11_marked.pdf, 2011.

1600 Thompson, D. M., Cole, J. E., Shen, G. T., Tudhope, A. W., and Meehl, G. A.: Early twentieth-century
1601 warming linked to tropical Pacific wind strength. *Nature Geosci.*, 8, doi:10.1038/ngeo2321, 2014.

1602 Thomason, L., Vernier, J.-P., Bourassa, A., Arfeuille, F., Bingen, C., Peter, T., and Luo, B.:
1603 Stratospheric Aerosol Data Set (SADS Version 2) Prospectus, to be submitted to Geosci. Model Dev.
1604 Discuss., 2016.

1605 Trenberth, K. E., and Shea, D. J.: Atlantic hurricanes and natural variability in 2005, Geophys. Res.
1606 Lett., 33, L12704, doi:10.1029/2006GL026894, 2006.

1607 van Marle, M.J.E., and co-authors: Historic global biomass burning emissions for CMIP6 (BB4CMIP)
1608 based on merging satellite observations with proxies and fire models (1750-2015), Geosci. Model Dev.,
1609 10, 3329-3357, doi:10.5194/gmd-10-3329-2017, 2017.

1610 Waliser, D. E., Li, J.-L. F., L'Ecuyer, T. S., and Chen, W.-T.: The impact of precipitating ice and snow
1611 on the radiation balance in global climate models, Geophys. Res. Lett., 38, L06802,
1612 doi:10.1029/2010GL046478, 2011.

1613 Wallace, J. M. and Gutzler, D. S.: Teleconnections in the geopotential height field during the northern
1614 hemisphere winter, Mon. Wea. Rev., 109, 784-812, 1981.

1615 Watanabe, M., Suzuki, T., O'ishi, R., Komuro, Y., Watanabe, S., Emori, S., Takemura, T., Chikira, M.,
1616 Ogura, T., Sekiguchi, M., Takata, K., Yamazaki, D., Yokohata, T., Nozawa, T., Hasumi, H., Tatebe, H.,
1617 and ~~M.~~Kimoto, M.: Improved climate simulation by MIROC5: Mean states, variability, and climate
1618 sensitivity, J. Clim., 23, 6312-6335, DOI: 10.1175/2010JCLI3679.1, 2010.

1619 [Watanabe, M., Chikira, M., Imada, Y., and Kimoto, M.: Convective control of ENSO, J. Climate, 24,](#)
1620 [543-562, 2011.](#)

1621 Watanabe, M., Shiogama, H., Tatebe, H., Hayashi, M., Ishii, M., and Kimoto, M.: Contribution of
1622 natural decadal variability to global warming acceleration and hiatus, Nature Clim. Change, 4, 893-
1623 897, 2014.

1624 Watanabe, M., Shiogama, H., Imada, Y., Mori, M., Ishii, M., and Kimoto, M.: Event attribution of the
1625 August 2010 Russian heat wave, SOLA, 9, 65-68, 2013.

1626 [Watanabe, S.: Constraints on a non-orographic gravity wave drag parameterization using a gravity](#)
1627 [wave resolving general circulation model, SOLA\(Scientific Online Letters on the Atmosphere\), 4, 61–](#)
1628 [64, doi:10.2151/sola.2008-016, 2008.](#)

1629 [Watanabe, S., Kawatani, Y., Tomikawa, Y., Miyazaki, K., Takahashi, M., and Sato, K.: General aspects](#)
1630 [of a T213L256 middle atmosphere general circulation model, J. Geophys. Res., 113, D12110,](#)
1631 [doi:10.1029/2008JD010026, 2008.](#)

1632

1633 Watanabe, S., Hajima, T., Sudo, K., Nagashima, T., Takemura, T., Okajima, H., Nozawa, T., Kawase,
1634 H., Abe, M., Yokohata, T., Ise, T., Sato, H., Kato, E., Takata, K., Emori, S., and Kawamiya, M.:
1635 MIROC-ESM 2010: model description and basic results of CMIP5-20c3m experiments, Geosci.
1636 Model Dev., 4, 845-872, doi:10.5194/gmd-4-845-2011, 2011.

1637 Watanabe, M., and Kawamiya, M.: Remote effects of mixed layer development on ocean acidification
1638 in the subsurface layers of the North Pacific, J. Oceanogr., 73, 771-784, 2017.

1639 Wood, R. and Bretherton, C. S.: On the relationship between stratiform low cloud cover and lower-
1640 tropospheric stability, J. Clim., 19, 6425-6432, 2006.

1641 Webster, P. J., Moore, A. M., Loschnigg, J. P., and Leben, R. R.: Coupled ocean-atmosphere dynamics
1642 in the Indian Ocean during 1997-98, Nature, 401, 35-360, 1999.

1643 Wheeler, M. and Kiladis, G. N.: Convectively coupled equatorial waves: Analysis of clouds and
1644 temperature in the wavenumberfrequency domain, J. Atmos. Sci., 56, 374-399, 1999.

1645 Yamazaki, D., Oki, T., and Kanae, S.: Deriving a global river network map and its sub-grid topographic
1646 characteristics from a fine-resolution flow direction map, Hydrol. Earth Syst. Sci., 13, 2241–2251,
1647 2009.

1648 Yang, P., Lei, B., Baum, B.A., Liou, K-N., Kattawar, G.W., Mischenko, M. I., and Cole, B.: Spectrally
1649 consistent scattering, absorption, and polarization properties of atmospheric ice crystals at

1650 wavelengths from 0.2 to 100 μm , *J. Atm. Sci.*, 70, 330-347, 2013.

1651 Yoo, C. and Son, S. W.: Modulation of the boreal wintertime Madden Julian oscillation by the
1652 stratospheric quasi-biennial oscillation, *Geophys. Res. Lett.*, 43, 1392-1398, 2016.

1653 Zappa, G., Shaffrey, L. C., Hodges, K. I., Sansom, P. G., and Stephenson, D. B.: A multi-model
1654 assessment of future projections of North Atlantic and European extratropical cyclones in the CMIP5
1655 climate models, *J. Clim.*, doi:10.1175/JCLI-D-12-00573.1, 2013.

1656 Zhang, X. B., and co-authors: Detection of human influence on twentieth-century precipitation trends,
1657 *Nature*, 448, 461-464, 2007.

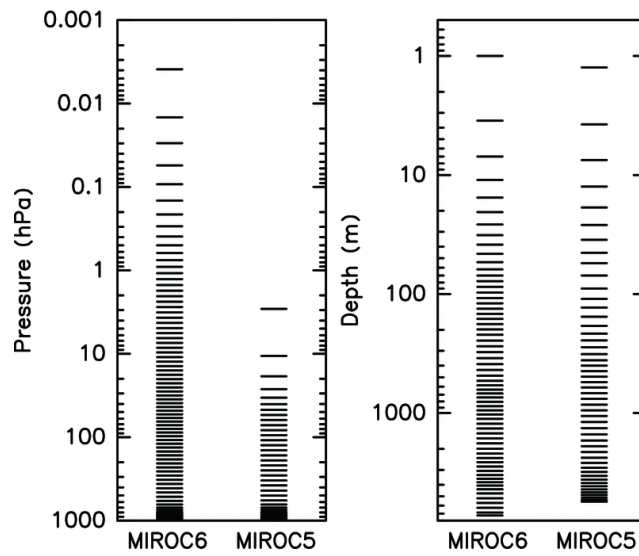
1658 Zhang, Y., Sperber, K. R., and Boyle, J. S.: Climatology and interannual variation of the East Asian
1659 winter monsoon: Results from the 1979-95 NCEP/NCAR reanalysis, *Mon. Wea. Rev.*, 125, 2605-2619,
1660 1997.

1661 Zhang, Y., Rossow, W. B., Lacis, A. A., Oinas, V., and Mishchenko, M. I.: Calculation of radiative
1662 fluxes from the surface to top of atmosphere based on ISCCP and other global data sets: Refinements
1663 of the radiative transfer model and the input data, *J. Geophys. Res.*, 109, doi:10.1029/2003JD004457,
1664 2004.

1665

1666

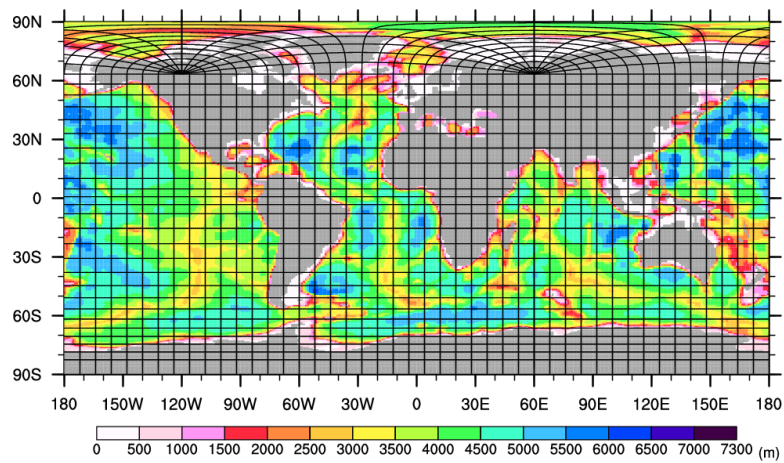
1667



1668

1669 Fig. 1. Vertical half levels for the atmospheric (left panel) and the oceanic (right panel) components of
1670 MIROC6 and MIROC5.

1671



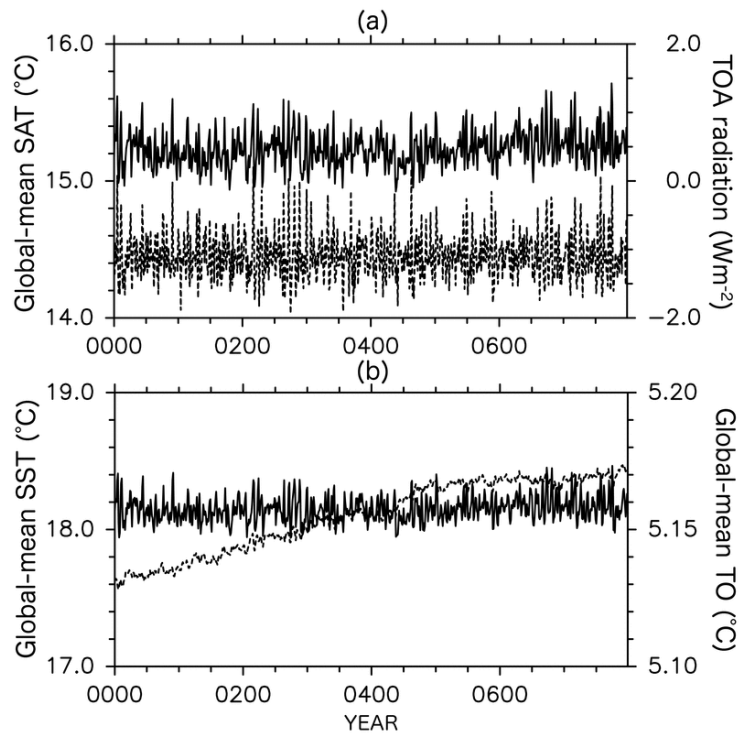
1672

1673 Fig. 2. Horizontal grid coordinate system and model bathymetry of the ocean component of MIROC6.

1674

1675

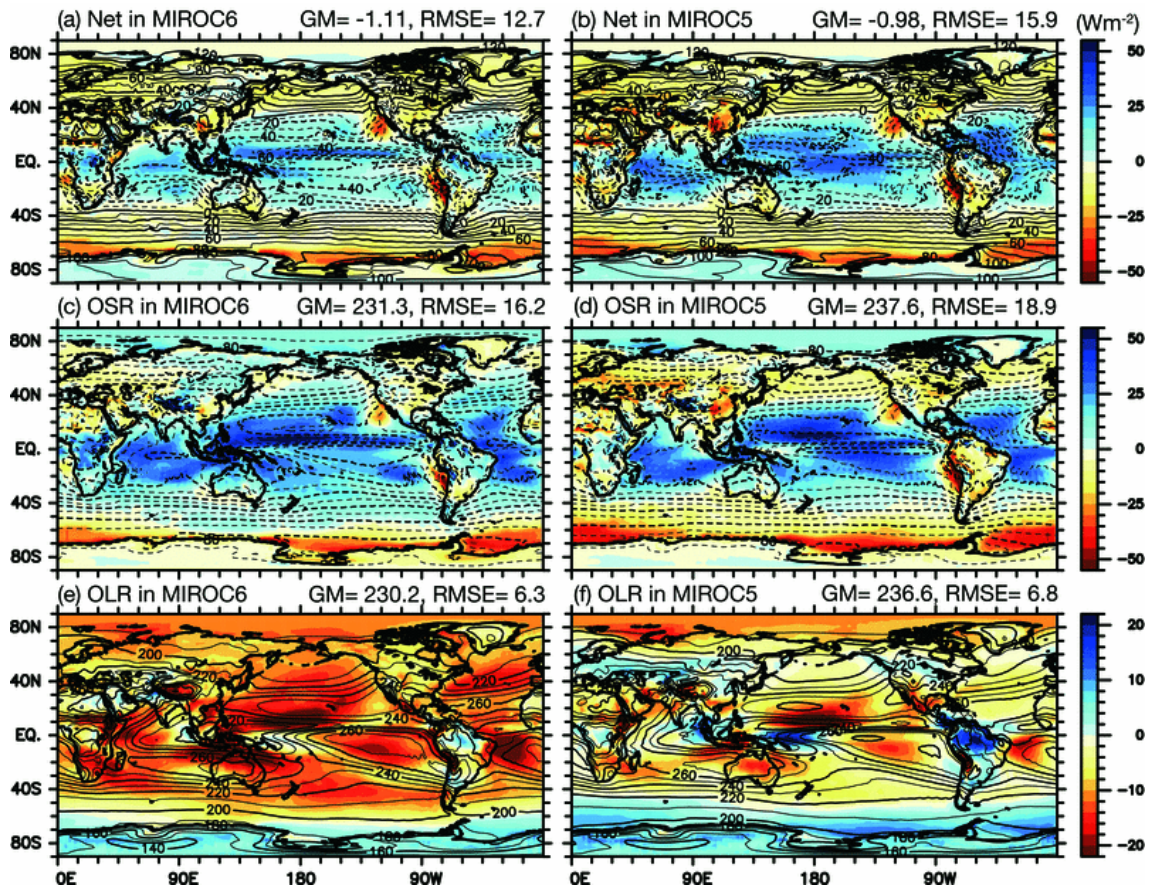
1676



1677

1678 Fig. 3. (a) Time series of the global-mean SAT (solid) and the TOA radiation budget (dashed; upward
1679 positive). (b) Same as (a), but for the global-mean SST (solid) and the ocean temperature through the
1680 full water column (dashed).

1681



1683

1684 Fig. 4. Annual-mean TOA radiative fluxes in MIROC6 (left panels) and MIROC5 (right panels).

1685 Upward is defined as positive. The net, shortwave and longwave radiative fluxes, and the sum of

1686 the two fluxes are denoted as OSR, OLR, and NET, respectively. outgoing shortwave, and outgoing

1687 longwave radiations are aligned from the top to the bottom. Colors indicate errors with respect to

1688 observations (CERES) and contours denote values in each model. Note that a different color scale is

1689 used for the longwave radiations. The global-mean values and root-mean-squared errors are indicated

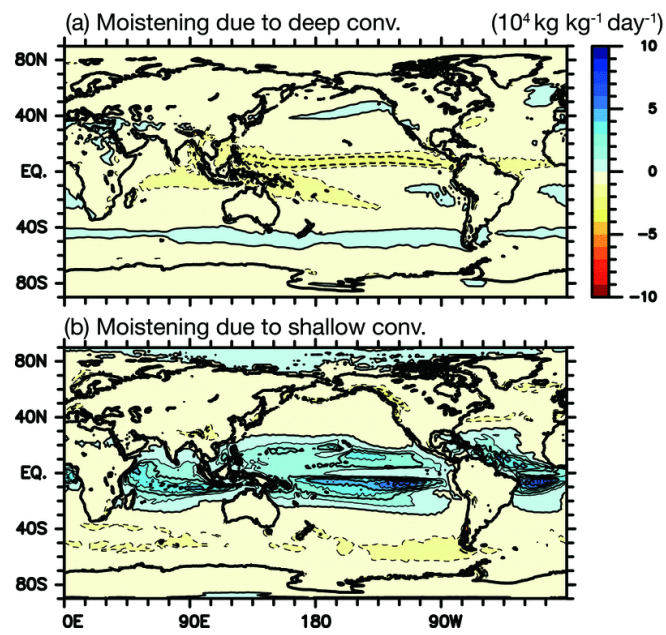
1690 by GM and RMSE, respectively. In the present manuscript, RMSE is computed without model and

1691 observed global-mean quantities unless otherwise noted.

1692 Note that a different color scale is used for the longwave radiations.

1693

1695

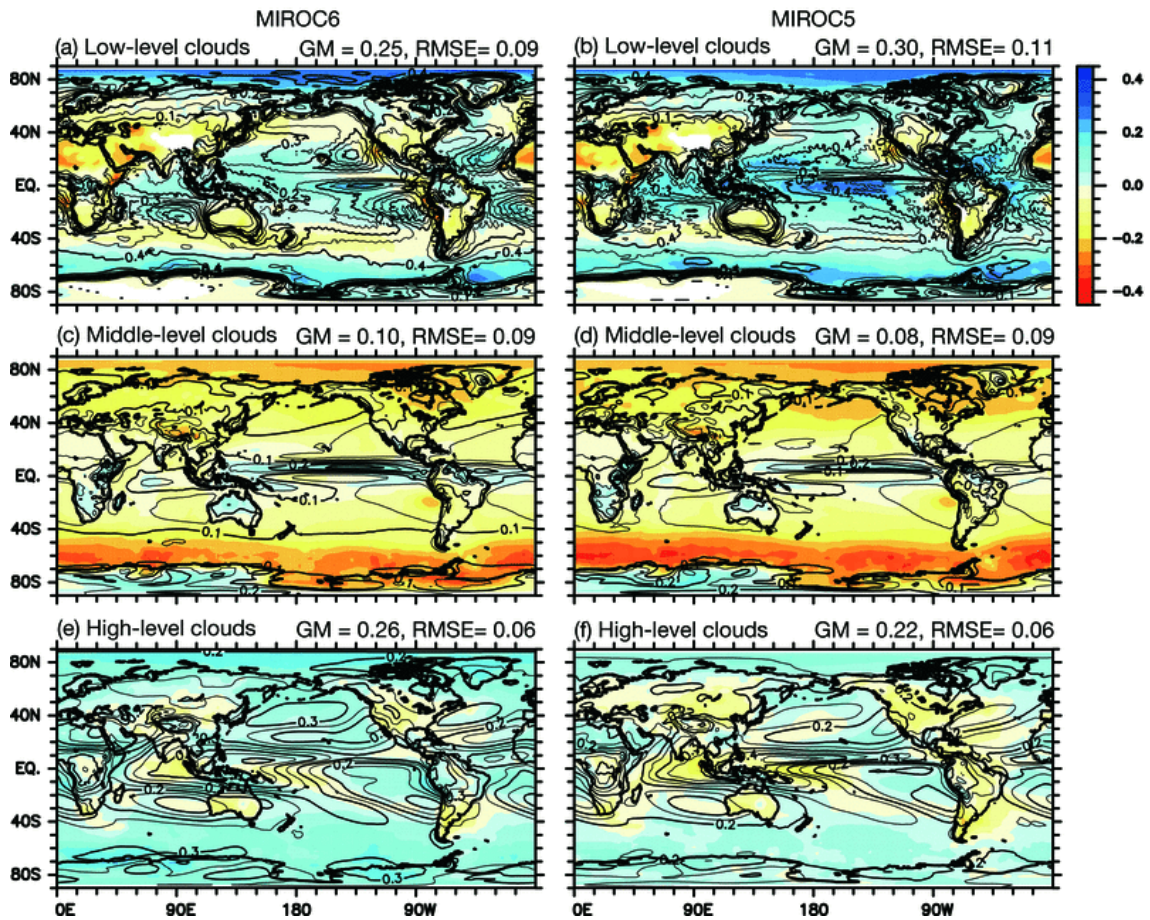


1696

1697 Fig. 5. Annual-mean moistening rate associated with (a) deep convections and (b) shallow convections

1698 in MIROC6 at the 850 hPa pressure level.

1699



1700

1701 Fig. 6. Same as Fig. 4, but for cloud covers in MIROC6 (left panels) and MIROC5 (right panels).

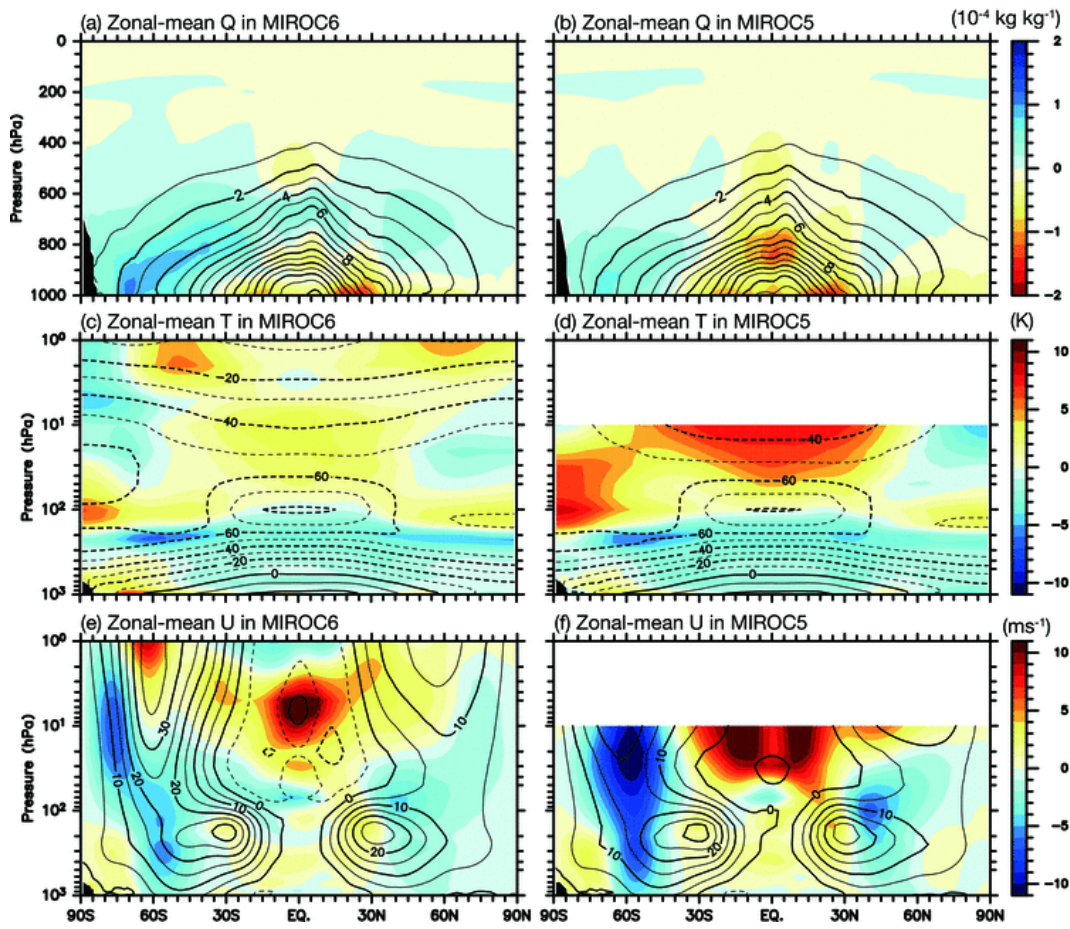
1702 Low-, middle-, and high-level cloud covers are aligned from the top to the bottom. The tops for low-,

1703 middle-, and high-level clouds are defined to exist below the 680 hPa, between the 680 hPa and 440

1704 hPa, and above the 440 hPa pressure levels, respectively. The unit is non-dimensional. ISCCP

1705 climatology is used as observations.

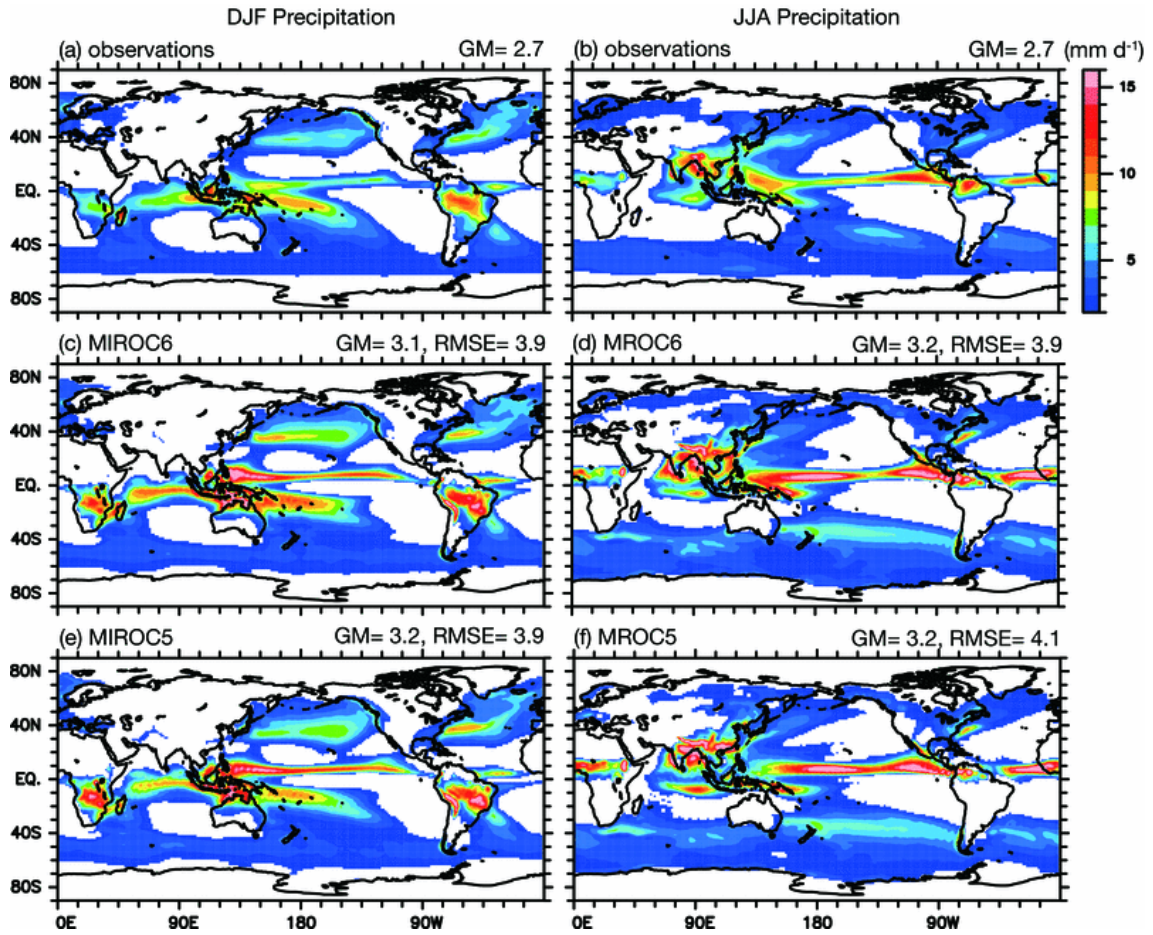
1706



1707

1708 Fig. 7. Annual and zonal-mean specific humidity (top panels), temperature (middle), and zonal wind
 1709 (bottom) in MIROC6 (left) and MIROC5 (right). Colors indicate errors with respect to observations
 1710 (ERA-I) and contours denote values in each model.

1711



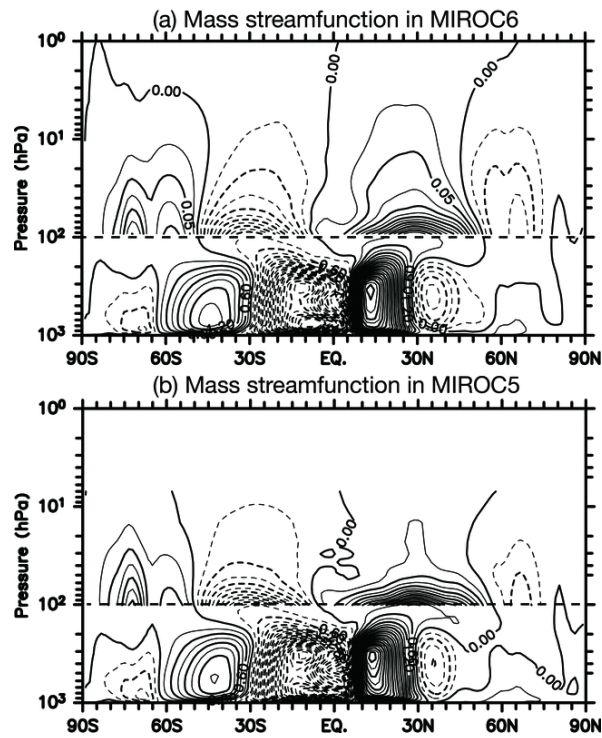
1712

1713 Fig. 8. Precipitation in boreal winter (December–February; left panels) and summer (June–August;
 1714 right panels) in observations (top; GPCP), MIROC6 (middle), and MIROC5 (bottom). Areas with
 1715 precipitation smaller than 3 mm d⁻¹ are not colored.

1716

1717

1718



1719

1720 Fig. 9. Annual-mean mass stream functions in (a) MIROC6 and (b) MIROC5. Contour interval is 0.3

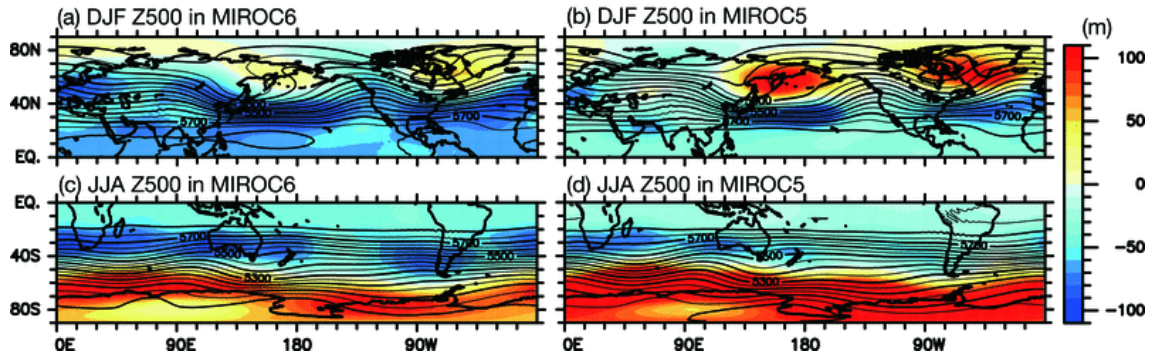
1721 $(0.025) \times 10^{10} \text{ kg s}^{-1}$ below (above) the 100 hPa pressure level. Negative values are denoted by dashed

1722 contours, and the horizontal dashed lines indicate the 100 hPa pressure level.

1723

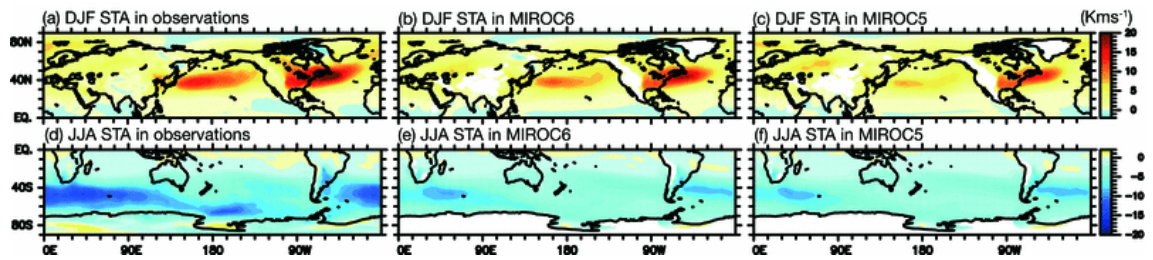
1724

1725



1726 Fig. 10. Same as Fig. 4, but for the wintertime 500 hPa pressure level in MIROC6 (left panels) and
1727 MIROC5 (right panels). Maps for boreal (austral) winter are shown in the upper (lower) panels. ERA-
1728 I is used as observations.

1729



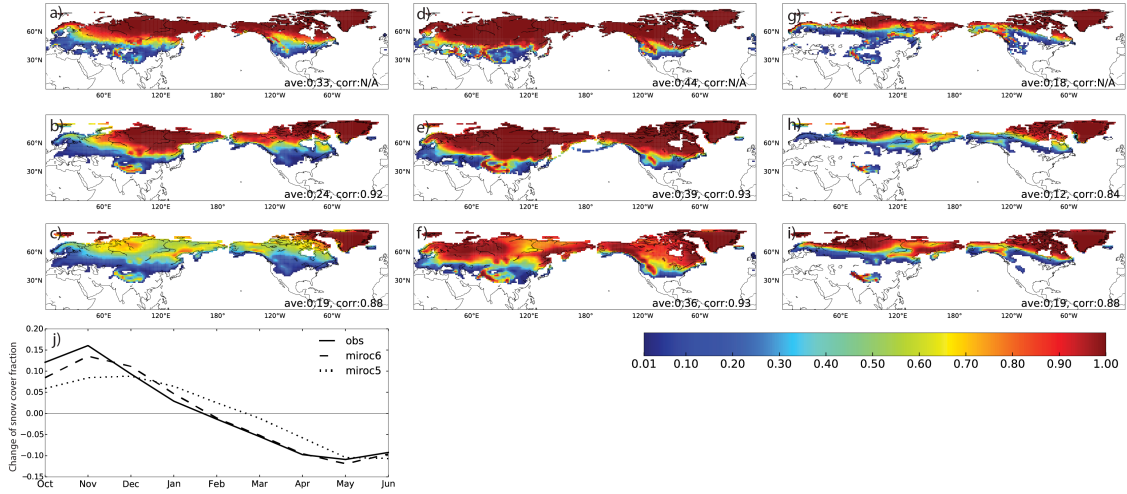
1730 Fig. 11. Wintertime storm track activity (STA) in observations (left), MIROC6 (center), and MIROC5
1731 (right). STA is defined as 8-day-highpass-filtered eddy meridional temperature flux at the 850 hPa
1732 pressure level. Maps for boreal (austral) winter are shown in the upper (lower) panels. ERA-I is used
1733 as observations.

1734

1735

1736

1737



1738

1739 Fig. 12. Snow cover fractions for observations (top panels), MIROC6 (middle), and MIROC5 (bottom).

1740 Maps in November, February, and May are aligned from the left to the right. The unit is non-

1741 dimensional. Areas where snow cover fractions are less than 0.01 are masked. Ave and corr. in the

1742 panels indicate spatial averages and correlation coefficients between observations and models over the

1743 land surface in the Northern Hemisphere, respectively. Time series in the bottom-left panel shows

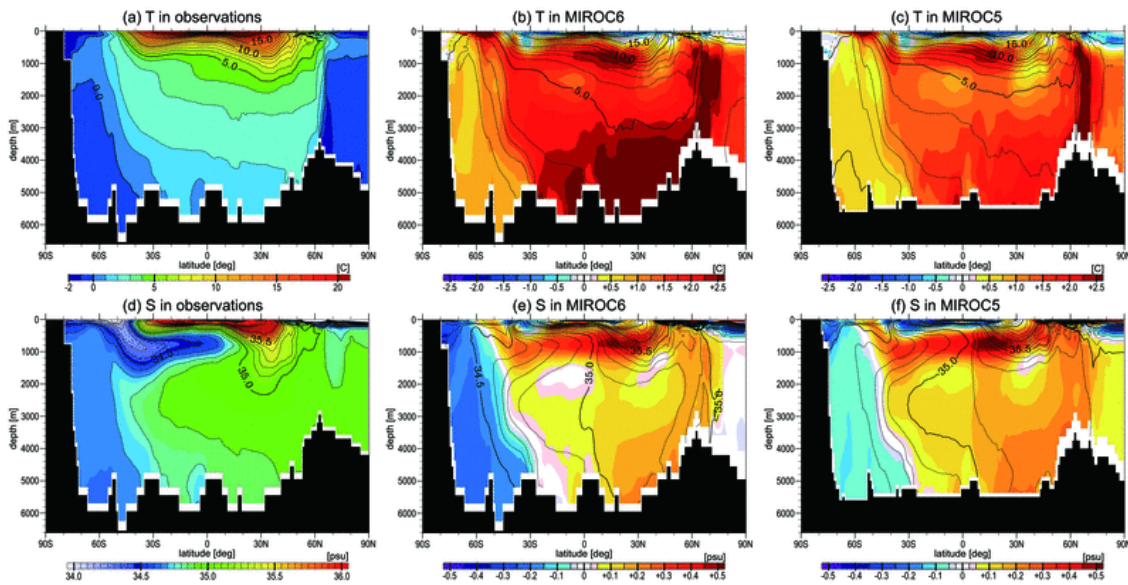
1744 temporal rate of change of the monthly spatial averages. Snow-cover dataset of the Northern

1745 Hemisphere EASE-Grid 2.0 is used as observations.

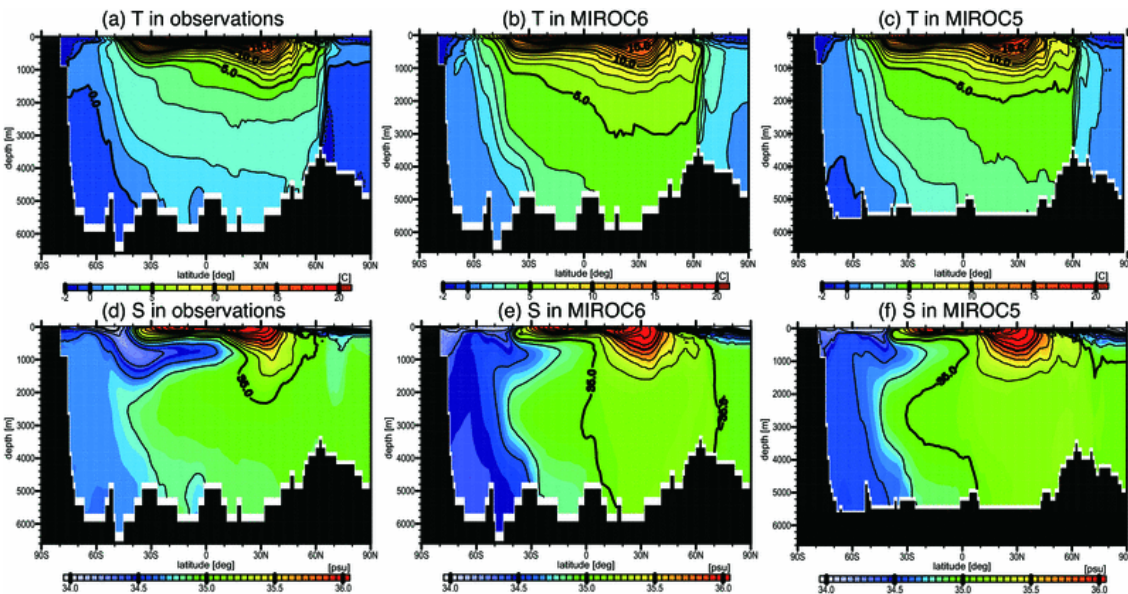
1746

1747

1748



1749



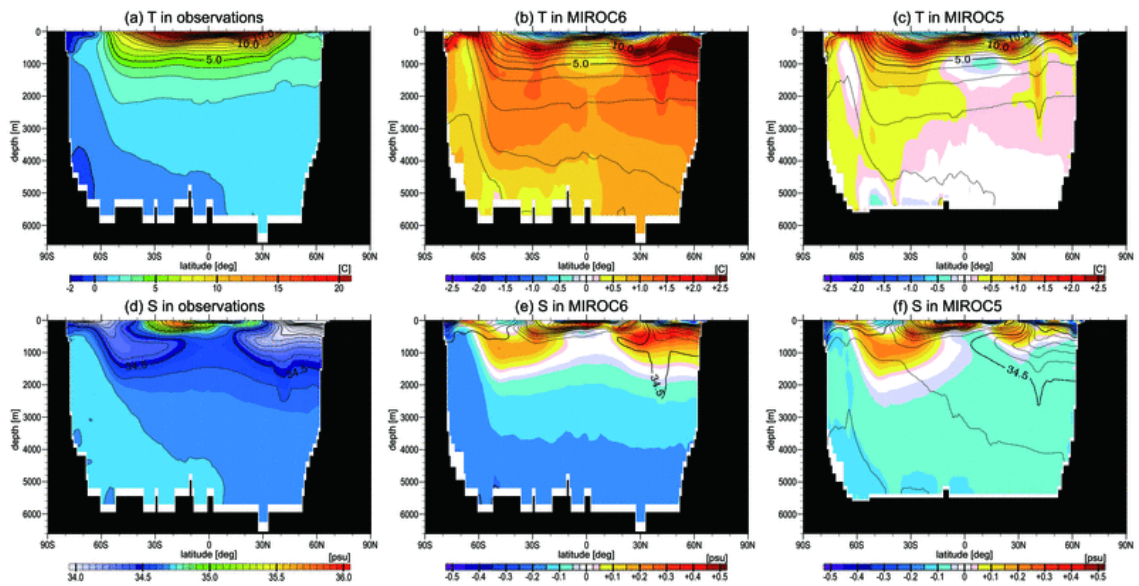
1750

1751 Fig. 13. Annual-mean potential temperature (upper panels; unit is °C) and salinity (lower; psu) in the
 1752 Atlantic sector ~~for from~~ observations (left), MIROC6 (middle), and MIROC5 (right). Colors indicate
 1753 errors with respect to observations (ProjD) and contours denote model values in the middle and right
 1754 panels.

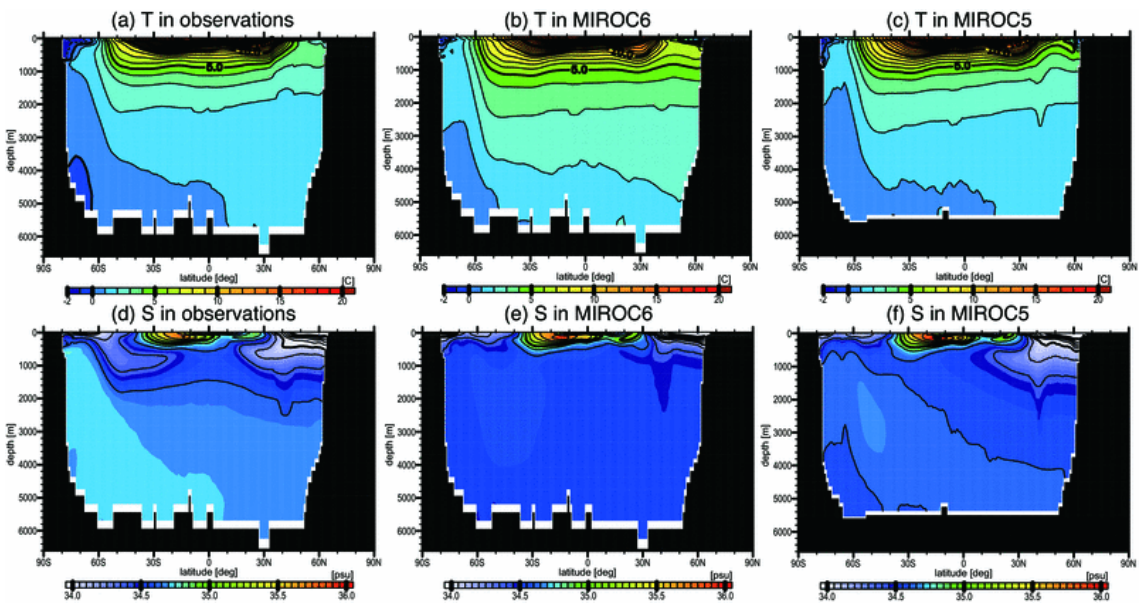
1755 ProjD is used as observations.

1756

1757



1758

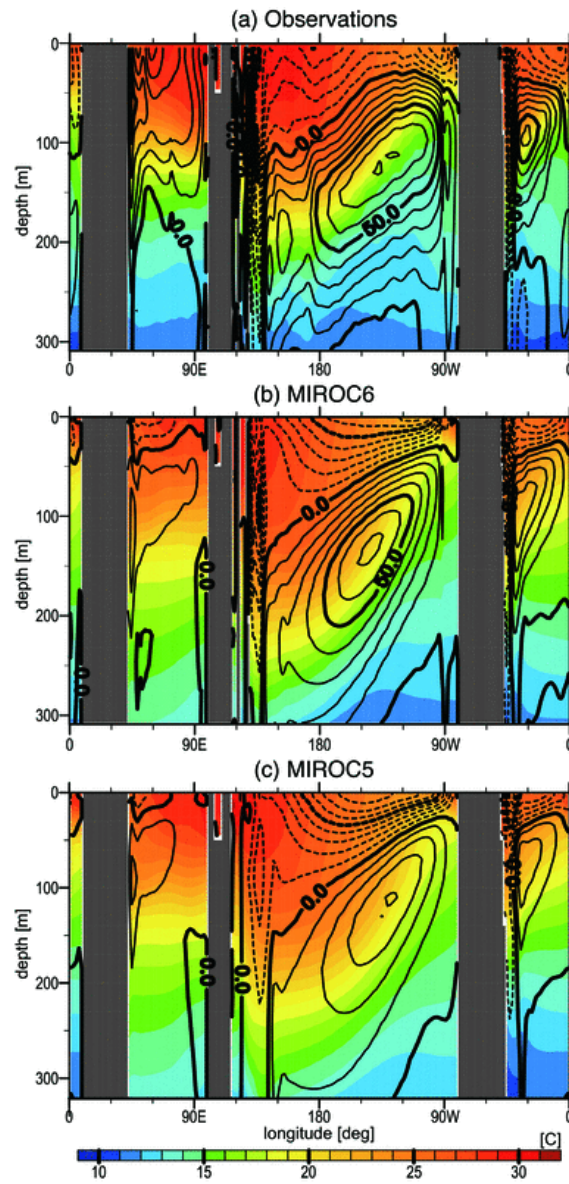


1759

1760 Fig. 14. Same as Fig. 13, but for the Pacific sector.

1761

1762



1764

1765

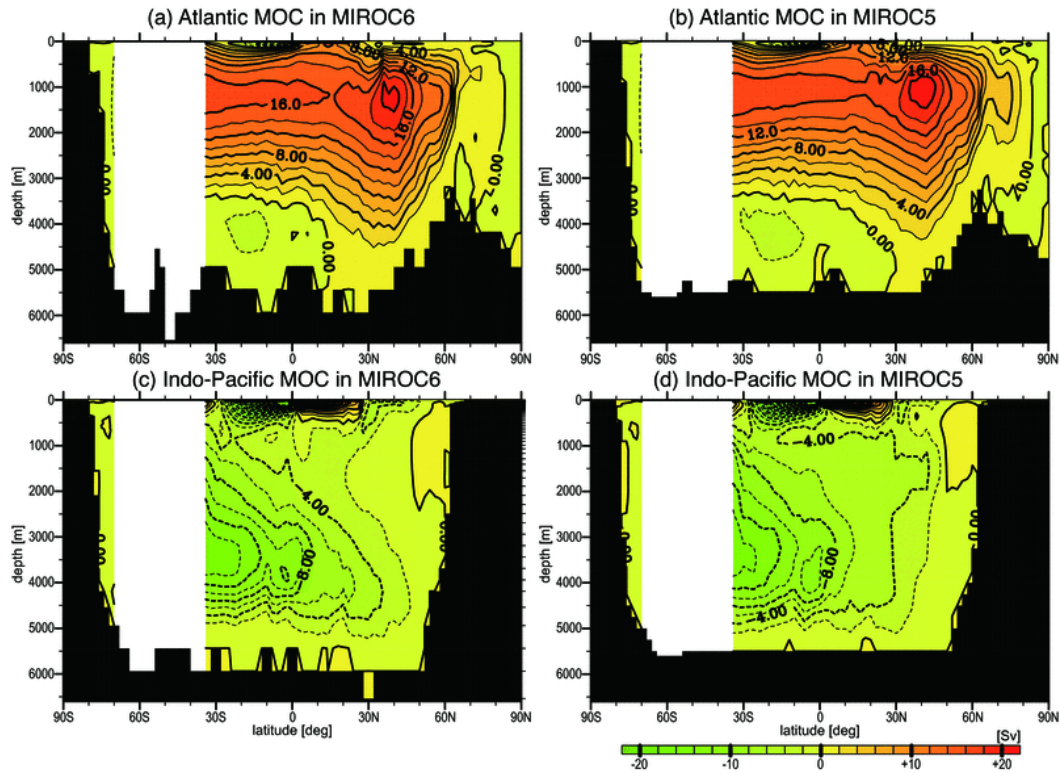
1766

1767

1768

Fig. 15. Annual-mean climatology of potential temperature ($^{\circ}\text{C}$; colors) and zonal current speed (cm s^{-1} ; contours) along the equator (1°S – 1°N) in (a) observations (ProjD and SODA), (b) MIROC6, and (c) MIROC5.

1769



1770

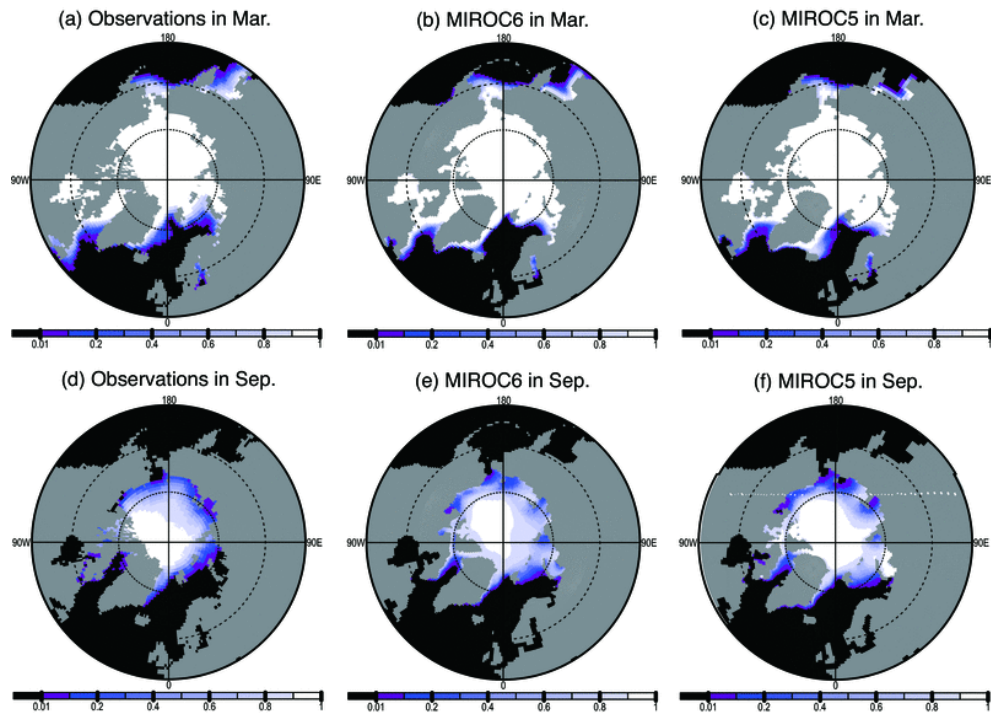
1771 Fig. 16. Annual-mean meridional overturning circulations in the Atlantic (upper panels) and the Indo-

1772 Pacific sectors (lower) in MIROC6 (left) and MIROC5 (right). The unit is Sv ($\equiv 10^6 \text{ m}^3 \text{ s}^{-1}$).

1773

1774

1775



1776

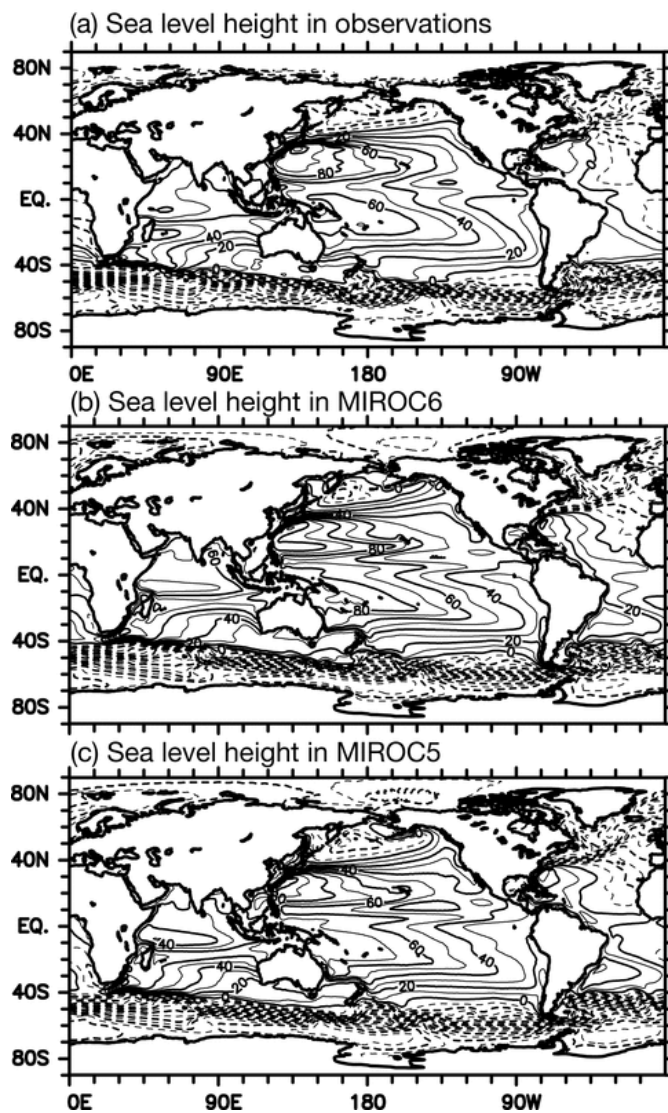
1777 Fig. 17. Northern Hemisphere sea-ice concentrations in March (upper panels) and September (lower
1778 panels) for observations (left), MIROC6 (middle), and MIROC5 (right). The unit is non-dimensional.

1779 Satellite-based sea-ice concentration data of the SSM/I are used as observations.

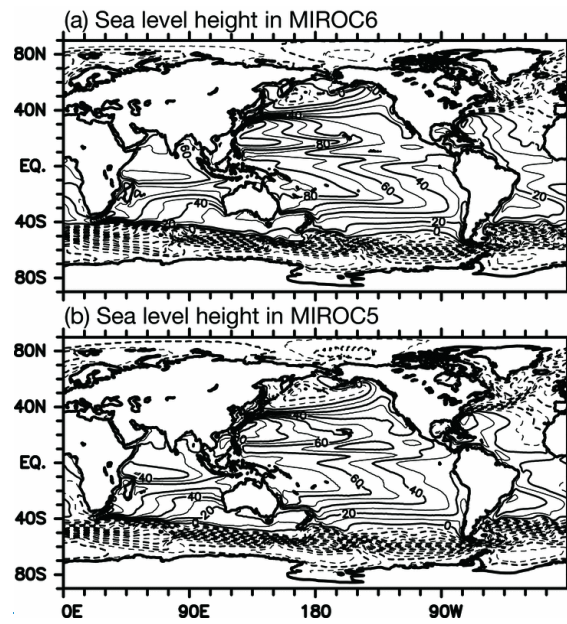
1780

1781

1782



1783



1784

1785 Fig. 18. Annual-mean sea level height relative to the geoid in (a) observations, (b) MIROC6, and (c)

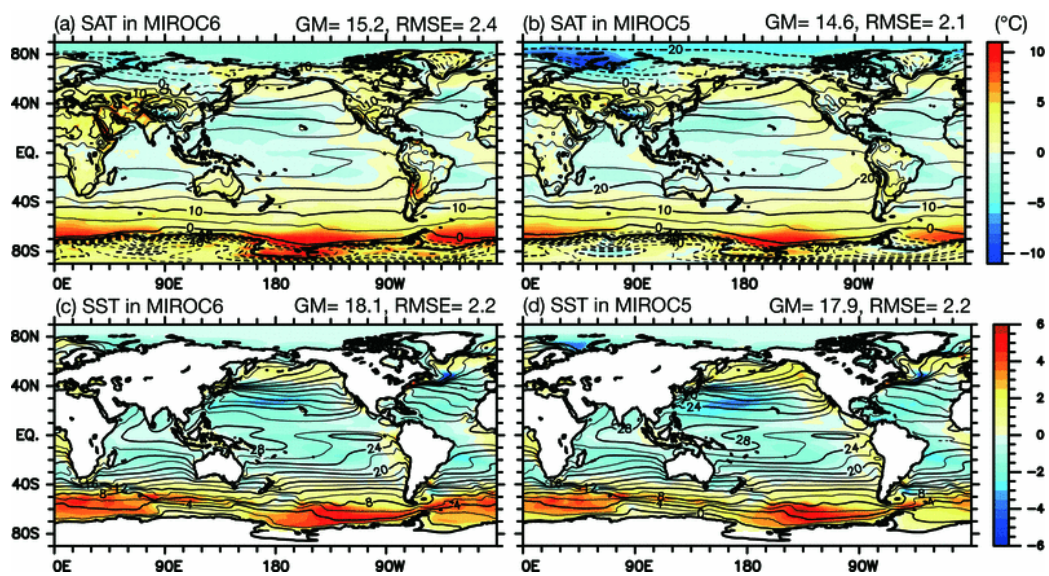
1786 MIROC5. Contour interval is 20 cm. Negative values are denoted by dashed lines. Note that loading

1787 due to sea-ice and accumulated snow on sea-ice are removed from the model sea level height and that

1788 the global-mean value is is also eliminated.

1789

1790



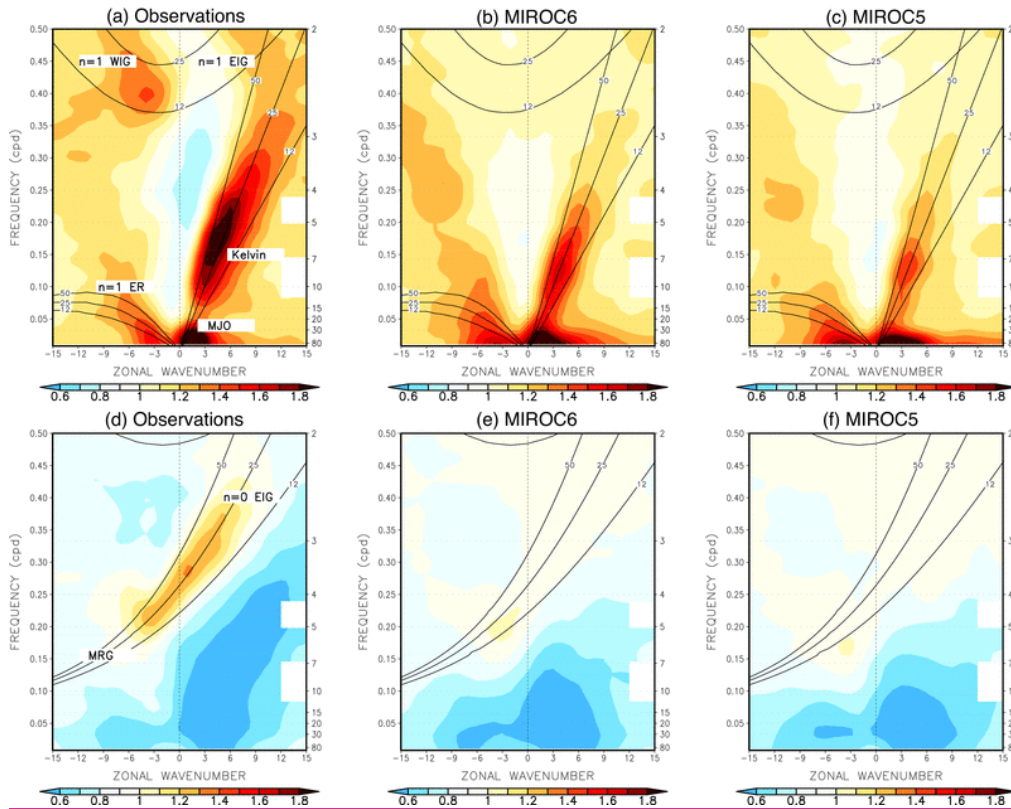
1791

1792 Fig. 19. Same as Fig. 4, but for annual-mean SAT (upper panels) and SST (lower panels). ERA-I for

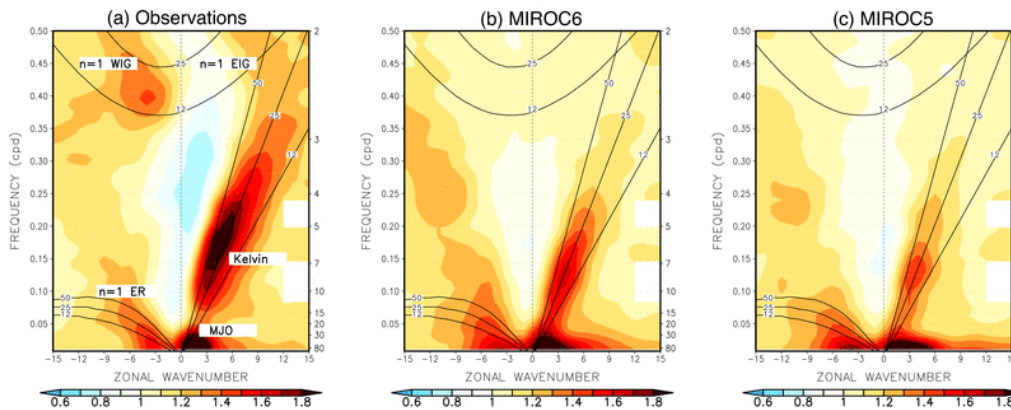
1793 the SAT and the ProjD for the SST are used as observations.

1794

1795



1797



1798

1799

1800

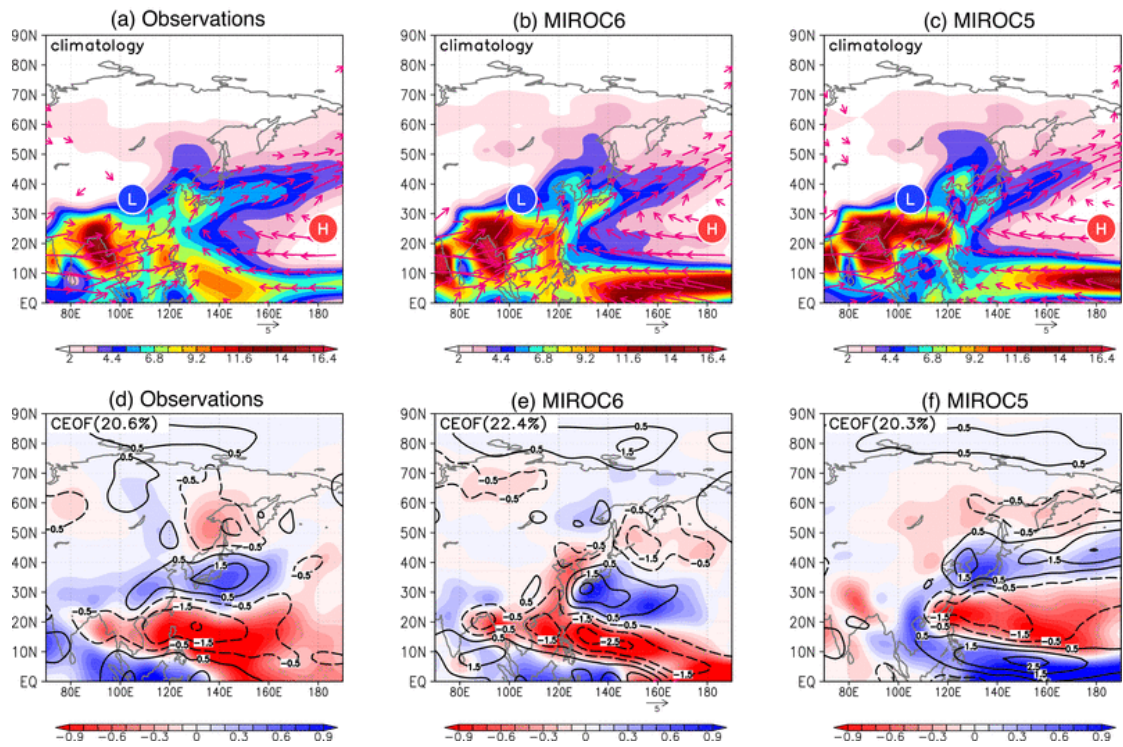
1801

1802

Fig. 20. Zonal wavenumber–frequency power spectra of the (a-c) symmetric and (d-f) antisymmetric component of OLR divided by background power in (a,d) observations (NOAA OLR), (b,e) MIROC6, and (c,f) MIROC5. Dispersion curves of equatorial waves for the three equivalent depths of 12, 25, and 50 m are indicated by black lines. Signals corresponding to the westward and eastward inertia-

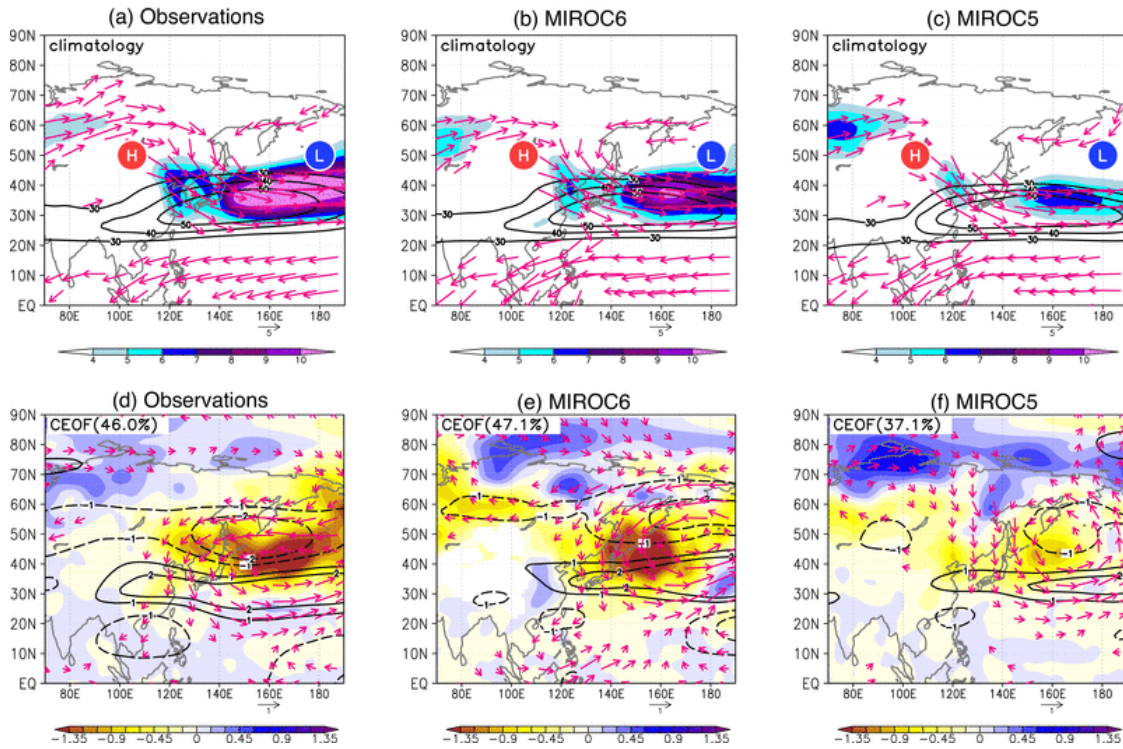
1803 gravity (WIG and EIG) waves, the equatorial Rossby (ER) waves, equatorial Kelvin waves, the mix-
1804 ed Rossby-gravity waves (MRG), and Madden-Julian oscillation (MJO) are labeled in (a). The unit of
1805 the vertical axes is cycle per day (cpd).
1806

1807



1808

1809 Fig. 21. (a-c) Summertime (JJA) climatology of precipitation (color shading, mm day^{-1}) and the 850
1810 hPa horizontal wind (vector; m s^{-1}) for (a) observations (ERA-I), (b) MIROC6, and (c) MIROC5. (d-
1811 f) Anomalies of summertime precipitation (shading; mm day^{-1}) and the 850 hPa vorticity (contour;
1812 10^{-6} s^{-1}) regressed to the time series of EOF1 of the 850 hPa vorticity over $[100^{\circ}\text{E}-150^{\circ}\text{E}, 0^{\circ}\text{N}-60^{\circ}\text{N}]$
1813 for (d) observations, (e) MIROC6, and (f) MIROC5.



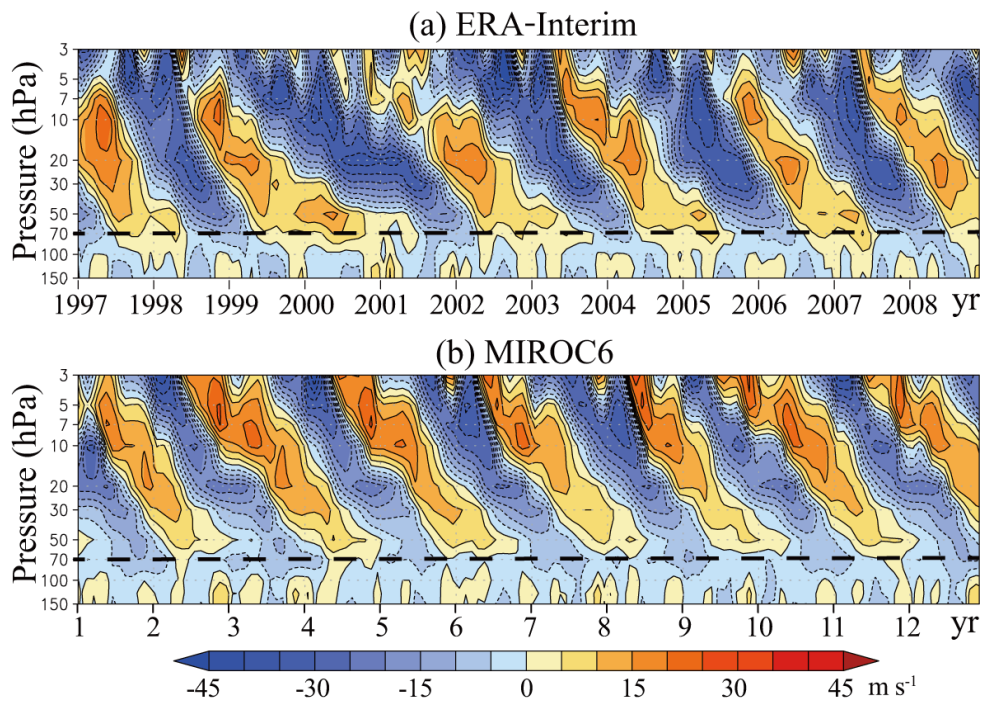
1814

1815 Fig. 22. (a-c) Wintertime (DJF) climatology of STA (color shading; K m s^{-1}), the 300 hPa zonal wind
 1816 (contour; m s^{-1}), and the 300 hPa horizontal wind (vector; m s^{-1}) for (a) observations (ERA-I), (b)
 1817 MIROC6, and (c) MIROC5. (d-f) As in (a-c), but for anomalies regressed onto the time series of the
 1818 EOF1 of the 850 hPa meridional wind over [120°E–150°E, 30°N–60°N].

1819

1820

1821

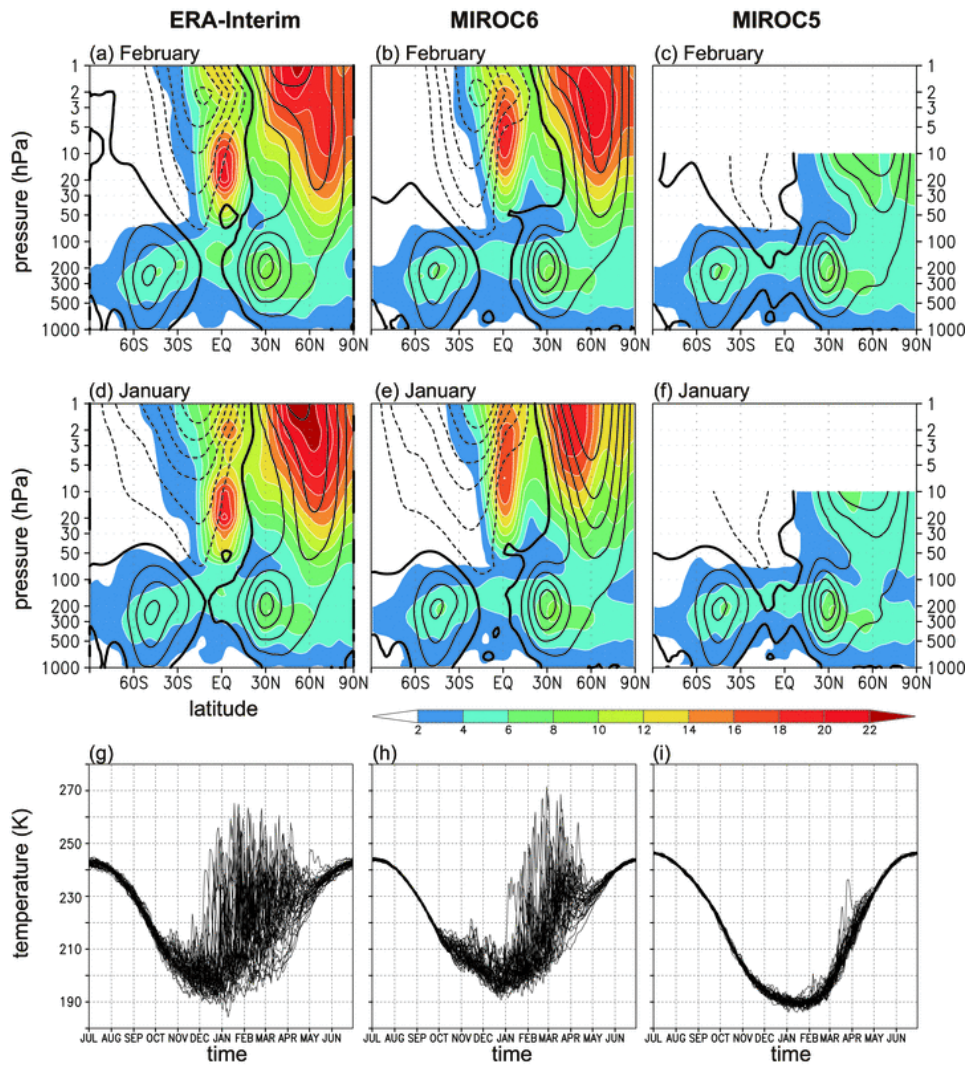


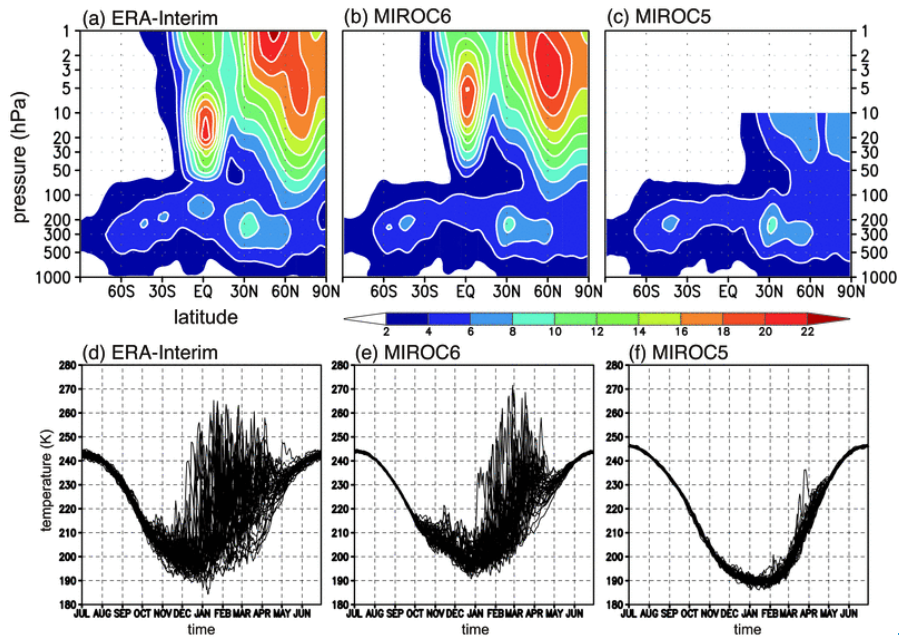
1822

1823 Fig. 23. Time-height cross section of the monthly mean, zonal mean zonal wind over the equator for
1824 (a) observations (ERA-I) and (b) MIROC6. The contour intervals are 5 m s^{-1} . Dashed lines correspond
1825 to the altitude of the 70 hPa pressure level. The red and blue colors correspond to westerlies and
1826 easterlies, respectively.

1827

1828





1830

1831 Fig. 24. (a)-(e) Standard deviation of monthly and zonal-mean zonal wind (colors; unit is m s^{-1})

1832 superimposed on monthly climatology of zonal-mean zonal wind (black contours; unit is m s^{-1}) in

1833 (a-c) February and (d-f) January for observations (ERA-I in 1979-2014; left panels), MIROC6

1834 (middle) and MIROC5 (right) during 60-year period. In panels (g-i), the daily-mean temperatures at

1835 the 10 hPa pressure level on the North Pole are plotted. for (a) observations (ERA-I) in 1979-2014;

1836 (b) MIROC6, and (e) MIROC5 during 60-year period.

1837 Unit is m s^{-1} . (d-f) Daily variation of temperature at the 10 hPa pressure level on the North Pole for

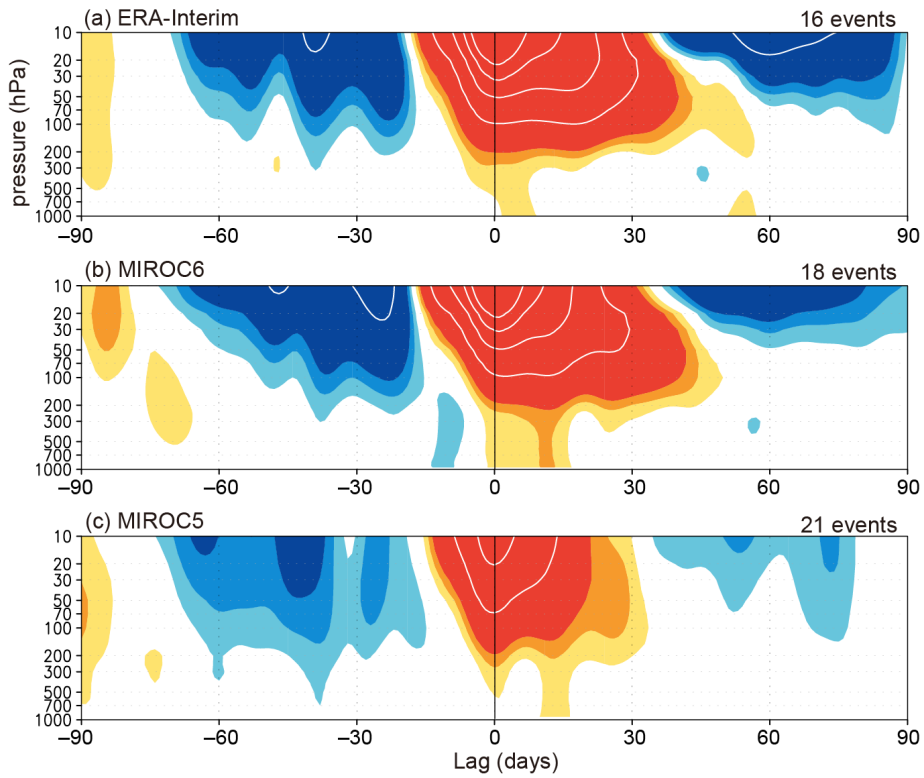
1838 (d) observations (ERA-I), (e) MIROC6, and (f) MIROC5. Daily mean data during 36-year period are

1839 included in each panel (1979-2014 for observations).

1840

1841

1842

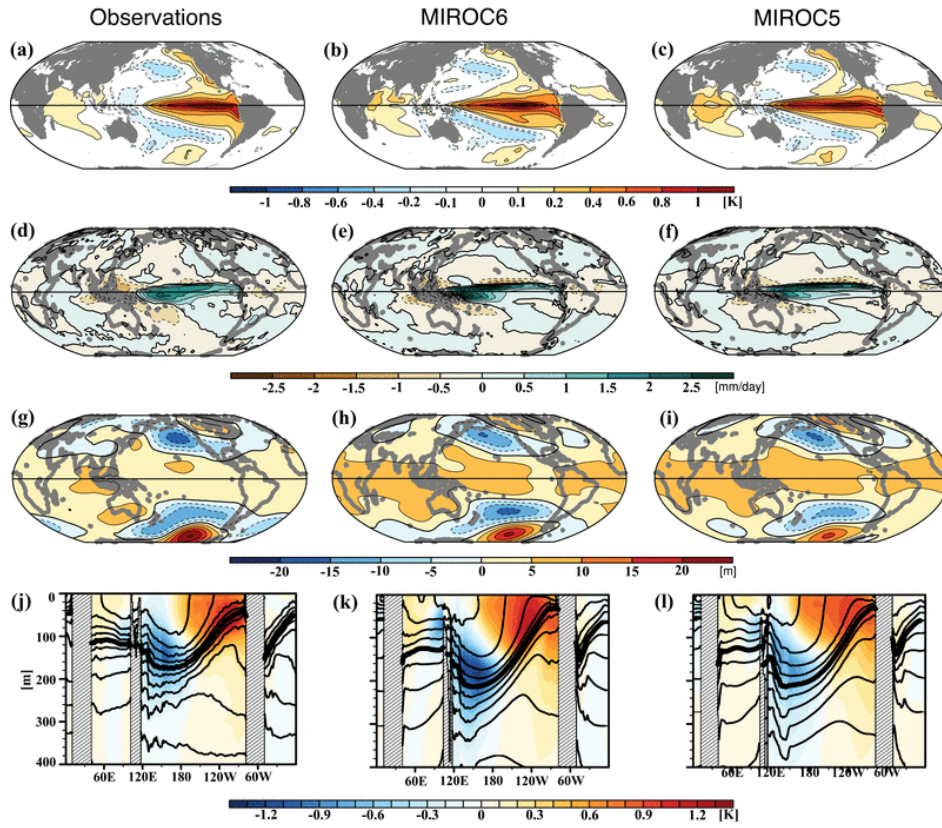


1843

1844 Fig. 25. Composites of time development of the zonal-mean NAM index for stratospheric weak polar
1845 vortex events in (a) observations (ERA-I), (b) MIROC6, and (c) MIROC5. The indices having
1846 dimension of geopotential height (m), and red colors denote negative values. Interval of colors
1847 (contours) is 50 (400) m. The number of events included in the composite are indicated above each
1848 panel.

1849

1850



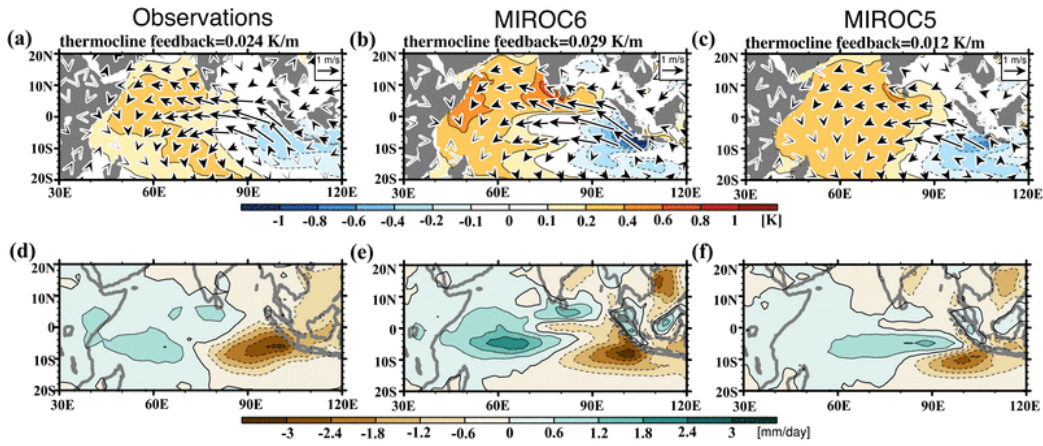
1851

1852 Figure 26. Anomalies of SST (K), precipitation (mm day^{-1}), the 500 hPa pressure height (m), and the
1853 equatorial ocean temperature averaged in $5^{\circ}\text{S}-5^{\circ}\text{N}$ (K) which are regressed onto the Niño3 index.

1854 Monthly anomalies with respect to monthly climatology are used here. From the left to the right, the
1855 anomalies in observations (ProjD and ERA-I), MIROC6, and MIROC5 are aligned. In the bottom
1856 panels, contours denote annual-mean climatological temperature with the 20°C isotherms thickened
1857 and the contour interval is 2°C .

1858

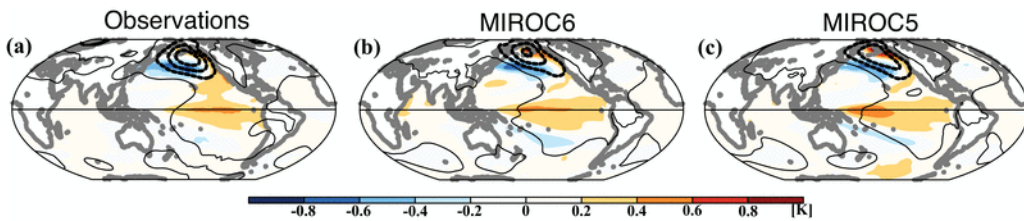
1859



1860

1861 Figure 27. Same as Fig. 26, but for anomalies of SST (colors), 10 m wind vectors (upper panels) and
1862 precipitation (lower panels) regressed onto the autumn DMI. The values of the regression slope
1863 between anomalies of the 20°C isotherm depth and the SST over the eastern IOD region, which
1864 indicates the thermocline feedback, are displayed on the top of the upper panels.

1865

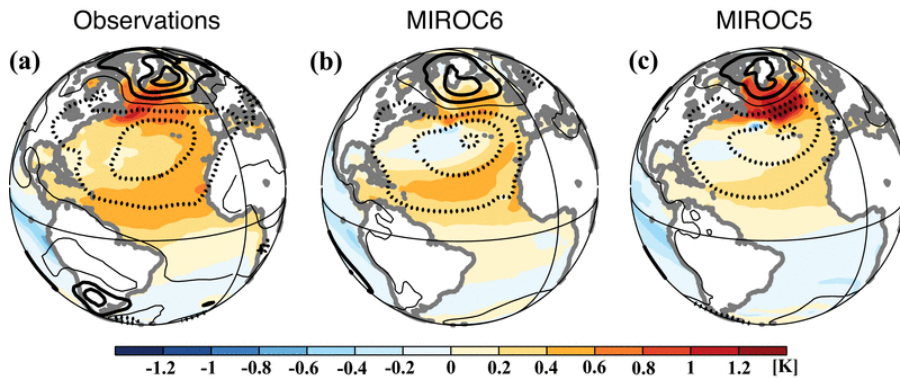


1866

1867 Figure 28. Same as Fig. 26, but for anomalies of monthly SST and wintertime SLP regressed onto the
1868 PDO index (see the text). COBE-SST2/SLP2 data in 1900–2013 are used as observations.

1869

1870

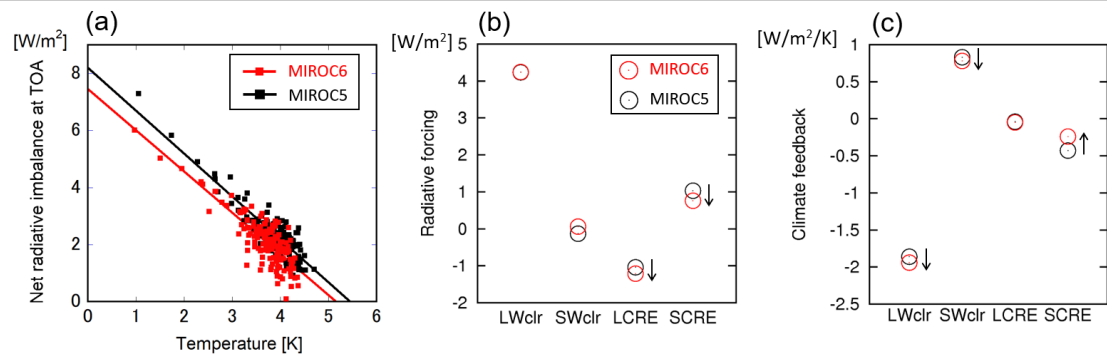


1871

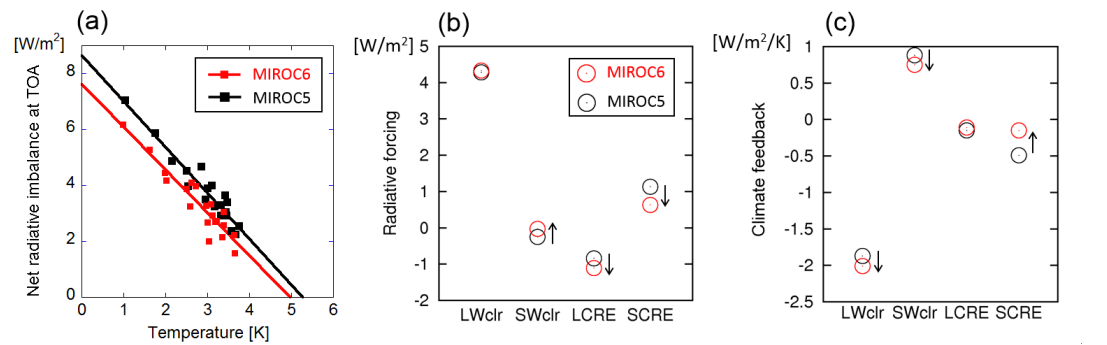
1872 Figure 29. Same as Fig. 26, but for anomalies of SST (colors) and SLP (contours; 0.2 hPa) regressed

1873 onto the AMO index (see the text). Negative values are denoted by dashed contours.

1874



1875



1876

1877 Fig. 30. (a) Global mean net radiative imbalance at the TOA plotted against the global mean SAT

1878 increase. Data from the first 150±20 years after the abrupt CO₂ quadrupling are used. (b) 2 × CO₂

1879 radiative forcing estimated by regressing four components of TOA radiation against the global-mean

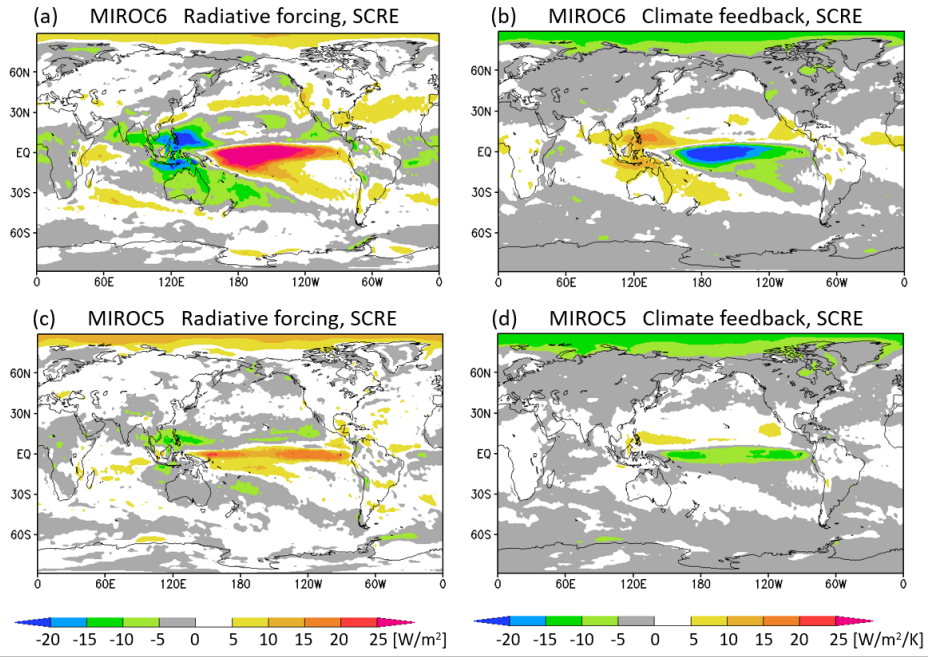
1880 SAT, following Gregory and Webb (2008). (c) Same as (b) but for climate feedback. In Figs. 30bc,

1881 LWclr (SWclr) and LCRE (SCRE) denote a clear-sky longwave (shortwave) component and a
1882 longwave (shortwave) cloud component, respectively. The arrows in (b) and (c) indicate that the results
1883 of MIROC6 are different from MIROC5 at the 5% level.
1884 _____

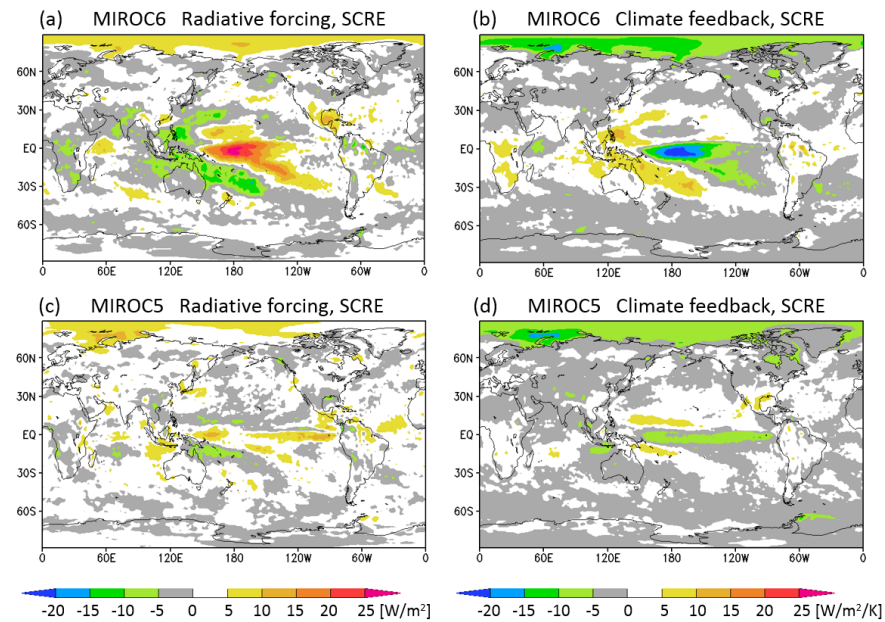
1885

1886

1887



1888



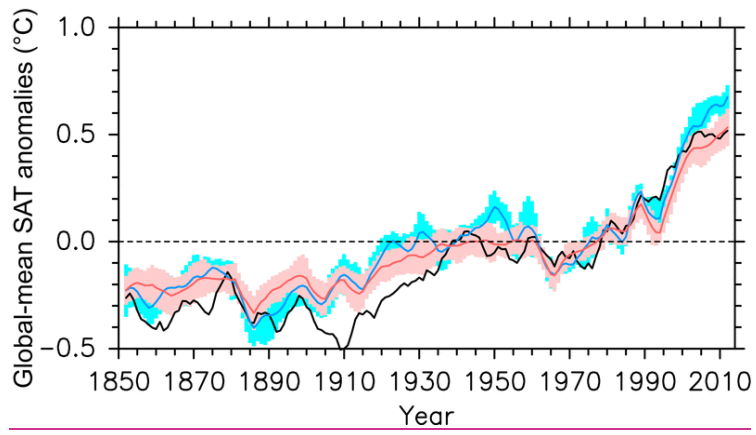
1889

1890

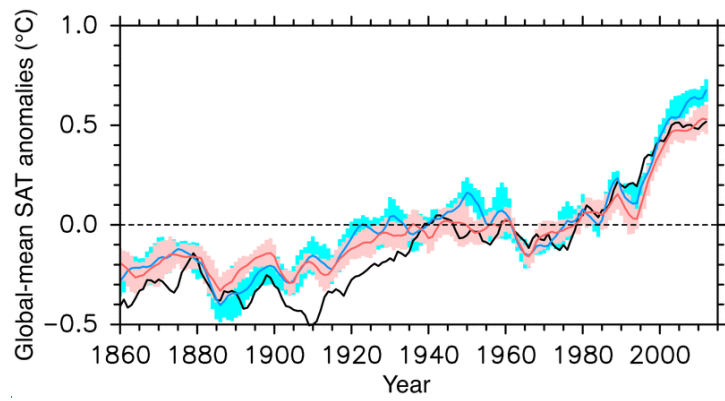
1891

Figure 31. Shortwave cloud component of (a, c) $2 \times \text{CO}_2$ radiative forcing (left panels) and (b, d) climate feedback (right panels) in MIROC6 (upper panels) and MIROC5 (lower panels).

1892



1893



1894

1895 Figure 32. Time series of the global-mean SAT anomalies for observations (black), MIROC6 (red),
1896 and MIROC5 (blue). A 5-yr running-mean filter is applied to the anomalies with respect to the 1961–
1897 1990 mean. Colors indicate spreads of ensemble experiments for each model (1 standard deviation).

1898

1899

1900

Dataset	Used data period (year)	Reference
CERES (edition 2.8)	2001–2013	Loeb et al. (2009)
ISCCP	Climatology	Zhang et al. (2004)
ERA-Interim	1980–2009	Dee et al. (2011)
GPCPv2	1980–2009	Adler et al. (2003)
EASE-Grid 2.0	1980–2009	Brodzik and Armstrong (2013)
ProjD	1980–2009	Ishii et al. (2013)
SODA	1980–2009	Carton and Giese (2008)
SSM/I	1980–2009	Cavarieli et al. (1991)
NOAA OLR	1974–2013	Liebmann and Smith (1996)
COBE-SST2/SLP2	1900–2013	Hirahara et al. (2014)
HadCRUT	1850–2015	Morice et al. (2012)

1901 Table 1. Summary of observation and reanalysis datasets used as the references in the present
 1902 manuscript.

1903

1904

Model	ECS [K]	Radiative forcing [W/m ²]	Climate feedback [W/m ² /K]
MIROC6	2.56	3.7281*	-1.4453
MIROC5	2.67	4.1033	-1.5063

1905 Table 2. Effective climate sensitivity (ECS), radiative forcing of CO₂ doubling, and climate feedback
 1906 for MIROC6 and MIROC5. The result of MIROC6 with ‘*’ is different from MIROC5 at the 5% level.

1907

1908

1909

1910

Model	Radiative forcing [W/m ²]				Climate feedback [W/m ² /K]			
	LWclr	SWclr	LCRE	SCRE	LWclr	SWclr	LCRE	SCRE
MIROC6	4.2433	-0.036*	-1.2+1*	0.7663*	-	0.758*	-0.4+05	-
					21.9401*			0.2415*
MIROC5	4.2328	-0.1325	-	1.403	-1.876	0.883	-0.4504	-0.493
			0.10484					

1911 Table 3. Radiative forcing of CO₂ doubling and climate feedback for MIROC6 and MIROC5,

1912 evaluated with different components of TOA radiation as longwave clear sky (LWclr), shortwave clear

1913 sky (SWclr), longwave cloud radiative effect (LCRE), and shortwave cloud radiative effect (SCRE).

1914 The results of MIROC6 with ‘*’ are different from MIROC5 at the 5% level.

1915

Appendix

	MIROC5 (Watanabe et al., 2010)	MIROC6 (this issue)
Atmosphere		
Core	CCSR-NIES AGCM (Numaguti et al., 1997)	Same as MIROC5
Resolution	T85 (150 km), 40 levels up to 3 hPa	T85 (150 km), 81 levels up to 0.004 hPa
Cumulus	An entrainment plume model with multiple cloud-types (Chikira and Sugiyama, 2010)	Same as MIROC5
Shallow conv.	N/A	A mass flux-based single plume model based on Park and Bretherton (2009)
Aerosol	SPRINTARS (Takemura et al., 2000, 2005, 2009)	Same as MIROC5, but with prognostic precursor gases of organic matters and diagnostic oceanic primary and secondary organic matters.
Radiation	<i>k</i> -distribution scheme (Sekiguchi and Nakajima, 2008)	Same as MIROC5, but with a hexagonal solid column as ice particle habit and extended mode radius of cloud particles.
Gravity waves	An orographic gravity wave parameterization (McFarlane, 1987)	Same as MIROC5, but with a non-orographic gravity wave parameterization (Hines, 1997)
Land		
Core	MATSRIO (Takatani et al., 2003)	Same as MIROC5, but with parameterizations for subgrid snow distribution (Linston et al. 2004; Niita et al., 2014) and a snow-fed wetland (Niita et al., 2017)
Resolution	T85 (150 km), 3 snow layers and 6 soil layers down to 14 m depth	Same as MIROC5
Ocean/sea-ice		
Core	COCO4.9 (Hasumi, 2004)	Same as MIROC5
Resolution	Nominal 1.4° (bipolar grid system), 49 levels down to 5500 m	Nominal 1° (tripolar grid system), 63 levels down to 6300 m
Turbulence	1.5 level turbulent closure model (Noh and Kim, 1999)	Same as MIROC5, but modified turbulent kinetic energy input and smaller background vertical diffusivity under sea-ice (Komuro, 2014)

Table A. Summary of the updated configurations from MIROC5 to MIROC6